Photon Correlations in Two-Mode Cavity Quantum Electrodynamics

Matthias Kronenwett

A thesis submitted in fulfilment of the requirements
for the degree of Master of Science in Physics

The University of Auckland
2007

Matthias Kronenwett

Department of Physics
University of Auckland
Private Bag 92019
Auckland
New Zealand

Supervisors

Prof. Howard J. Carmichael

Department of Physics
University of Auckland
Private Bag 92019
Auckland
New Zealand

Dr. A. Scott Parkins

Department of Physics
University of Auckland
Private Bag 92019
Auckland
New Zealand

Abstract

Cavity quantum electrodynamics (cavity QED) systems, in which two-level atoms interact with a single cavity mode, have been studied extensively over the past years. Recently, the first explicitly two-mode cavity QED experiments were carried out. In this thesis, we compute photon correlation functions in a cavity QED system where a single atom couples to two cavity modes with orthogonal linear polarisations. We take into account the full atomic level structure for an $F = 3$ to $F' = 4$ transition, and consider the case where one cavity mode is resonantly driven by a coherent field, while light in the other cavity mode is generated only through atomic emission.

From analytic investigations in the weak-excitation limit, we find that two orthogonal manifolds of basis states exist, with transitions between the two manifolds occurring precisely whenever a photon from the non-driven mode is emitted. As a qualitative result, the system displays correlations on two distinct time scales: one, a short time scale, determined by the atomic and cavity-mode decay times; the other (not present in single-mode cavity QED), a much longer time scale, determined by the non-driven-mode emission rate.

For a quantitative treatment, we use standard quantum regression formulas and numerical solutions of the master equation for the system density operator to compute steady-state properties and photon correlation functions in the weak-excitation regime; for this, we truncate the cavity mode Hilbert spaces at two-photon states. As with our analytical investigations, we find an extremely long correlation time at the lowest level of excitation, and a shortening of this correlation time as the level of excitation is increased. From a Monte-Carlo simulation based on a quantum trajectory unravelling of the master equation, we recover this dynamic, and explore higher levels of excitations.

Für meine Eltern

Mehr als alles andere stärkt uns die Gewissheit,
dass es jemanden gibt, der an uns glaubt,
der zur Stelle ist, wenn wir ihn brauchen.

(frei nach Jochen Mariss)

Preface

The interaction of matter with electromagnetic radiation has emerged as a key to modern physics. The starting point might have been in 1859, when Gustav R. Kirchhoff formulated the *black-body problem* [1]: how does the intensity of the electromagnetic radiation that is emitted by a black body (an object that absorbs all incident electromagnetic radiation) depend on the frequency of the radiation and the temperature of the body?

In the ensuing years, Kirchhoff's question was explored experimentally through precise observations of black-body spectra; first for short wavelengths and later for long wavelengths by Lummer and Pringsheim [2], and Rubens and Kurlbaum [3]. Although the then-current theory of light, *Maxwell's electromagnetic wave theory* [4], failed to explain the experimentally observed spectra, two formulae that fitted the experimental data in the limiting case of short and long wavelengths were found by Wilhelm Wien [5] and Lord Rayleigh [6] respectively; but these formulae failed when applied to the opposite limits.

In 1900, with the aim of improving Wien's formula, Max Planck developed his *Interpolationsformel* [7] (today known as *Planck's law*), which was consistent with the experimentally observed black-body spectra and interpolated Wien's and Rayleigh's formulae in the appropriate limits. In developing his formula, Planck assumed that a black body can emit electromagnetic energy only in discrete steps, i. e. the emitted energy is *quantised*; this idea was originally suggested by Ludwig Boltzmann in 1877 [8].

To explain Philipp Lenard's observations of the photoelectric effect in 1902, Albert Einstein took Planck's idea a step further and proposed in 1905 [9] that light itself is quantised and consists of individual particles—christened '*photons*' by Gilbert N. Lewis in 1926 [10]. In subsequent years, further work on the spectral radiation of atoms led to the genesis of modern *quantum mechanics* in the late 1920s. Merging Maxwell's electromagnetic wave theory and quantum mechanics resulted in the development of *quantum electrodynamics* (QED), today the most accurate theory in physics. QED describes the interaction of matter with electromagnetic radiation, and involves de Broglie's concept [11] of wave-particle duality.

After the formulation of quantum mechanics, of fundamental interest to physicists was studying the difference between the classical (wave) and quantum (particle) behaviour of light. One method of doing this is to study the intensity of a light beam. The light intensity can be understood not only in terms of a classical electromagnetic field amplitude, but also as a photon flux.

In the 1950s, Robert Hanbury Brown and Richard Q. Twiss [12] investigated temporal correlations of the intensity fluctuations in a light beam emitted by a thermal source. They found that the photons in the light beam tended to arrive in bunches, rather than strictly at random; this phenomenon is called *photon bunching*. Nonetheless, their observations can also be explained classically as a pure wave effect of the electromagnetic light field.

In contrast to photon bunching, photons can also tend to arrive more evenly spread out than strictly at random. This phenomenon is called *photon antibunching*, and was first experimentally observed by Kimble *et al.* [13] in 1977. Antibunching is understandable only in the quantum mechanical description of light; it has no classical explanation and is, therefore, direct evidence for the existence of photons.

The study of the nature of atom-light interactions and resulting phenomena such as photon antibunching is the domain of *quantum optics*; the interaction of a single two-level atom with a single mode of the radiation field is the standard textbook example. However, the reproduction of this idealised example in laboratory experiments is not so simple, and it took until the early 1990s for this to be realised in experiments where atoms interact with light inside an optical cavity. These types of experiments are the subject of *cavity quantum electrodynamics* (cavity QED).

The first photon correlation measurements for optical frequency cavity QED were made by Rempe *et al.* in 1991 [14]. Similar measurements were later performed by Mielke *et al.* [15] and Foster *et al.* [16]. All of these experiments used a beam of thermal atoms intersecting the cavity axis; the atoms interact with the cavity modes during their transit through the cavity. These experiments showed a photon-antibunching effect, the size of which was set by the one-atom coupling strength, even though they were performed on many-atom systems. This provided evidence for a strong coupling between the cavity mode and single atoms [17], and motivated the first truly single-atom measurements in cavity QED taken by the groups of Rempe [18] and Kimble [19].

A promising application of cavity QED with single atoms is found in *quantum information processing* [20], where it is necessary to manipulate atomic and photon states (so-called *qubits*) to store and transfer information. The decay mechanisms of quantum systems are essential for the information transfer as they allow the flow of information into and out of the quantum system. In cavity QED systems, there are two types of decay channel available: the cavity mode decay due to photon loss through the cavity mirrors, and spontaneous emission of the atom. Photons from spontaneous emission events normally exit out the side of the cavity, which, in practice, makes it impossible to detect them efficiently.

In a recent cavity QED experiment carried out by Luis A. Orozco's group [21], a single rubidium atom interacts on resonance with two orthogonally polarised modes of an optical cavity, one mode of which is resonantly driven by a coherent laser field. Due to the experimental set-up and the internal structure of the atom, the light in the driven cavity mode could come from the driving field, and from atomic spontaneous or stimulated emission. The light in the other cavity mode originates only from photon

emission events by the atom. This allows information about the atomic emission channel to be gained by detection of photons emitted from this non-driven mode.

The initial aim of our project is to develop a model of the two-mode cavity QED experiment of Orozco's group, while our ultimate goal is to reproduce their data. For this purpose, we focus on results of temporal correlation measurements of the photons leaking from the two cavity modes through the cavity mirrors.

This thesis is divided into two parts. In the first three chapters, we provide the background knowledge required to understand the methods used to find the results presented in the next three chapters. We assume the reader to be at a postgraduate level in physics. However, we aim to present a generally consistent derivation of the main ideas, and give references for further reading where necessary.

Chapter 1 We give a schematic set-up of the two-mode cavity QED system under consideration, and introduce a typically measured quantity, the second-order correlation function. We then discuss the interactions present in our cavity QED system, and derive the system Hamiltonian for two possible models that differ in the description of the atom. The first model ignores the detailed atomic level structure and uses a simple non-degenerate two-level atom that couples to two cavity modes, whereas the second model takes the full atomic level structure for the electric dipole transitions into account.

Chapter 2 Due to the interaction of the driven cavity QED system with the environment (which enables observations), the system is not closed and the dynamics cannot be described by von Neumann's equation. Hence, we derive an appropriate equation of motion for the system density operator: the so-called master equation. Besides this, we briefly introduce quantum trajectory theory, another approach to open quantum systems.

Chapter 3 We give a brief introduction to cavity quantum electrodynamics on the basis of the standard textbook example, the Jaynes-Cummings model. Afterwards, we adopt the master equation formalism to describe an empty cavity and the two-level atom. Subsequently, we derive the master equation for our two-mode cavity QED system.

Chapter 4 In the weak excitation limit, we perform analytic investigations based on an expansion of the density operator by making a perturbation expansion in the driving field strength. From this, we calculate steady-state correlation functions for a two-mode cavity QED system with a non-degenerate two-level atom. In addition, we find that the level structure is crucial for the dynamics of the system; correlations on a second time scale appear if the full atomic level structure is taken into account.

Chapter 5 In the weak excitation regime, where we make a truncation of the cavity mode Hilbert spaces at two-photon states, we compute the steady-state photon correlation functions using standard quantum regression formulae and a numerical solution of the master equation. Our results confirm the correlations on two distinct time-scales, as predicted by our analytic investigations, if the full atomic level structure for the resonant dipole transition is treated.

Chapter 6 With Monte-Carlo simulations based on a quantum trajectory unravelling of the master equation, we recover the dynamic found from the numerical solution of the master equation in the previous chapter. We also sketch the behaviour displayed when the excitation strength is increased away from the weak-excitation regime.

Chapter 7 We summarise our results and give a brief outlook on future work in this project.

Throughout this thesis the main ideas and results are summarised or highlighted in grey boxes. However, this is only for better comprehension and easier consultation; no attempt is made to formulate them in a fully self-consistent manner.

I would like to acknowledge and thank the people that have contributed to the content of my thesis. First and foremost, I would like to thank my supervisors, Prof. Howard Carmichael and Dr. Scott Parkins, for giving me a rich learning experience, and for their guidance during this project.

Special thanks go to Fabienne, who found a lot of time for moral and editorial support even when she lacked spare time herself. Many thanks go to Simon and Neha for taking the time to proof-read several parts of my thesis. Thanks go to my fellow students Andrew, Andy, Chang, Felipe, Jonathan, Levente, and Malkhaz for all the discussions that positively influenced my thesis work.

This thesis is dedicated to my parents, without whom my studies had not been possible. I thank them for all their support throughout my studies.

Matthias Kronenwett

Auckland, Aotearoa
July 2007

Contents

1 Atom-Light Interactions in a Driven Atom-Cavity System **1**
- 1.1 Schematic set-up of a two-mode cavity QED experiment 2
- 1.2 Photon correlation measurements 3
  - 1.2.1 Hanbury Brown-Twiss experiment for classical intensity fluctuations 3
  - 1.2.2 Hanbury Brown-Twiss experiments with photons 5
- 1.3 Interactions in a driven atom-cavity system 8
  - 1.3.1 The two-level atom 8
  - 1.3.2 Atom-light interactions 10
  - 1.3.3 Selection rules for electric dipole transitions in one-electron atoms 14
  - 1.3.4 Cavity-laser interactions 18
- 1.4 Hamiltonian of a driven single-atom two-mode cavity system 20
  - 1.4.1 Non-degenerate two-level atom 20
  - 1.4.2 Two-level atom with Zeeman substructure 21

2 Open Quantum Systems **23**
- 2.1 The master equation approach 24
  - 2.1.1 The integro-differential von Neumann equation 24
  - 2.1.2 The master equation for the reduced density operator 26
  - 2.1.3 Born approximation 26
  - 2.1.4 Markov approximations 28
  - 2.1.5 General Lindblad master equation 30
  - 2.1.6 Quantum regression formula 34
- 2.2 Quantum trajectories 36
  - 2.2.1 Unravelling the master equation 36
  - 2.2.2 Stochastic wavefunctions 38

3 Cavity Quantum Electrodynamics (Cavity QED) **43**
- 3.1 The Jaynes-Cummings model 44
- 3.2 The damped electromagnetic cavity field 44
  - 3.2.1 The master equation for the non-driven multi-mode cavity . . 44
  - 3.2.2 The single-mode cavity 47
  - 3.2.3 The coherently-driven single-mode cavity 48
- 3.3 The radiatively damped two-level atom 50
- 3.4 The driven single-atom two-mode cavity QED system 52
  - 3.4.1 Two-level atom 53

3.4.2 Two-level atom with Zeeman sub-structure 53

4 Two-Mode Cavity QED I: Analytic Investigations 55
4.1 Method 56
4.1.1 Pure-state factorisation 56
4.1.2 Expansion of the density operator 57
4.2 Non-degenerate two-level atom 57
4.2.1 Steady state 59
4.2.2 Steady state photon correlation functions 60
4.3 Two-level atom with Zeeman substructure 63
4.3.1 Possible system states 63
4.3.2 Identification of two correlation time-scales 64

5 Two-Mode Cavity QED II: Numerical Solutions of the Master Equation 67
5.1 Computational considerations 68
5.1.1 Dimensionless master equation 68
5.1.2 Fock space truncation 68
5.2 Results for the steady state in the weak excitation regime 69
5.2.1 Steady state properties 69
5.2.2 Second-order photon correlation functions 72

6 Two-Mode Cavity QED III: Quantum Simulations 77
6.1 Stochastic wavefunction for a two-mode cavity QED system 78
6.2 Monte-Carlo simulation 79
6.2.1 Computational considerations 79
6.2.2 Monte-Carlo algorithm 80
6.3 Results for the steady state 81
6.3.1 Steady state properties 81
6.3.2 Second-order photon correlation functions 83

7 Conclusion 87
7.1 Summary 87
7.2 Future work 88

A Different Pictures in Quantum Mechanics 89
A.1 Some general properties of non-relativistic quantum mechanics 89
A.2 The Schrödinger, Heisenberg, and Dirac pictures 91

Bibliography 93

List of Figures

1.1 Schematic set-up of the single-atom two-mode cavity QED experiment under investigation . . . 3
1.2 Hanbury Brown-Twiss experiment for the detection of classical intensity fluctuations . . . 4
(a) Schematic set-up of the detection unit . . . 4
(b) Second-order correlation function for perfectly coherent and chaotic monochromatic light . . . 4
1.3 Hanbury Brown-Twiss experiment with photons . . . 6
(a) Schematic set-up of the detection unit . . . 6
(b) Possible computer output . . . 6
1.4 Energy level scheme of the two-level atom . . . 9
1.5 Atomic level structure and allowed electromagnetic dipole transitions for an $F = 3$ to $F' = 4$ transition . . . 18

3.1 The Jaynes-Cummings ladder . . . 45

4.1 Analytic second-order correlation functions for a non-degenerate single atom in a two-mode cavity in the weak-excitation regime . . . 62
4.2 Initial condition of the investigated two-mode cavity QED system . . . 63
4.3 Two orthogonal manifolds of basis states in the weak-excitation limit 64
4.4 Back-and-forth switching of the system between the two manifolds of basis states . . . 65

5.1 Mean photon number in the driven and non-driven cavity modes in the weak excitation regime . . . 71
(a) for varying coupling constant . . . 71
(b) for varying driving field strength . . . 71
5.2 Mean field amplitude of the driven cavity mode for varying coupling constant and driving strength in the weak excitation regime . . . 71
5.3 Atomic population distribution for a varying coupling constant in the weak excitation regime . . . 73
5.4 Atomic population distribution for a varying driving strength in the weak excitation regime . . . 74
5.5 Steady state second-order photon correlation functions for various driving field strengths in the weak excitation regime . . . 75

6.1 Mean photon numbers of the two cavity modes for various driving field strengths 82
6.2 Photon flux out the side of the cavity for various driving field strengths 83
6.3 Steady state second-order photon correlation functions at zero time delay for various driving field strengths 84
6.4 Steady state second-order photon correlation functions for various driving field strengths 85

Chapter 1

Atom-Light Interactions in a Driven Atom-Cavity System

The starting point for our project is a cavity quantum electrodynamics (cavity QED) experiment carried out by L. A. Orozco's group at the University of Maryland [21]. We aim to predict data for their measurements. In this first chapter we familiarise the reader with basic ideas on how to model this type of experiment.

In the first section, we present a schematic set-up of Orozco's experiment, thereby looking at the elements necessary for the development of a theoretical model.

In the second section we introduce a typical measured quantity, the *second-order correlation function* $g^{(2)}$. This function is a normalised two-time average of delayed coincidence measurements.

Even though Orozco's experiment investigates photon correlations, we begin this section with its classical analogue—correlations of time-dependent intensity fluctuations in a light beam. These correlations were first investigated in detail by R. Hanbury Brown and R. Q. Twiss in the 1950s [12]; their experiments led to the concept of the classical intensity correlation function. Different types of classical light, for example coherent light and chaotic light, give correlation functions with different specific properties.

The quantum theory of light predicts some properties for photon correlation functions that are impossible for classical intensity correlation functions. For example, for so-called *antibunched light* we find $g^{(2)}(0) < 1$, which has no classical analogue. Thus, antibunching is a clear signature of the quantum nature of light.

The third section covers interactions in a driven atom-cavity system, namely the atom-cavity and the laser-cavity interactions. Both of these interactions are fairly complicated processes and certain approximations are necessary to make a model calculation feasible.

The complexity of the interaction between the atom and the cavity field lies in the large number of possible transitions of the atomic electrons when interacting with electromagnetic radiation. However, the present experiment uses light with a frequency that is near an atomic transition frequency; this means that the interaction can be well-approximated as the interaction of the light with an effective two-level atom, although each level may itself consist of a number of (Zeeman) sublevels.

The interaction between the driving laser and the cavity field is also a complicated process. The laser light is transmitted through and reflected at several layers of the cavity mirror. Nevertheless, by assuming a simple linear coupling between the driving laser and the cavity field, a good approximation of this process can be achieved.

In the last section we bring together knowledge acquired in the previous sections to write down the Hamiltonian of a driven single-atom two-mode cavity system. In an interaction picture this system Hamiltonian consists of two parts, one for each of the above mentioned interactions:

$$H = (\text{laser-cavity interaction}) + (\text{atom-cavity interaction}) \ .$$

1.1 Schematic set-up of a two-mode cavity quantum electrodynamics experiment

We consider a system consisting of a single ^{85}Rb atom resting in the centre of a high-finesse optical cavity. A schematic set-up of the experimental apparatus is shown in figure 1.1. Two optical cavity modes with orthogonal linear polarisations interact on resonance with the atom via the D_2-line $F = 3$ to $F' = 4$ transition. The dipole coupling strength of the atom light interaction is denoted as g; we will say more about this in subsection 1.3.2. A small external magnetic field with negligible Zeeman effect induces a quantisation axis such that one mode couples the $F = 3$ atomic ground state to the $F' = 4$ excited state via $\Delta m_F = 0$ transitions. This mode is driven on-axis by a coherent field of amplitude $\mathcal{E}$. The other mode, with orthogonal polarisation to the driven mode, couples the atomic levels via $\Delta m_F = \pm 1$ transitions. Thus, any light in this non-driven mode originates only from a spontaneous emission event of the atom with $\Delta m_F = \pm 1$.

The cavity-mode and atomic excited-state decay rates are denoted as κ and γ, respectively. They describe the damping of the system due to light emission through the cavity mirror and atomic spontaneous emission out the side of the cavity, respectively. The light leaking out through the cavity mirror is split by a polarising beam splitter (PBS), such that the output from each mode can be detected separately.

To determine and characterise properties of such systems one typically measures photon arrival times at the detectors. In the two-mode cavity QED system being considered our main interests are the photon self- and cross-correlations for the two modes.

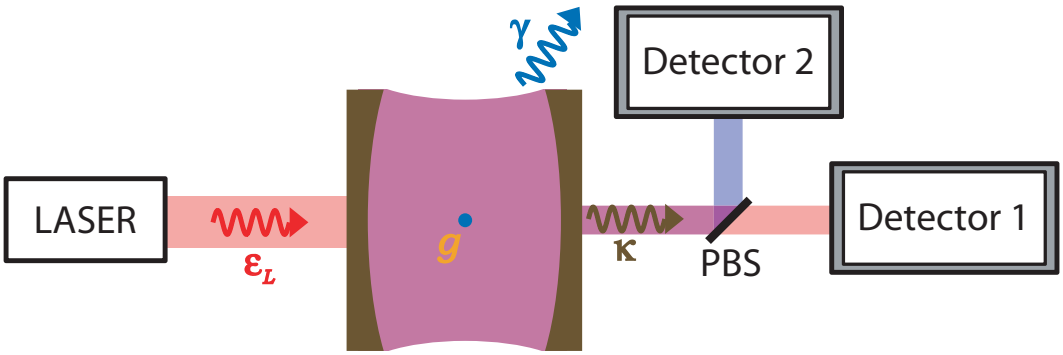

Figure 1.1 Schematic set-up of the single-atom two-mode cavity QED experiment under investigation. The atom is localised in the centre of the cavity.

1.2 Photon correlation measurements

To investigate photon correlations, fast single-photon detectors with a high time resolution are essential. Such fast detectors were not yet available in the 1950s when correlations in a light beam were analysed for the first time in detail. With photo-multiplier tubes (PMT) available at this time it was only possible to measure intensity correlations of a light beam, the classical analogue to photon correlation measurements.

1.2.1 Hanbury Brown-Twiss experiment for classical intensity fluctuations

The classic Hanbury Brown-Twiss experiment [12] investigates temporal correlation effects in the intensity $I(t)$ of a light beam. Figure 1.2a shows a schematic experimental set-up of a Hanbury Brown-Twiss detection unit. Note that the intensity incident on the photomultiplier tubes defines $I(t)$—which assumes the light beam impingent on the 50:50 beam splitter to be a classical wave with intensity $2I(t)$ that is split into two identical beams. One PMT-signal is delayed by some time $\tau \geq 0$. The capacitors subtract the DC part of the current from the photomultiplier tubes. Thus, if we restrict our considerations to light beams with constant mean intensity $\langle I \rangle$ and denote the intensity fluctuation from the mean intensity as $\Delta I(t)$ with $\langle \Delta I(t) \rangle = 0$, i. e.

$$I(t) = \langle I \rangle + \Delta I(t) \ , \tag{1.1}$$

the output of the multiplier and integrator gives $\langle \Delta I(t) \Delta I(t+\tau) \rangle$, where $\langle \cdot \rangle$ indicates the time average. This motivates the introduction of the classical *second-order intensity correlation function* $g^{(2)}(\tau)$ as a normalised time average of delayed coincidence

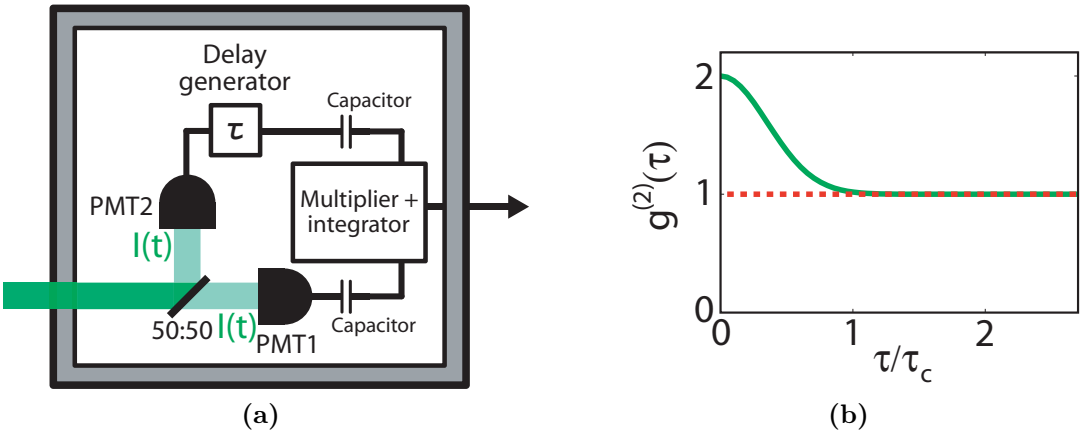

Figure 1.2 (a) Schematic of the Hanbury Brown-Twiss experiment investigating classical intensity fluctuations of an incident light beam. (b) From the output of the multiplier and integrator, correlation functions are extracted: the figure shows the second-order correlation function for perfectly coherent light (red, dashed line) and chaotic light from a monochromatic discharge lamp (green, solid line).

intensity measurements:

$$g^{(2)}(\tau) \equiv \frac{\langle I(t)I(t+\tau)\rangle}{\langle I(t)\rangle\langle I(t+\tau)\rangle} \tag{1.2a}$$

$$= 1 + \frac{\langle \Delta I(t)\Delta I(t+\tau)\rangle}{\langle I\rangle^2} \ , \tag{1.2b}$$

where equation (1.1) has been used. The intensity correlation function $g^{(2)}(\tau)$ is normalised such that it is unity if the intensities separated by some time τ are uncorrelated.

Without explicitly specifying the time dependence of the intensity fluctuation $\Delta I(t)$, we can find some general properties of $g^{(2)}(\tau)$. For time delays τ smaller than the coherence time τ_c of the light source we expect the intensity fluctuations to be correlated, since they share some electromagnetic wave trains. For the case $\tau = 0$, we have

$$g^{(2)}(0) = 1 + \frac{\langle \Delta I(t)^2\rangle}{\langle I\rangle^2} \geq 1 \ . \tag{1.3}$$

For time delays $\tau \gg \tau_c$, the intensity fluctuations of the light beam are uncorrelated, since $\Delta I(t)\Delta I(t+\tau)$ randomly changes its sign with time. Thus,

$$\langle \Delta I(t)\Delta I(t+\tau)\rangle_{\tau\gg\tau_c} = 0 \ , \tag{1.4}$$

and $g^{(2)}(\tau \gg \tau_c)$ becomes unity. In addition, by using Cauchy's inequality

$$I(t_1)^2 + I(t_2)^2 \geq 2I(t_1)I(t_2) \ , \tag{1.5}$$

it can be shown that $g^{(2)}(\tau)$ has a global maximum at $\tau = 0$.

Classical second-order intensity correlation function

Given the time-varying intensity

$$I(t) = \langle I \rangle + \Delta I(t) \ , \tag{1.6}$$

of a light beam with fluctuations $\Delta I(t)$ from a constant mean intensity $\langle I \rangle$, the second-order intensity correlation function

$$g^{(2)}(\tau) \equiv \frac{\langle I(t) I(t+\tau) \rangle}{\langle I(t) \rangle \langle I(t+\tau) \rangle} = 1 + \frac{\langle \Delta I(t) \Delta I(t+\tau) \rangle}{\langle I \rangle^2} \ , \qquad \tau \geq 0 \ , \tag{1.7}$$

characterises the temporal coherence of the light source. It has the properties

$$g^{(2)}(0) \geq g^{(2)}(\tau) \geq 1 \qquad \text{and} \qquad g^{(2)}(\tau \gg \tau_c) = 1 \ , \tag{1.8}$$

where τ_c is the coherence time of the source. For perfectly coherent light, where the intensity is constant in time, the second-order intensity correlation function is unity for all times.

The second-order intensity correlation function for chaotic light from a monochromatic discharge lamp and for perfectly coherent light is illustrated in figure 1.2b.

When faster light detectors became available it was possible to probe the quantum nature of the light and to detect single photons; this will be covered in the following subsection.

1.2.2 Hanbury Brown-Twiss experiments with photons

By using high-precision photomultiplier tubes it is possible to probe the quantum nature of light by detecting single photons. In the photon interpretation of light, the intensity is related to a photon flux: the more photons present the higher the intensity. Classical intensity correlation measurements thus become correlation measurements of photon detection probabilities.

The experimental set-up of a Hanbury Brown-Twiss experiment with photons is shown in figure 1.3a. Though the set-up is similar to the classical one, the physical difference in the detection process is crucial. After the detection of a photon at one detector it is no longer available for a detection at the second detector. The 50:50 splitter no longer divides the incident light beam into two identical beams.

A computer stores all photon arrival times. It is common to visualise the statistics of these arrival times in a histogram, as in figure 1.3b: The separation times of each photon to the others are determined from the arrival times. Each bin of the histogram displays the relative frequency of the separation times in a certain time interval. The envelope of these bins characterises the photon correlations in the light beam.

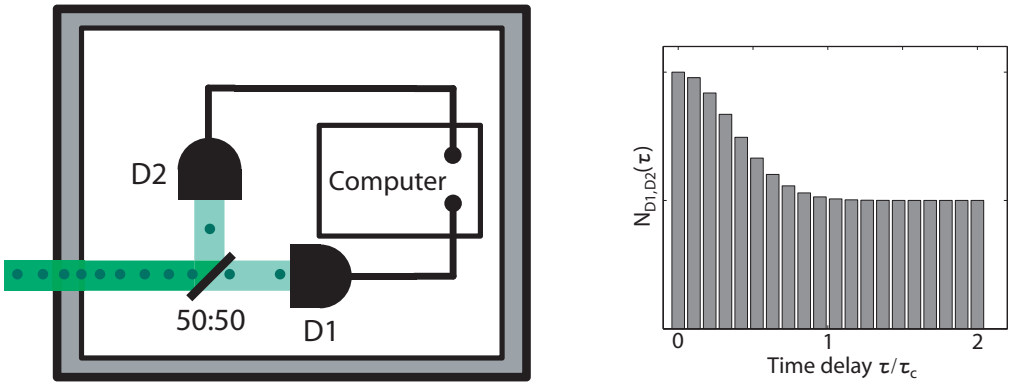

(a) **(b)**

Figure 1.3 (a) Set-up scheme of the Hanbury Brown-Twiss experiment investigating photon arrival times of an incident light beam. (b) Visualisation of the photon arrival time statistics. Each bin contains the number of photon pairs with a separation time in a certain time interval.

Thus, if $P(E_1)$ and $P(E_2)$ are the probabilities for the events E_1 and E_2 of a photon detection at times t_1 and $t_2 = t_1 + \tau \geq t_1$, respectively, and $P(E_1 \cap E_2)$ is the joint probability of the two events, then the normalised *second-order photon correlation function* is defined as

$$g^{(2)}_{E_1E_2}(\tau) \equiv \frac{\langle P(E_1 \cap E_2)\rangle}{\langle P(E_1)\rangle\langle P(E_2)\rangle} \tag{1.9a}$$

$$= \frac{\langle P(E_1)\rangle\langle P(E_2|E_1)\rangle}{\langle P(E_1)\rangle\langle P(E_2)\rangle} = \frac{\langle P(E_2|E_1)\rangle}{\langle P(E_2)\rangle} \ , \tag{1.9b}$$

where $P(E_2|E_1)$ is the *conditional probability*, that is the probability of the event E_2, given the event E_1 did happen. For *statistically independent* events E_1 and E_2

$$\langle P(E_1 \cap E_2)\rangle = \langle P(E_1)\rangle\langle P(E_2)\rangle \ , \tag{1.10}$$

and the correlation function is unity. An experimental advantage of the normalisation is that in this way the correlation function is independent of the quantum efficiency η of the detectors. Both the numerator and the denominator in equation (1.9) have a factor of η^2 (since two photons are detected) that cancel each other.

In an actual experiment, photon numbers rather than detection probabilities are observed. In the photon interpretation of light the number n of photons determines the intensity. The second-order photon correlation function (1.9) can thus be written as

$$g^{(2)}(\tau) = \frac{\langle : \hat{n}_1(t)\hat{n}_2(t+\tau) : \rangle}{\langle \hat{n}_1(t)\rangle\langle \hat{n}_2(t+\tau)\rangle} = \frac{\langle \hat{a}_1^\dagger(t)\hat{a}_2^\dagger(t+\tau)\hat{a}_2(t+\tau)\hat{a}_1(t)\rangle}{\langle \hat{a}_1^\dagger(t)\hat{a}_1(t)\rangle\langle \hat{a}_2^\dagger(t+\tau)\hat{a}_2(t+\tau)\rangle} \ , \tag{1.11}$$

where $\hat{n}_i \equiv \hat{a}_i^\dagger\hat{a}_i$ is the occupation number operator of the light impinging on detector $i = 1, 2$; $\hat{a}_i$ represents an annihilation of a photon by detection of detector $i = 1, 2$.

$:\cdot:$ denotes normal and time ordering: all the creation operators appear to the left of the annihilation operators, and all operators are ordered from outside to inside by increasing time. This ordering of operators is a consequence of the photoelectric detection process that annihilates photons and converts them to a photocurrent.

One of the main properties the second-order correlation function provides is determined by its value for $\tau = 0$:

$$g^{(2)}(0) = \frac{\langle \hat{n}(\hat{n}-1)\rangle}{\langle \hat{n}\rangle^2} \ , \tag{1.12}$$

where $\hat{n}$ is the occupation number operator of the light field incident on the 50:50 beam splitter in the detection unit.

- For a coherent state, i. e. an eigenstate of the annihilation operator, expression (1.12) is unity.
- For a photon number state $|n\rangle$ we find

  $$g^{(2)}(0) = \frac{n(n-1)}{n^2} \ , \tag{1.13}$$

  which is zero for sources that emit single-photons, i. e. photon number states with $n = 1$. The value zero of the second-order correlation function is classically impossible and thus a clear signature of the quantum nature of light.

Due to the above properties of the correlation function at zero time-delay, it is common to classify light as *bunched*, *coherent*, or *antibunched* dependent on whether $g^{(2)}(0)$ is larger, equal to, or smaller than unity, respectively. The first verification of antibunched light was demonstrated by Kimble *et al.* in 1977 [13].

The second-order photon correlation function, and photon bunching and antibunching

The second-order photon correlation function of the electromagnetic field for a single mode is given by

$$g^{(2)}(\tau) = \frac{\langle \hat{a}^\dagger(0)\hat{a}^\dagger(\tau)\hat{a}(\tau)\hat{a}(0)\rangle}{\langle \hat{a}^\dagger(0)\hat{a}(0)\rangle\langle \hat{a}^\dagger(\tau)\hat{a}(\tau)\rangle} \ . \tag{1.14}$$

One classifies light into three categories according to the value of $g^{(2)}(0)$, with

$g^{(2)}(0) > 1$: bunched light ,
$g^{(2)}(0) = 1$: coherent light , and
$g^{(2)}(0) < 1$: antibunched light .

Antibunched light has no classical analogue, and is therefore a clear signature of the quantum nature of light.

Note 1.1 The above classification of light into bunched, coherent and antibunched should not be mistaken for the classification of light according to its photon number statistics. Comparing the mean photon number $\bar{n}$ and its variance $(\Delta n)^2$, one can distinguish between

$$\begin{aligned} (\Delta n)^2 > \bar{n} \ : &\quad \text{super-Poissonian statistics ,} \\ (\Delta n)^2 = \bar{n} \ : &\quad \text{Poissonian statistics ,} \\ (\Delta n)^2 < \bar{n} \ : &\quad \text{sub-Poissonian statistics .} \end{aligned}$$

The classical equivalents to these photon statistics are partially coherent, incoherent, or thermal light for super-Poissonian statistics, and perfectly coherent light for Poissonian statistics. Sub-Poissonian statistics has no classical equivalent and is another signature of the quantum nature of light; it is reflected in an initial rise of the $g^{(2)}(\tau)$-function at zero time delay.

Even though antibunching and sub-Poissonian photon statistics frequently occur simultaneously, they are different phenomena and are not two manifestations of a single quantum phenomenon. [22] ◀

Cavity QED experiments are a good tool to visualize atom-light interactions with the help of the photon correlations in the light that leaks through the cavity mirrors. An empty cavity is simply a Fabry-Pérot interferometer; if it is coherently driven, the output field will be coherent, too, and consequently the measured correlation function will be unity. With an atom inside the cavity, any deviation of the correlation function from unity is therefore due to the interaction of the cavity field with the atom. The theoretical description of atom-light interactions as well as the laser-cavity interaction is the content of the following section.

1.3 Interactions in a driven atom-cavity system

In a driven-atom cavity system two dominant interactions are present: the interaction of the driving laser with the cavity field through the cavity mirror, and the interaction of the cavity field with the atom inside the cavity. This section presents the theory that describes these two interactions. Atom-light interactions are discussed in all quantum optics books; we mainly follow Friedrich [23].

1.3.1 The two-level atom

Consider a two-level atom with a ground state $|g\rangle$, an excited state $|e\rangle$, and corresponding energies E_g and E_e with $E_g < E_e$. If we use these energy eigenstates as a basis for the two-level atom, the internal atomic Hamiltonian H_A can be written as

$$H_A = E_g|g\rangle\langle g| + E_e|e\rangle\langle e| \quad . \tag{1.15}$$

The first term in equation (1.15) may be removed by choosing the zero of energy at the ground state energy E_g (see figure 1.4). By introducing the *atomic lowering and raising operators*

$$\hat{\sigma}_- \equiv |g\rangle\langle e| \qquad \text{and} \qquad \hat{\sigma}_+ \equiv |e\rangle\langle g| \ , \tag{1.16}$$

we can rewrite the internal atomic Hamiltonian as follows:

Hamiltonian of a two-level atom

The internal Hamiltonian of a two-level atom with ground state energy $E_g \equiv 0$ and excited state energy E_e can be written in the Schrödinger picture as

$$H_A = \hbar\omega_A \hat{\sigma}_+ \hat{\sigma}_- \ , \tag{1.17}$$

where $\omega_A \equiv (E_e - E_g)/\hbar$ is the atomic transition frequency.

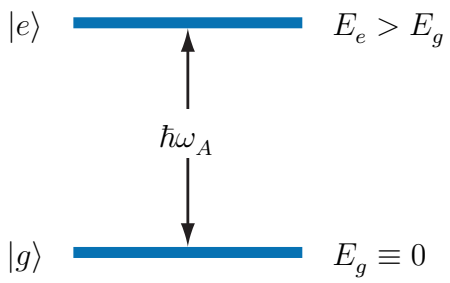

Figure 1.4 Energy level scheme of the two-level atom.

When light interacts with an atom in quantum optical systems, it is often the case that the light is resonant with a certain transition frequency of the atom. Under these circumstances only two levels of the atom play an essential role in the interaction and we can neglect all other atomic levels in our model. In these situations the two-level approximation is valid.

Two-level atom approximation

If the electromagnetic field interacting with an atom is near resonance with the atomic transition frequency between the two states $|g\rangle$ and $|e\rangle$, transitions between other states are negligible and the atom may be approximated as a two-level atom.

In the next section we discuss the interaction of light with an atom in more detail.

1.3.2 Atom-light interactions

We consider a hydrogenic atom interacting with an electromagnetic field. If the electromagnetic field is treated as a classical field represented by the vector and scalar potentials $\boldsymbol{A}$ and Φ, the Hamiltonian of such an atom-field system is

$$H = \left(\frac{[\hat{\boldsymbol{p}}_\mathrm{e} + (\mathrm{e}/c)\boldsymbol{A}(\boldsymbol{r}_\mathrm{e}, t)]^2}{2\mu} - \mathrm{e}\,\Phi(\boldsymbol{r}_\mathrm{e}, t) \right) + \hat{V} \ , \tag{1.18}$$

where μ is the *reduced mass* of the atomic nucleus and the electron, $\boldsymbol{p}_\mathrm{e}$ and $\boldsymbol{r}_\mathrm{e}$ are the momentum and position of the valence electron, respectively, c is the speed of light, and the electron charge is $-\mathrm{e}$.

For many aspects of the atom-light interaction it is sufficient to represent the light as a classical electromagnetic field. However, for the description of some phenomena such as spontaneous emission of light from an atom into a cavity mode it is necessary to quantise the electromagnetic field [24]. To achieve this, we replace the potentials in equation (1.18) by the corresponding quantum mechanical operators $\hat{\boldsymbol{A}}$ and $\hat{\Phi}$, and for a consistent quantum mechanical treatment we also add the Hamiltonian H_F of the free electromagnetic field to equation (1.18). The free Hamiltonian generates the time-dependence of the electromagnetic field such that there is no need for an explicit time-dependence of the field itself.

Multiplying out the expressions in equation (1.18) and choosing the radiation (Coulomb) gauge for a source-free field, i. e. $\Phi = 0$, we get the full Hamiltonian for a hydrogenic atom interacting with a quantised electromagnetic field in the radiation gauge,

$$H = H_0 + W \ , \tag{1.19}$$

which contains a term describing the free atom and field,

$$H_0 = H_A + H_F = \underbrace{\frac{\hat{\boldsymbol{p}}_\mathrm{e}^2}{2\mu} + \hat{V}}_{\text{atom}} + \underbrace{\sum_{\boldsymbol{k},\lambda} \hbar\omega_k \hat{b}^\dagger_{\boldsymbol{k},\lambda} \hat{b}_{\boldsymbol{k},\lambda}}_{\text{el.mag. field}} \ , \tag{1.20}$$

and an interaction term

$$W = \frac{\mathrm{e}}{2\mu c} \left(\hat{\boldsymbol{p}}_\mathrm{e} \cdot \hat{\boldsymbol{A}}(\boldsymbol{r}_\mathrm{e}) + \hat{\boldsymbol{A}}(\boldsymbol{r}_\mathrm{e}) \cdot \hat{\boldsymbol{p}}_\mathrm{e} \right) + \frac{\mathrm{e}^2}{2\mu c^2} \left(\hat{\boldsymbol{A}}(\boldsymbol{r}_\mathrm{e}) \right)^2 \tag{1.21}$$

with

$$\hat{\boldsymbol{A}}(\boldsymbol{r}) = \sum_{\boldsymbol{k},\lambda} \sqrt{\frac{2\pi\hbar c^2}{\omega_k L^3}} \left(\boldsymbol{\pi}_{\boldsymbol{k},\lambda} e^{\mathrm{i}\boldsymbol{k}\cdot\boldsymbol{r}} \hat{b}_{\boldsymbol{k},\lambda} + \boldsymbol{\pi}^*_{\boldsymbol{k},\lambda} e^{-\mathrm{i}\boldsymbol{k}\cdot\boldsymbol{r}} \hat{b}^\dagger_{\boldsymbol{k},\lambda} \right) \ , \tag{1.22}$$

where $\boldsymbol{\pi}_{\boldsymbol{k},\lambda}$ is the complex polarisation vector of the electromagnetic field mode with wavevector $\boldsymbol{k}$, polarisation state λ and frequency ω_k.

When modelling quantum optical experiments there are often several approximations allowed to simplify the interaction Hamiltonian.

The interaction Hamiltonian (1.21) contains both linear and quadratic terms in the vector potential. The quadratic term represents two-photon processes that may be neglected in the spirit of first-order perturbation theory.

One-photon interaction

We neglect terms in the interaction Hamiltonian involving $\hat{\boldsymbol{A}}^2$. They refer to two-photon processes and are much smaller than the others.

It is usually the case in quantum optical experiments that the wavelength of the electromagnetic field interacting with the atom is much larger than the size of the atom itself. Thus, if we label the position of the atom with $\boldsymbol{r}_A$ we can approximate the exponentials in the vector potential (1.22) by:

$$\begin{aligned} e^{\pm \mathrm{i}\boldsymbol{k}\cdot\boldsymbol{r}_e} &= e^{\pm \mathrm{i}\boldsymbol{k}\cdot(\boldsymbol{r}_A+(\boldsymbol{r}_e-\boldsymbol{r}_A))} \\ &= e^{\pm \mathrm{i}\boldsymbol{k}\cdot\boldsymbol{r}_A}\left(1 \pm 2\pi\mathrm{i}\frac{|\boldsymbol{r}_e-\boldsymbol{r}_A|}{2\pi/|\boldsymbol{k}|}\frac{\boldsymbol{k}\cdot(\boldsymbol{r}_e-\boldsymbol{r}_A)}{|\boldsymbol{k}||\boldsymbol{r}_e-\boldsymbol{r}_A|} - \cdots\right) \\ &\approx e^{\pm \mathrm{i}\boldsymbol{k}\cdot\boldsymbol{r}_A} \ . \end{aligned} \tag{1.23}$$

This is known as the dipole approximation, and it will become clearer why this name is appropriate later on this subsection.

Dipole approximation

If the wavelengths $2\pi/|\boldsymbol{k}|$ of the electromagnetic field are much larger than the size of the atom, i. e.

$$\frac{2\pi}{|\boldsymbol{k}|} \gg |\boldsymbol{r}_e - \boldsymbol{r}_A| \ , \tag{1.24}$$

we can evaluate the electromagnetic field at the position $\boldsymbol{r}_A$ of the the atom instead of the position $\boldsymbol{r}_e$ of the electron.

Applying these approximations, the interaction Hamiltonian (1.21) can be written more compactly as

$$W = \frac{\mathrm{e}}{\mu c}\sum_{\boldsymbol{k},\lambda}\sqrt{\frac{2\pi\hbar c^2}{\omega_k L^3}}\ \hat{\boldsymbol{p}}_\mathrm{e}\cdot\left(\boldsymbol{\pi}_{\boldsymbol{k},\lambda}e^{\mathrm{i}\boldsymbol{k}\cdot\boldsymbol{r}_A}\hat{b}_{\boldsymbol{k},\lambda} + \boldsymbol{\pi}^*_{\boldsymbol{k},\lambda}e^{-\mathrm{i}\boldsymbol{k}\cdot\boldsymbol{r}_A}\hat{b}^\dagger_{\boldsymbol{k},\lambda}\right) \ . \tag{1.25}$$

Furthermore, we can express the momentum in terms of position,

$$\hat{\boldsymbol{p}}_{\mathrm{e}} = \frac{\mu}{\mathrm{i}\hbar}\left[\hat{\boldsymbol{r}}_{\mathrm{e}}, H_A\right], \tag{1.26}$$

where $\dot{\hat{\boldsymbol{r}}}_{\mathrm{e}} = \hat{\boldsymbol{p}}_{\mathrm{e}}/\mu$ is substituted into Heisenberg's equation of motion. Combining equation (1.26) with the two-level approximation we get

$$\begin{aligned}
\hat{\boldsymbol{p}}_{\mathrm{e}} &= \sum_{\alpha=g,e}\sum_{\alpha'=g,e}\left(|\alpha\rangle\langle\alpha|\hat{\boldsymbol{p}}_{\mathrm{e}}|\alpha'\rangle\langle\alpha'|\right) \\
&= \langle g|\hat{\boldsymbol{p}}_{\mathrm{e}}|g\rangle\ |g\rangle\langle g| + \langle e|\hat{\boldsymbol{p}}_{\mathrm{e}}|e\rangle\ |e\rangle\langle e| + \langle g|\hat{\boldsymbol{p}}_{\mathrm{e}}|e\rangle\ |g\rangle\langle e| + \langle e|\hat{\boldsymbol{p}}_{\mathrm{e}}|g\rangle\ |e\rangle\langle g| \\
&= -\mathrm{i}\mu\omega_A\big(\langle g|\hat{\boldsymbol{r}}_{\mathrm{e}}|e\rangle\ |g\rangle\langle e| - \langle e|\hat{\boldsymbol{r}}_{\mathrm{e}}|g\rangle\ |e\rangle\langle g|\big) \\
&= \frac{\mathrm{i}\mu\omega_A}{\mathrm{e}}\big(\boldsymbol{d}_{ge}\ \hat{\sigma}_- - \boldsymbol{d}^*_{ge}\ \hat{\sigma}_+\big)\ ,
\end{aligned} \tag{1.27}$$

where we have defined the *atomic dipole matrix element* $\boldsymbol{d}_{ge} \equiv -\mathrm{e}\langle g|\hat{\boldsymbol{r}}_{\mathrm{e}}|e\rangle$. Substituting equation (1.27) in (1.25) the interaction part of the Hamiltonian reads as

$$W = \mathrm{i}\hbar\sum_{\boldsymbol{k},\lambda}\sqrt{\frac{2\pi\omega_A^2}{\hbar\omega_k L^3}}\ \left(\boldsymbol{d}_{ge}\hat{\sigma}_- - \boldsymbol{d}^*_{ge}\hat{\sigma}_+\right)\cdot\left(\boldsymbol{\pi}_{\boldsymbol{k},\lambda}e^{\mathrm{i}\boldsymbol{k}\cdot\boldsymbol{r}_A}\hat{b}_{\boldsymbol{k},\lambda} + \boldsymbol{\pi}^*_{\boldsymbol{k},\lambda}e^{-\mathrm{i}\boldsymbol{k}\cdot\boldsymbol{r}_A}\hat{b}^\dagger_{\boldsymbol{k},\lambda}\right)\ . \tag{1.28}$$

Note 1.2 Now it is clear why the name 'dipole approximation' has been chosen. The interaction between light of optical frequency and the atom is essentially via the dipole moment of the atom. ◀

For a further approximation we transform into the Dirac picture (see Appendix):

$$\tilde{b}_{\boldsymbol{k},\lambda} = e^{-\frac{1}{\mathrm{i}\hbar}\hat{H}_0 t}\hat{b}_{\boldsymbol{k},\lambda}e^{\frac{1}{\mathrm{i}\hbar}\hat{H}_0 t} = \hat{b}_{\boldsymbol{k},\lambda}e^{-\mathrm{i}\omega_k t}\ , \tag{1.29a}$$

$$\tilde{b}^\dagger_{\boldsymbol{k},\lambda} = e^{\frac{1}{\mathrm{i}\hbar}\hat{H}_0 t}\hat{b}^\dagger_{\boldsymbol{k},\lambda}e^{-\frac{1}{\mathrm{i}\hbar}\hat{H}_0 t} = \hat{b}^\dagger_{\boldsymbol{k},\lambda}e^{\mathrm{i}\omega_k t}\ , \tag{1.29b}$$

$$\tilde{\sigma}_- = e^{-\frac{1}{\mathrm{i}\hbar}\hat{H}_0 t}\hat{\sigma}_- e^{\frac{1}{\mathrm{i}\hbar}\hat{H}_0 t} = \hat{\sigma}_- e^{-\mathrm{i}\omega_A t}\ , \tag{1.29c}$$

$$\tilde{\sigma}_+ = e^{\frac{1}{\mathrm{i}\hbar}\hat{H}_0 t}\hat{\sigma}_+ e^{-\frac{1}{\mathrm{i}\hbar}\hat{H}_0 t} = \hat{\sigma}_+ e^{\mathrm{i}\omega_A t}\ , \tag{1.29d}$$

where we have used the commutation relations

$$\left[\hat{b}_{\boldsymbol{k},\lambda}, \hat{\sigma}_+\hat{\sigma}_-\right] = \left[\hat{b}^\dagger_{\boldsymbol{k},\lambda}, \hat{\sigma}_+\hat{\sigma}_-\right] = 0\ , \tag{1.30a}$$

$$\left[\hat{b}_{\boldsymbol{k},\lambda}, \hat{b}^\dagger_{\boldsymbol{k}',\lambda'}\right] = \delta_{\boldsymbol{k}\lambda,\boldsymbol{k}'\lambda'}\ , \qquad \left[\hat{\sigma}_\pm, \hat{\sigma}_+\hat{\sigma}_-\right] = \mp 2\hat{\sigma}_\pm\ . \tag{1.30b}$$

By transforming equation (1.28), we find the Hamiltonian in the interaction picture

$$\begin{aligned}
\tilde{W}(t) \equiv \mathrm{i}\hbar\sum_{\boldsymbol{k},\lambda}\sqrt{\frac{2\pi\omega_A^2}{\hbar\omega_k L^3}}\Big(&\boldsymbol{d}_{ge}\tilde{\sigma}_-\cdot\boldsymbol{\pi}_{\boldsymbol{k},\lambda}\tilde{b}_{\boldsymbol{k},\lambda}e^{-\mathrm{i}\left(2\omega_A t + \Delta\omega_k t - \boldsymbol{k}\cdot\boldsymbol{r}_A\right)} \\
&+ \boldsymbol{d}_{ge}\tilde{\sigma}_-\cdot\boldsymbol{\pi}^*_{\boldsymbol{k},\lambda}\tilde{b}^\dagger_{\boldsymbol{k},\lambda}e^{\mathrm{i}(\Delta\omega_k t - \boldsymbol{k}\cdot\boldsymbol{r}_A)} \\
&- \boldsymbol{d}^*_{ge}\tilde{\sigma}_+\cdot\boldsymbol{\pi}_{\boldsymbol{k},\lambda}\tilde{b}_{\boldsymbol{k},\lambda}e^{-\mathrm{i}(\Delta\omega_k t - \boldsymbol{k}\cdot\boldsymbol{r}_A)} \\
&- \boldsymbol{d}^*_{ge}\tilde{\sigma}_+\cdot\boldsymbol{\pi}^*_{\boldsymbol{k},\lambda}\tilde{b}^\dagger_{\boldsymbol{k},\lambda}e^{\mathrm{i}\left(2\omega_A t + \Delta\omega_k t - \boldsymbol{k}\cdot\boldsymbol{r}_A\right)}\Big)\ ,
\end{aligned} \tag{1.31}$$

where $\Delta\omega_k \equiv \omega_k - \omega_A$ is the detuning between the frequency of the electromagnetic field mode and the atomic resonance frequency.

Typically, an integration with $\tilde{W}(t)$ inside the integrand is involved when finding the time-evolution of the system. Since rapidly oscillating terms average out over time when integrating much longer than the oscillation period, this allows an approximation that is commonly used when describing quantum optical systems:

Rotating-wave approximation

If the atomic resonance frequency is in the optical regime ($\omega_A \approx 10^{15}\,\mathrm{Hz}$) and the field is near resonant ($\Delta\omega_k \lessapprox 10^9\,\mathrm{Hz}$), we can neglect the rapidly oscillating terms in the interaction Hamiltonian (1.31), i. e. terms involving $e^{\pm 2\mathrm{i}\omega_A t}$.

Adopting this approximation and also assuming $\omega_A \approx \omega_k$, we find

$$\begin{aligned}\tilde{W}(t) = \mathrm{i}\hbar \sum_{\boldsymbol{k},\lambda} \sqrt{\frac{2\pi\omega_k}{\hbar L^3}} \Big(& \boldsymbol{d}_{ge}\tilde{\sigma}_- \cdot \boldsymbol{\pi}^*_{\boldsymbol{k},\lambda} \tilde{b}^\dagger_{\boldsymbol{k},\lambda} e^{\mathrm{i}(\Delta\omega_k t - \boldsymbol{k}\cdot\boldsymbol{r}_A)} \\ & - \boldsymbol{d}^*_{ge}\tilde{\sigma}_+ \cdot \boldsymbol{\pi}_{\boldsymbol{k},\lambda} \tilde{b}_{\boldsymbol{k},\lambda} e^{-\mathrm{i}(\Delta\omega_k t - \boldsymbol{k}\cdot\boldsymbol{r}_A)} \Big) .\end{aligned} \tag{1.32}$$

Finally, we transform back into the Schrödinger picture.

Hamiltonian for a hydrogenic atom in a near resonant field

In the Schrödinger picture the Hamiltonian for a hydrogenic atom in the two-level approximation interacting with a near resonant field can be written in the rotating-wave and dipole approximations as

$$H = H_0 + W \tag{1.33}$$

with free Hamiltonian

$$H_0 = \hbar\omega_A \hat{\sigma}_+ \hat{\sigma}_- + \sum_{\boldsymbol{k},\lambda} \hbar\omega_k \hat{b}^\dagger_{\boldsymbol{k},\lambda} \hat{b}_{\boldsymbol{k},\lambda} \tag{1.34}$$

and interaction Hamiltonian

$$W = \mathrm{i}\hbar \sum_{\boldsymbol{k},\lambda} \left(g^*_{\boldsymbol{k},\lambda} \hat{b}^\dagger_{\boldsymbol{k},\lambda} \hat{\sigma}_- - g_{\boldsymbol{k},\lambda} \hat{b}_{\boldsymbol{k},\lambda} \hat{\sigma}_+ \right) , \tag{1.35}$$

where

$$g_{\boldsymbol{k},\lambda} = e^{-\mathrm{i}\boldsymbol{k}\cdot\boldsymbol{r}_A} \sqrt{\frac{2\pi\omega_k}{\hbar L^3}}\ \boldsymbol{\pi}_{\boldsymbol{k},\lambda} \cdot \boldsymbol{d}^*_{ge} \tag{1.36}$$

is the dipole coupling constant between the $(\boldsymbol{k},\lambda)$-mode and the atom.

Note 1.3 It is quite common to absorb the complex phase of the coupling constant into the definitions of the field and atomic operators to get a real coupling constant

$$g_{\boldsymbol{k},\lambda} = \sqrt{\frac{2\pi\omega_k}{\hbar L^3}}\, |\boldsymbol{\pi}_{\boldsymbol{k},\lambda} \cdot \boldsymbol{d}^*_{ge}| \ . \tag{1.37}$$

◀

1.3.3 Selection rules for electric dipole transitions in one-electron atoms

So far we have restricted all our derivations to a one-electron two-level atom. We now want to take into account that these two levels may each contain degenerate sub-levels. If so, the question arises as to how light interacts with the sub-levels of the multiplet, and especially how the relative strengths of transitions within the multiplet are determined.

Starting with Fermi's golden rule we will deduce selection rules. This rule describes which transitions we have to take into account and what the relative strengths of the transitions are. Our derivation of the selection rules partly follows reference [23].

Fermi's golden rule

Fermi's golden rule is the central result of first-order time-dependent perturbation theory for transitions of a quantum system into a continuous spectrum of final states with density $\rho(E_\mathrm{f})$, where E_f is the energy of the final state. The derivation of Fermi's golden rule can be found in reference [25].

Fermi's golden rule

The probability per unit time for a transition of a quantum system from an initial state $|\phi_\mathrm{i}\rangle$ with energy E_i to a final state $|\phi_\mathrm{f}\rangle$ with energy E_f, due to a perturbation W is

$$P_{\mathrm{i}\to\mathrm{f}} = \frac{2\pi}{\hbar} \left|\langle\phi_\mathrm{f}|W|\phi_\mathrm{i}\rangle\right|^2 \rho\left(E_\mathrm{i}\right) \ , \tag{1.38}$$

where $|\phi_\mathrm{i}\rangle$ and $|\phi_\mathrm{f}\rangle$ are eigenstates of the unperturbed system.

The main quantity characterising the strength of transitions between states is thus the matrix element

$$W_\mathrm{fi} \equiv \langle\phi_\mathrm{f}|W|\phi_\mathrm{i}\rangle \ . \tag{1.39}$$

In the case of atomic transitions induced by absorbing or emitting photons, the momenta of the photons vary continuously. Therefore, if we assume that the interaction between the atom and the electromagnetic field can be regarded as a small perturbation, Fermi's golden rule can be applied. 'Small' perturbation means that we look at

transitions in which only one photon is absorbed or emitted at a time. Transitions in which several photons are absorbed or emitted simultaneously occur, and become important, only when an atom interacts with a very strong electromagnetic field.

For a one-photon interaction between a one-electron atom (not in the two-level approximation) and a field, we use the interaction Hamiltonian (1.25)—but instead of the summation over all modes we keep only the term for one mode $(\boldsymbol{k}, \lambda)$—as the perturbing interaction to calculate the matrix elements

$$W_{\mathrm{fi}} = \frac{\mathrm{e}}{\mu c}\sqrt{\frac{2\pi\hbar c^2}{\omega_k L^3}}\left(\langle\Phi_{\mathrm{f}}|\hat{\boldsymbol{p}}_{\mathrm{e}}\cdot\boldsymbol{\pi}_{\boldsymbol{k},\lambda}e^{\mathrm{i}\boldsymbol{k}\cdot\boldsymbol{r}_A}|\Phi_{\mathrm{i}}\rangle F^{\mathrm{abs}}_{\boldsymbol{k},\lambda} + \langle\Phi_{\mathrm{f}}|\hat{\boldsymbol{p}}_{\mathrm{e}}\cdot\boldsymbol{\pi}^*_{\boldsymbol{k},\lambda}e^{-\mathrm{i}\boldsymbol{k}\cdot\boldsymbol{r}_A}|\Phi_{\mathrm{i}}\rangle F^{\mathrm{em}}_{\boldsymbol{k},\lambda}\right), \quad (1.40)$$

where the initial and final states have been written as a product of an atomic state $|\Phi_{\mathrm{i}}\rangle$ and $|\Phi_{\mathrm{f}}\rangle$ with respective eigenvalues ε_{i} and ε_{f} of H_A, and a field state $|n_{\boldsymbol{k},\lambda,\mathrm{i}}\rangle$ and $|n_{\boldsymbol{k},\lambda,\mathrm{f}}\rangle$ of the mode $(\boldsymbol{k}, \lambda)$,

$$|\phi_{\mathrm{i}}\rangle \equiv |\Phi_{\mathrm{i}}\rangle|n_{\boldsymbol{k},\lambda,\mathrm{i}}\rangle\ , \qquad |\phi_{\mathrm{f}}\rangle \equiv |\Phi_{\mathrm{f}}\rangle|n_{\boldsymbol{k},\lambda,\mathrm{f}}\rangle\ , \quad (1.41)$$

while

$$F^{\mathrm{abs}}_{\boldsymbol{k},\lambda} \equiv \langle n_{\boldsymbol{k},\lambda,\mathrm{f}}|b_{\boldsymbol{k},\lambda}|n_{\boldsymbol{k},\lambda,\mathrm{i}}\rangle\ , \qquad F^{\mathrm{em}}_{\boldsymbol{k},\lambda} \equiv \langle n_{\boldsymbol{k},\lambda,\mathrm{f}}|b^\dagger_{\boldsymbol{k},\lambda}|n_{\boldsymbol{k},\lambda,\mathrm{i}}\rangle \quad (1.42)$$

stand for the field contribution to the transition matrix element. Note that $F^{\mathrm{abs}}_{\boldsymbol{k},\lambda}$ is non-zero only if $n_{\boldsymbol{k},\lambda,\mathrm{f}} = n_{\boldsymbol{k},\lambda,\mathrm{i}} - 1$ and $F^{\mathrm{em}}_{\boldsymbol{k},\lambda}$ is non-zero only if $n_{\boldsymbol{k},\lambda,\mathrm{f}} = n_{\boldsymbol{k},\lambda,\mathrm{i}} + 1$. The energies of the initial and final state can be written as

$$E_{\mathrm{i}} = \varepsilon_{\mathrm{i}} + n_{\boldsymbol{k},\lambda,\mathrm{i}}\hbar\omega_k + \text{energy of all other modes}, \quad (1.43a)$$
$$E_{\mathrm{f}} = \varepsilon_{\mathrm{f}} + n_{\boldsymbol{k},\lambda,\mathrm{f}}\hbar\omega_k + \text{energy of all other modes}, \quad (1.43b)$$

and energy conservation, $E_{\mathrm{i}} = E_{\mathrm{f}}$, requires

$$\varepsilon_{\mathrm{f}} - \varepsilon_{\mathrm{i}} = \left(n_{\boldsymbol{k},\lambda,\mathrm{i}} - n_{\boldsymbol{k},\lambda,\mathrm{f}}\right)\hbar\omega_k\ . \quad (1.44)$$

Together with equation (1.26) we get

$$P_{\mathrm{i}\to\mathrm{f}} = 4\pi^2\frac{c}{L^3}\frac{\mathrm{e}^2}{\hbar c}\hbar\omega_k\left|\boldsymbol{r}_{\mathrm{fi}}\cdot\boldsymbol{\pi}_{\boldsymbol{k},\lambda}e^{\mathrm{i}\boldsymbol{k}\cdot\boldsymbol{r}_A}F^{\mathrm{abs}}_{\boldsymbol{k},\lambda} + \boldsymbol{r}_{\mathrm{fi}}\cdot\boldsymbol{\pi}^*_{\boldsymbol{k},\lambda}e^{-\mathrm{i}\boldsymbol{k}\cdot\boldsymbol{r}_A}F^{\mathrm{em}}_{\boldsymbol{k},\lambda}\right|^2\rho\left(E_{\mathrm{i}}\right) \quad (1.45)$$

where we have defined the *atomic matrix element*

$$\boldsymbol{r}_{\mathrm{fi}} = \langle\Phi_{\mathrm{f}}|\boldsymbol{r}_{\mathrm{e}}|\Phi_{\mathrm{i}}\rangle\ . \quad (1.46)$$

Note that the dimensionless constant $\mathrm{e}^2/(\hbar c) \approx 1/137$ in equation (1.45), which is called the fine-structure constant, characterises the strength of electromagnetic interactions.

The selection rules

The selection rules are based on the observation that the interaction W induces no transition between the states $|\phi_\mathrm{i}\rangle$ and $|\phi_\mathrm{f}\rangle$ if the matrix element $\langle\phi_\mathrm{f}|W|\phi_\mathrm{i}\rangle$ vanishes. Transitions with vanishing matrix element are called *forbidden* in the W-interaction (e. g. the electric dipole interaction), but may occur due to another interaction (the magnetic dipole or electric quadrupole interaction, for example).

The electromagnetic transition probability depends on the atomic matrix element (1.46). Since the electron wavefunction of an atom involves spherical harmonics, it is convenient to evaluate the vector operator $\boldsymbol{r}_\mathrm{e} \equiv (x_\mathrm{e}, y_\mathrm{e}, z_\mathrm{e})$ inside this matrix element via its *spherical vector components* defined as

$$r_{\pm1} \equiv \frac{\mp1}{\sqrt{2}}(x_\mathrm{e} \pm \mathrm{i}y_\mathrm{e}) \ , \qquad\qquad r_0 \equiv z_\mathrm{e} \ . \tag{1.47}$$

The advantage is that for the angular-momentum state matrix elements of the spherical vector components of any vector, one can find a factorisation of a particular practical form. This is stated in one of the most important theorems in quantum mechanics [26, 27]:

Wigner-Eckart Theorem

The matrix elements of a spherical tensor operator $T_q^{(k)}$ (of rank k with $2k+1$ components $\{q\}$) with respect to angular-momentum eigenstates $|j_\mathrm{i}m_\mathrm{i}\rangle$ satisfy

$$\langle j_\mathrm{f}m_\mathrm{f}|T_q^{(k)}|j_\mathrm{i}m_\mathrm{i}\rangle = \langle j_\mathrm{f}m_\mathrm{f}|j_\mathrm{i}m_\mathrm{i};k,q\rangle\langle j_\mathrm{f}||T^{(k)}||j_\mathrm{i}\rangle \ , \tag{1.48}$$

where $\langle j_\mathrm{f}m_\mathrm{f}|j_\mathrm{i}m_\mathrm{i};k,q\rangle$ is a Clebsch-Gordan coefficient.

A proof of this theorem can be found in [25]. For us it is important that the left hand side of equation (1.48) factorises into two parts, one term that does not depend on m_i, m_f and q, and a Clebsch-Gordan coefficient that contains all the dependence on these parameters. Thus, we can determine selection rules based on the well-known properties of the Clebsch-Gordan coefficients.

Fine structure If we neglect for the moment the atomic nuclear spin, the angular-momentum eigenstates can be labelled with the quantum numbers j and m, i. e.

$$|\Phi_\mathrm{i}\rangle = |j_\mathrm{i}m_\mathrm{i}\rangle \ , \qquad\qquad |\Phi_\mathrm{f}\rangle = |j_\mathrm{f}m_\mathrm{f}\rangle \ . \tag{1.49}$$

In the language of spherical tensors the vector operator $\boldsymbol{r}_\mathrm{e}$ is of rank one, and hence the Wigner-Eckart theorem gives us

$$\langle j_\mathrm{f}m_\mathrm{f}|r_q|j_\mathrm{i}m_\mathrm{i}\rangle = \langle j_\mathrm{f}m_\mathrm{f}|j_\mathrm{i}m_\mathrm{i};1,q\rangle\langle j_\mathrm{f}||\boldsymbol{r}_\mathrm{e}||j_\mathrm{i}\rangle \ , \tag{1.50}$$

with $q = -1, 0, 1$. This has a clear interpretation when thinking in terms of adding angular momentum. The Clebsch-Gordan coefficients are identical to those that couple the initial atom angular-momentum state $|j_\mathrm{i}, m_\mathrm{i}\rangle$ and the photon angular-momentum $k = j_\mathrm{Photon} = 1$ with $q = m_\mathrm{Photon} = -1, 0, 1$ to the final atom-angular momentum state $|j_\mathrm{f}, m_\mathrm{f}\rangle$. Thus, allowed transitions are those with non-vanishing Clebsch-Gordan coefficients $\langle j_\mathrm{f} m_\mathrm{f} | j_\mathrm{i} m_\mathrm{i}; 1, \nu\rangle$.

Selection rules for fine structure

The selection rules for electromagnetic dipole transitions for the fine structure are

$$m_\mathrm{f} - m_\mathrm{i} = -1, 0, +1 \ , \tag{1.51a}$$
$$j_\mathrm{f} - j_\mathrm{i} = -1, 0, +1 \tag{1.51b}$$

as the allowed transitions, but

$$j_\mathrm{i} = 0 \to j_\mathrm{f} = 0 \quad \text{and} \tag{1.51c}$$
$$m_\mathrm{i} = 0 \to m_\mathrm{f} = 0 \ , \quad j_\mathrm{f} - j_\mathrm{i} = 0 \tag{1.51d}$$

are forbidden.

Hyperfine structure If we include the atomic nucleus spin, the angular-momentum eigenstates can be labelled with the quantum numbers F (for the total angular momentum) and m_F, i. e.

$$|\Phi_\mathrm{i}\rangle = |F_\mathrm{i} m_{F,\mathrm{i}}\rangle \ , \qquad |\Phi_\mathrm{f}\rangle = |F_\mathrm{f} m_{F,\mathrm{f}}\rangle \ , \tag{1.52}$$

and the Wigner-Eckart theorem reads as

$$\langle F_\mathrm{f} m_{F,\mathrm{f}} | r_\nu | F_\mathrm{i} m_{F,\mathrm{i}}\rangle = \langle F_\mathrm{f} m_{F,\mathrm{f}} | F_\mathrm{i} m_{F,\mathrm{i}}; 1, \nu\rangle \langle F_\mathrm{f} || \boldsymbol{r}_\mathrm{e} || F_\mathrm{i}\rangle \ , \tag{1.53}$$

with $\nu = -1, 0, 1$. Thus, the resulting selection rules are similar to those of the fine structure.

Selection rules for hyperfine structure

The selection rules for electromagnetic dipole transitions for the hyperfine structure are

$$m_{F,\mathrm{f}} - m_{F,\mathrm{i}} = -1, 0, +1 \ , \tag{1.54a}$$
$$F_\mathrm{f} - F_\mathrm{i} = -1, 0, +1 \ , \tag{1.54b}$$

as the allowed transitions, but

$$F_\mathrm{i} = 0 \to F_\mathrm{f} = 0 \quad \text{and} \tag{1.54c}$$
$$m_{F,\mathrm{i}} = 0 \to m_{F,\mathrm{f}} = 0 \ , \quad F_\mathrm{f} - F_\mathrm{i} = 0 \tag{1.54d}$$

are forbidden.

Example. Figure 1.5 shows the allowed electric dipole transitions for an $F = 3$ to $F' = 4$ transition of the D_2-line of a ^{85}Rb-atom ($I = 5/2$).

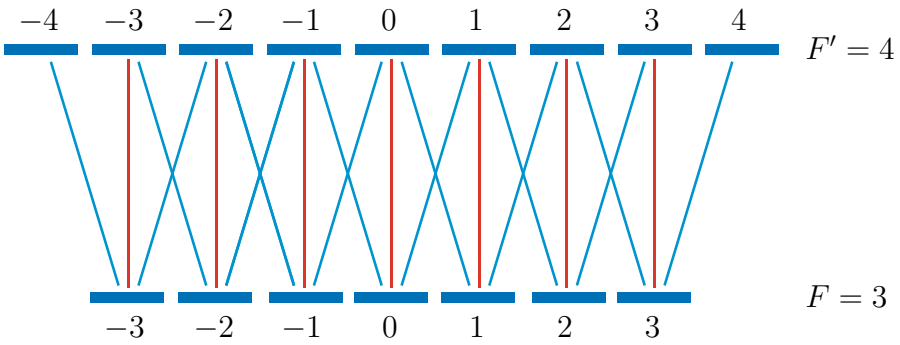

Figure 1.5 Atomic level structure and allowed electromagnetic dipole transitions for an $F = 3$ to $F' = 4$ transition. The relative transition strengths are determined by the appropriate Clebsch-Gordan coefficients. The colour coding refers to the two-mode cavity QED set-up described in section 1.1: the driven mode interacts with the atom via $\Delta m_F = 0$ transitions, and the non-driven mode via $\Delta m_F = \pm 1$ transitions.

Having described the interaction of light with an atom, the next step toward the description of our atom-cavity system is the interaction between the cavity field and the driving laser.

1.3.4 Cavity-laser interactions

The interaction of a driving laser with a cavity is a fairly complicated process. The incoming laser light is transmitted and reflected on the many layers of the cavity mirrors.

A coherent driving laser is described by a classical electromagnetic field represented by the vector potential

$$\boldsymbol{A}(\boldsymbol{r}, t) = \boldsymbol{\pi} \frac{c\mathcal{E}_0}{\omega_L} \sin(\omega_L t - \boldsymbol{k} \cdot \boldsymbol{r} + \phi) \ , \tag{1.55}$$

where $\boldsymbol{\pi}$ is the complex polarisation vector, and $\mathcal{E}_0$ the amplitude of the electric field. When this laser interacts with the cavity via the cavity mirror, the mirror is fixed in space over the whole interaction time, and we can absorb the (constant) spatial dependence into the phase:

$$\boldsymbol{A}(t) = \boldsymbol{\pi} \frac{c\mathcal{E}_0}{\omega_L} \sin(\omega_L t + \phi_0) \ . \tag{1.56}$$

The Hamiltonian for a coherently driven cavity is

$$H = H_0 + W_{LC} \quad , \tag{1.57}$$

with a free part for the quantised cavity mode

$$H_0 = \hbar\omega_a \hat{a}^\dagger \hat{a} \quad , \tag{1.58}$$

and an interaction part W_{LC}. If the laser frequency ω_L is near resonance with a cavity mode a of frequency ω_a, i. e. $\omega_L \approx \omega_a$, the atom-cavity interaction is well approximated by a linear coupling that is characterised by the coupling constant ε between the laser field and this driven cavity mode:

$$\hat{W}_{LC} = \varepsilon \frac{\mathrm{i}c\mathcal{E}_0}{2\omega_L} \left(\boldsymbol{\pi} e^{-\mathrm{i}\omega_L t - \mathrm{i}\phi_0} - \boldsymbol{\pi}^* e^{\mathrm{i}\omega_L t + \mathrm{i}\phi_0}\right) \cdot \sqrt{\frac{2\pi\hbar c^2}{\omega_a V}} \left(\boldsymbol{\pi} e^{\mathrm{i}\varphi_0} \hat{a} + \boldsymbol{\pi}^* e^{-\mathrm{i}\varphi_0} \hat{a}^\dagger\right) \ , \tag{1.59}$$

where we have assumed that the driving laser only interacts with a cavity mode with the same polarisation; the phase ϕ_0 includes the constant spatial dependence of the cavity mode at the cavity mirror. In the rotating-wave approximation this Hamiltonian becomes

$$\hat{W}_{LC} = \mathrm{i}\varepsilon \frac{c\mathcal{E}_0}{2\omega_L} \sqrt{\frac{2\pi\hbar c^2}{\omega_a V}} \left(\hat{a}^\dagger e^{-\mathrm{i}\omega_L t - \mathrm{i}\varphi} + \hat{a} e^{\mathrm{i}\omega_L t + \mathrm{i}\varphi}\right) \ , \tag{1.60}$$

where we have used the fact that $\boldsymbol{\pi}^* \cdot \boldsymbol{\pi} = 1$. The phase $\varphi \equiv \phi_0 - \varphi_0$ is arbitrary and can be absorbed into the definition of the ladder operator.

Hamiltonian of a coherently driven cavity mode

The Hamiltonian of a classical laser interacting near resonance with a cavity mode a can be written in the Schrödinger picture as

$$H = H_0 + W_{LC} \ , \tag{1.61}$$

with a free part for the quantised cavity mode

$$H_0 = \hbar\omega_a \hat{a}^\dagger \hat{a} \ , \tag{1.62}$$

and an interaction part

$$W_{LC} = \mathrm{i}\hbar\mathcal{E} \left(\hat{a}^\dagger e^{-\mathrm{i}\hbar\omega_L t} - \hat{a} e^{\mathrm{i}\hbar\omega_L t}\right) \ , \tag{1.63}$$

with

$$\mathcal{E} \equiv \varepsilon \frac{c\mathcal{E}_0}{2\omega_L} \sqrt{\frac{2\pi c^2}{\hbar\omega_a V}} \ . \tag{1.64}$$

In the next section we bring together the acquired knowledge to describe a driven atom-cavity system.

1.4 Hamiltonian of a driven single-atom two-mode cavity system

With the background theory provided in the previous sections we are now able to develop a first model of the atom-cavity system that we introduced at the beginning of this chapter. In this thesis we investigate in fact two models that differ in the way that the atomic states of the $F = 3$ to $F' = 4$ transition are taken into account.

In a simple model we reduce the degeneracy such that we are left with a (non-degenerate) two-level atom. The Zeeman substructure is only reflected in different coupling constants between the atom and the two modes, which gives consideration to the various Clebsch-Gordan coefficients.

In a second, more realistic, model we take the Zeeman sublevels explicitly into account and look at the full level scheme of the dipole transition.

1.4.1 Non-degenerate two-level atom

Assuming that the two levels of the atom are non-degenerate and the atom couples to both cavity modes, the Hamiltonian of this system can be written as

$$H = H_0 + W \ , \tag{1.65}$$

with a free part H_0 for the two cavity modes and the atom,

$$H_0 = \hbar\omega_a \hat{a}^\dagger \hat{a} + \hbar\omega_b \hat{b}^\dagger \hat{b} + \hbar\omega_A \hat{\sigma}_+ \hat{\sigma}_- \ , \tag{1.66}$$

and an interaction part,

$$\begin{aligned} W = {} & \mathrm{i}\hbar\mathcal{E}\left(\hat{a}^\dagger e^{-\mathrm{i}\omega_L t} - \hat{a} e^{\mathrm{i}\omega_L t}\right) \\ & + \mathrm{i}\hbar g_a \left(\hat{a}^\dagger \hat{\sigma}_- - \hat{a}\hat{\sigma}_+\right) + \mathrm{i}\hbar g_b \left(\hat{b}^\dagger \hat{\sigma}_- - \hat{b}\hat{\sigma}_+\right) \ , \end{aligned} \tag{1.67}$$

where g_a and g_b are the coupling constants between the atom and the two cavity modes.

In a frame rotating at the laser frequency the Hamiltonian becomes

$$\begin{aligned} H = {} & \hbar\left(\omega_A - \omega_L\right)\hat{\sigma}_+\hat{\sigma}_- + \hbar\left(\omega_a - \omega_L\right)\hat{a}^\dagger\hat{a} + \hbar\left(\omega_b - \omega_L\right)\hat{b}^\dagger\hat{b} \\ & + \mathrm{i}\hbar\mathcal{E}\left(\hat{a}^\dagger - \hat{a}\right) + \mathrm{i}\hbar g_a \left(\hat{a}^\dagger\hat{\sigma}_- - \hat{a}\hat{\sigma}_+\right) + \mathrm{i}\hbar g_b \left(\hat{b}^\dagger\hat{\sigma}_- - \hat{b}\hat{\sigma}_+\right) \ . \end{aligned} \tag{1.68}$$

This simplifies if all frequencies are resonant, i. e. $\omega_L = \omega_a = \omega_b = \omega_A$:

Hamiltonian of a driven single-atom two-mode cavity system with a non-degenerate two-level atom

For a driven single-atom two-mode cavity system, where a non-degenerate two-level atom interacts resonantly with the two cavity modes, the system Hamiltonian in

the dipole and rotating-wave approximations, written in a frame rotating at the laser frequency, is

$$H = \mathrm{i}\hbar\mathcal{E}\big(\hat{a}^\dagger - \hat{a}\big) + \mathrm{i}\hbar g_a\big(\hat{a}^\dagger\hat{\sigma}_- - \hat{a}\hat{\sigma}_+\big) + \mathrm{i}\hbar g_b\big(\hat{b}^\dagger\hat{\sigma}_- - \hat{b}\hat{\sigma}_+\big)\ , \tag{1.69}$$

where g_a and g_b are the coupling strengths between the atom and cavity modes a and b, respectively.

1.4.2 Two-level atom with Zeeman substructure

For a two-level atom with Zeeman substructure we assume a quantisation axis, imposed, for example, by a weak magnetic field with negligible Zeeman effect, such that the driven mode a couples the atomic ground and excited state via $\Delta m_{_F} = 0$ transitions, and the non-driven mode b couples them via $\Delta m_{_F} = \pm 1$ transitions. We denote the maximum dipole coupling strength of the atomic F to F' transition as g, and the atomic lowering and raising operators have expansions in terms of atomic states and appropriate Clebsch-Gordan coefficients.

Hamiltonian of a driven single-atom two-mode cavity system with atomic Zeeman substructure

We consider a resonant driven single-atom two-mode cavity system with atomic Zeeman substructure, where the atom interacts on resonance with the two (orthogonal) linearly-polarised cavity modes. The system Hamiltonian in the dipole and rotating-wave approximations, written in a frame rotating with laser frequency, is given by

$$\begin{aligned} H = {} & \mathrm{i}\hbar\mathcal{E}(\hat{a}^\dagger - \hat{a}) + \mathrm{i}\hbar g\big(\hat{a}^\dagger\hat{\Sigma}_0 - \hat{a}\hat{\Sigma}_0\big) \\ & + \mathrm{i}\hbar(g/\sqrt{2})\Big(\hat{b}^\dagger\big(\hat{\Sigma}_{-1} + \hat{\Sigma}_{+1}\big) - \hat{b}\big(\hat{\Sigma}^\dagger_{-1} + \hat{\Sigma}^\dagger_{+1}\big)\Big)\ , \end{aligned} \tag{1.70}$$

where g is the dipole coupling strength of the atomic $F = F_{_g}$ to $F' = F_{_e}$ transition. The atomic lowering and raising operators, $\hat{\Sigma}_{0,\pm1}$ and $\hat{\Sigma}^\dagger_{0,\pm1}$, have expansions in terms of atomic states and appropriate Clebsch-Gordan coefficients.

For atomic transitions with $F_{_g} = F_{_e} - 1$ the atomic operators can be written as:

$$\hat{\Sigma}_p \equiv \sum_{m=-3}^{3} C_{F_e,m+p,F_g,m}\ |F_g, m\rangle\langle F_e, m+p| \tag{1.71}$$

with the Clebsch-Gordan coefficients

$$C_{F_e,m_e,F_g,m_g} \equiv \big\langle F_g, m_g; 1, m_g - m_e \big| F_e, m_e\big\rangle\ . \tag{1.72}$$

In the cavity QED experiment we aim to model, the atomic transition is an $F = 3$ to $F' = 4$ transition. In this case the atomic lowering and raising operator are given by

$$\begin{aligned}\hat{\Sigma}_{-1} = {} & |g_{-3}\rangle\langle e_{-4}| + \sqrt{\frac{3}{4}}|g_{-2}\rangle\langle e_{-3}| + \sqrt{\frac{15}{28}}|g_{-1}\rangle\langle e_{-2}| + \sqrt{\frac{5}{14}}|g_0\rangle\langle e_{-1}| \\ & + \sqrt{\frac{3}{14}}|g_{+1}\rangle\langle e_0| + \sqrt{\frac{3}{28}}|g_{+2}\rangle\langle e_{+1}| + \sqrt{\frac{1}{28}}|g_{+3}\rangle\langle e_{+2}| \ ,\end{aligned} \tag{1.73a}$$

$$\begin{aligned}\hat{\Sigma}_{0} = {} & \sqrt{\frac{1}{4}}|g_{-3}\rangle\langle e_{-3}| + \sqrt{\frac{3}{7}}|g_{-2}\rangle\langle e_{-2}| + \sqrt{\frac{15}{28}}|g_{-1}\rangle\langle e_{-1}| + \sqrt{\frac{16}{28}}|g_0\rangle\langle e_0| \\ & + \sqrt{\frac{15}{28}}|g_{+1}\rangle\langle e_{+1}| + \sqrt{\frac{3}{7}}|g_{+2}\rangle\langle e_{+2}| + \sqrt{\frac{1}{4}}|g_{+3}\rangle\langle e_{+3}| \ ,\end{aligned} \tag{1.73b}$$

$$\begin{aligned}\hat{\Sigma}_{+1} = {} & \sqrt{\frac{1}{28}}|g_{-3}\rangle\langle e_{-2}| + \sqrt{\frac{3}{28}}|g_{-2}\rangle\langle e_{-1}| + \sqrt{\frac{3}{14}}|g_{-1}\rangle\langle e_0| \\ & + \sqrt{\frac{5}{14}}|g_0\rangle\langle e_{+1}| + \sqrt{\frac{15}{28}}|g_{+1}\rangle\langle e_{+2}| + \sqrt{\frac{3}{4}}|g_{+2}\rangle\langle e_{+3}| + |g_{+3}\rangle\langle e_{+4}| \ .\end{aligned} \tag{1.73c}$$

We could use the system Hamiltonian and the Schrödinger or von Neumann equation to describe the dynamics of the atom cavity system if there was not one important detail still missing. The Schrödinger and von Neumann equations describe the dynamics of a closed quantum system. But in a cavity QED experiment the detectors are outside the atom cavity system, and we detect light that leaks out through the cavity mirror. Consequently, a cavity QED system cannot be considered to be closed. In fact, the light loss through the mirror is an essential part of the experiment, and therefore, something more than the simple description of a closed quantum system is necessary. In the next chapter we present two methods that can be used to describe such open quantum systems.

Chapter 2

Open Quantum Systems

An *open quantum system* is a quantum mechanical system that interacts with an external quantum system—the environment. Since the environment is typically infinitely large, we refer it in the following as the *reservoir* R. Thus, an open quantum system S can be seen as a distinguishable part of a larger *closed quantum system* $S \otimes R$. The interaction process perturbs both S and R from their equilibrium states and induces internal fluctuations in both of them. These fluctuations are correlated on some time scale; if the interaction was switched off the fluctuations would regress and the system/reservoir would relax to equilibrium. Thus, this time scale is often referred as the *correlation time* or the *relaxation time* of the system/reservoir.

Due to the dissipative nature of an open quantum system one generally does not have complete knowledge of the system state. Therefore, the system cannot be described by a state vector but, rather, is described by its density operator. In the Schrödinger picture, state vectors and therefore also the density operator are generally time dependent. The equation of motion for the *density operator* $\chi(t)$ of the combined closed system $S \oplus R$ is described by the *von Neumann equation*,

$$\dot{\chi}(t) = \frac{1}{\mathrm{i}\hbar}\big[H_{S\otimes R}, \chi(t)\big] \ ,$$

where $H_{S\otimes R}$ is the Hamiltonian of $S \otimes R$. The complexity of the reservoir often means that it is impossible to find an exact solution of this equation.

Even if it is impossible to solve von Neumann's equation, an equation of motion for the *reduced density operator* $\rho(t)$ of S can be derived. This so-called *master equation* is in integro-differential form, and its integration kernel is still too complicated for the equation to be solved exactly. However, the advantage of the master equation is that it allows the derivation of simpler, solvable equations that adopt only a few assumptions and approximations regarding both the interaction between S and R, and the properties of R: (1) the open system and the reservoir are initially uncorrelated and the reservoir is in

equilibrium; (2) the coupling between S and R is weak enough that the contributions of interaction processes higher than second-order can be neglected (Born approximation); (3) internal correlations in R are on a much shorter time scale than the relaxation time of S (Markov approximation); (4) terms in the interaction Hamiltonian that oscillate much more rapidly than the others are neglected (Secular approximation). The resulting modified master equation is in *Lindblad form*, similar to von Neumann's equation, but with additional terms describing the relaxation of S,

$$\dot{\rho}(t) = \frac{1}{\mathrm{i}\hbar}\big[H'_S, \rho(t)\big] + \text{decay terms} \ ,$$

where H'_S is a modified system-Hamiltonian that takes into account energy shifts arising from the interaction of the system with the reservoir. The derivation of the master equation in Lindblad form is the goal in the first section of this chapter.

The content of the second section is the *quantum trajectory theory* [28]. This theory provides another means of analysing and thinking about the master equation, and is especially attractive for the numerical investigations of systems with many possible states. It lays the groundwork for simulating the master equation for the reduced density operator $\rho(t)$ of the dissipative system S in terms of system wavefunctions. Similar methods to the quantum trajectory theory were independently developed by several groups in the last decade of the 20th century [29, 30, 31]. All these methods have the foundation that the *system wavefunction* $\psi(t)$ propagates in time according to the *Schrödinger equation*,

$$|\dot{\psi}(t)\rangle = \frac{1}{\mathrm{i}\hbar} H_{\text{eff}} |\psi(t)\rangle \ ,$$

with an *"effective" non-Hermitian Hamiltonian*

$$H_{\text{eff}} = H'_S + \text{decay terms} \ ,$$

and that dissipation occurs in the form of wavefunction collapses ("quantum jumps").

2.1 The master equation approach

Corresponding to the splitting of the composite closed quantum system $S \otimes R$ into the open quantum *system* S and the remaining *reservoir* R, we decompose the Hamiltonian $H_{S\otimes R}$,

$$H_{S\otimes R} = H_S + H_R + H_{SR} \ , \tag{2.1}$$

where H_S and H_R are the Hamiltonians for the system S and the reservoir R, respectively, and the interaction between the system and the reservoir is described by the interaction Hamiltonian H_{SR}.

2.1.1 The integro-differential von Neumann equation

In the Schrödinger picture the time evolution of the composite system $S\otimes R$, described by the *density operator* $\chi(t)$, is governed by the *von Neumann equation*

$$\dot{\chi}(t) = \frac{1}{\mathrm{i}\hbar}\left[H_{S\otimes R}, \chi(t)\right] \ , \tag{2.2}$$

where $H_{S\otimes R}$ is given by equation (2.1). In the interaction picture the total density operator is defined as

$$\tilde{\chi}(t) \equiv e^{(i/\hbar)(H_S+H_R)t}\chi(t)e^{-(i/\hbar)(H_S+H_R)t} \ , \tag{2.3}$$

and its time derivative provides the analogue to von Neumann's equation (2.2),

$$\begin{aligned}\dot{\tilde{\chi}}(t) &= \frac{\mathrm{i}}{\hbar}\left(H_S+H_R\right)\tilde{\chi}(t) - \tilde{\chi}(t)\frac{\mathrm{i}}{\hbar}\left(H_S+H_R\right) \\ &\quad + e^{(\mathrm{i}/\hbar)(H_S+H_R)t}\dot{\chi}(t)e^{-(\mathrm{i}/\hbar)(H_S+H_R)t} \\ &= \frac{1}{\mathrm{i}\hbar}\left[\tilde{H}_{SR}(t),\tilde{\chi}(t)\right] \ ,\end{aligned} \tag{2.4}$$

where $\tilde{H}_{SR}(t)$ is now explicitly time dependent,

$$\tilde{H}_{SR}(t) \equiv e^{(\mathrm{i}/\hbar)(H_S+H_R)t}H_{SR}e^{-(\mathrm{i}/\hbar)(H_S+H_R)t} \ . \tag{2.5}$$

Integrating equation (2.4) formally, we obtain

$$\tilde{\chi}(t) = \tilde{\chi}(0) + \frac{1}{\mathrm{i}\hbar}\int_0^t \mathrm{d}s\left[\tilde{H}_{SR}(t-s),\tilde{\chi}(t-s)\right] \ . \tag{2.6}$$

Substituting this solution into the r. h. s. of equation (2.4) gives an integro-differential form of von Neumann's equation.

Von Neumann equation in integro-differential form

The time evolution of the density operator $\chi(t)$ of a combined closed quantum system $S\otimes R$ with Hamiltonian $H_{S\otimes R}$ in the Schrödinger picture is governed by von Neumann's equation,

$$\dot{\chi}(t) = \frac{1}{\mathrm{i}\hbar}\left[H_{S\otimes R},\chi(t)\right] \ . \tag{2.7}$$

In the interaction picture it can be written in integro-differential form,

$$\dot{\tilde{\chi}}(t) = \frac{1}{\mathrm{i}\hbar}\left[\tilde{H}_{SR}(t),\tilde{\chi}(0)\right] - \frac{1}{\hbar^2}\int_0^t \mathrm{d}s\left[\tilde{H}_{SR}(t),\left[\tilde{H}_{SR}(t-s),\tilde{\chi}(t-s)\right]\right] \ , \tag{2.8}$$

where the interaction Hamiltonian $\tilde{H}_{SR}(t)$ describes the coupling between S and R.

The equations (2.2, 2.4, 2.8) are all equivalent and generally not exactly solvable. Nevertheless, it is possible to proceed and construct an equation of motion for the reduced density operator $\rho(t)$ of the open system S.

2.1.2 The master equation for the reduced density operator

If we are interested in describing the open system S and do not want to include any detailed information about the reservoir R, we may average over all possible reservoir states. Thus, we define the *reduced density operator* describing S by taking a partial trace over the the reservoir variables of the density operator for the composite system.

Reduced density operator of the open quantum system S

The reduced density operator $\rho(t)$ of the system S is defined by

$$\rho(t) \equiv \operatorname{tr}_R \{\chi(t)\} \ , \tag{2.9}$$

where the trace is taken over the reservoir variables only.

By taking the partial trace over the reservoir variables of equation (2.8) we find an equation of motion for the reduced density operator.

Master equation

The time evolution of the reduced density operator $\rho(t)$ describing the system S is governed by the master equation

$$\begin{aligned}\dot{\tilde{\rho}}(t) = &\frac{1}{i\hbar}\operatorname{tr}_R \left\{ \left[\tilde{H}_{SR}(t), \tilde{\chi}(0) \right] \right\} \\ &- \frac{1}{\hbar} \int_0^t \mathrm{d}s \operatorname{tr}_R \left\{ \left[\tilde{H}_{SR}(t), \left[\tilde{H}_{SR}(t-s), \tilde{\chi}(t-s) \right] \right] \right\} \ .\end{aligned} \tag{2.10}$$

Note 2.1 Tracing over the reservoir variables has of course a disadvantage—we lose all knowledge of measurements made on the reservoir that could give us a better knowledge of the system state. ◀

The advantage of the master equation is that it is in a convenient form for some reasonable approximations.

Even though the master equation describes the dynamics of the reduced density operator $\rho(t)$, it still contains the density operator $\chi(t)$ of the composite system. This prevents us from finding an exact solution of the master equation. In order to derive an eventually solvable equation for $\rho(t)$, one that does not contain $\chi(t)$, we have to make one major approximation.

2.1.3 Born approximation

In preparation for the approximation we first have to make an assumption about the correlation between the system and the reservoir: We assume the system and the

reservoir are uncorrelated at time $t = 0$ so that

$$\tilde{\chi}(0) = \chi(0) = R_0\tilde{\rho}(0) \ , \tag{2.11}$$

where R_0 is the density operator of the reservoir assumed to be at equilibrium. We further assume that the interaction has no diagonal elements in the reservoir energy representation, i. e.

$$\mathrm{tr}_R\left\{\tilde{H}_{SR}(t)R_0\right\} = 0 \ . \tag{2.12}$$

In general this condition can be arranged by including $\mathrm{tr}_R\{\tilde{H}_{SR}(t)R(0)\}$ in the system Hamiltonian [32, 33]. Applying equations (2.11) and (2.12) we can simplify the master equation (2.10):

$$\dot{\tilde{\rho}} = -\frac{1}{\hbar^2}\int_0^t \mathrm{d}s\,\mathrm{tr}_R\left\{\left[\tilde{H}_{SR}(t),\left[\tilde{H}_{SR}(t-s),\tilde{\chi}(t-s)\right]\right]\right\} \ . \tag{2.13}$$

If there was no interaction between the system and the reservoir, the density operator $\tilde{\chi}(t)$ could be written as a direct product not only at time zero, but also at all other times. All deviations from the direct product are consequently due to the interaction. Thus, if the interaction is very weak we expect that at all times $\tilde{\chi}(t)$ deviates from an uncorrelated state in first or higher order of H_{SR},

$$\tilde{\chi}(t) = R_0\tilde{\rho}(t) + \mathcal{O}\left(H_{SR}\right) \ . \tag{2.14}$$

In the spirit of the Born approximation in perturbation theory we may neglect deviations from the factorised form of $\tilde{\chi}(t)$ for an uncorrelated state, and keep in the master equation only terms up to second order in H_{SR}.

Born approximation

For a very weak coupling between the system and the reservoir we neglect contributions higher than second order in the interaction H_{SR} in the master equation (2.13) for the reduced density operator $\rho(t)$.

Replacing $\tilde{\chi}(t-s)$ by $R_0\tilde{\rho}(t-s)$ in equation (2.13) results in a master equation that no longer contains the density operator for the composite system $S \otimes R$.

Master equation in the Born approximation

If the system and the reservoir are uncorrelated at time $t = 0$,

$$\tilde{\chi}(0) = \chi = R_0\tilde{\rho}(0) \ , \tag{2.15}$$

where R_0 is the density operator of the reservoir assumed to be in equilibrium, and for times $t > 0$ the coupling between the system and the reservoir is very weak,

then the time-evolution of the reduced density operator $\rho(t)$ is governed by the master equation in the Born approximation,

$$\dot{\tilde{\rho}}(t) = -\frac{1}{\hbar^2}\int_0^t \mathrm{d}s\, \mathrm{tr}_R\left\{\left[\tilde{H}_{SR}(t), \left[\tilde{H}_{SR}(t-s), R_0\tilde{\rho}(t-s)\right]\right]\right\} \ . \tag{2.16}$$

Note 2.2 The master equation in the Born approximation is the simplest possible equation of motion for $\rho(t)$ that still contains retardation effects—the future behaviour of the system depends on its past, since we have to integrate over $\tilde{\rho}(t-s)$. ◀

A detailed discussion about the Born approximation can be found in [34, 35]. The following example illustrates the physical meaning of the Born approximation:

Example. If a photon escapes a cavity into the electromagnetic reservoir field, the cavity field may have become entangled with the reservoir field. This perturbation of the reservoir field could act back on the cavity field. But the emitted photon travels away from the cavity after its escape and its presence in the reservoir field will not affect the dynamics of the cavity field at later times. The leading effect of the emitted photon on the cavity field occurs immediately at the time of emission and is taken into account by interactions of first order in $\tilde{H}_{SR}$. ◁

Even though we turned the exact master equation into an eventually solvable equation using the Born approximation, the resulting equation (2.16) is still a complicated expression containing retardation effects. In the next subsection we will simplify the master equation in the Born approximation further by neglecting these retardation effects. The resulting master equation will be Markovian, i. e. the dynamics of the system will depend on its present state only and not on any past state.

2.1.4 Markov approximations

Retardation effects are of course physically possible, since the reservoir could in principle preserve changes due to its interaction with the system and reflect them back into the future evolution of the system. However, the reservoir is typically a large system with many degrees of freedom, and if it is in equilibrium we expect it to be essentially unaffected by the interaction with the system. Thus, we can assume that its correlation time is short compared to the relaxation time of the system. This motivates the first Markov approximation.

First Markov approximation

If the reservoir correlation time is much smaller than the time scale of correlated fluctuations in the system S we may replace $\tilde{\rho}(t-s)$ by $\tilde{\rho}(t)$ in the master equation (2.16).

Applying this approximation, equation (2.16) becomes local in time, and is known as the *Redfield master equation* [36],

$$\dot{\tilde{\rho}}(t) = -\frac{1}{\hbar^2}\int_0^t \mathrm{d}s\,\mathrm{tr}_R\left\{\left[\tilde{H}_{SR}(t),\left[\tilde{H}_{SR}(t-s),R_0\tilde{\rho}(t)\right]\right]\right\}\ , \tag{2.17}$$

which is still not Markovian, since the time evolution depends on our choice of the time origin, represented by the upper integration limit.

Note 2.3 The Redfield equation (2.17) is a coarse-grained version of the master equation. It describes only effects on an intermediate time scale, smaller than the relaxation time of the system and much longer then the reservoir correlation time.◀

Equation (2.17) is in the interaction picture where the only relevant time scale dominating the integration is for times s on the order of the reservoir correlation time. Thus, for times s much larger than the reservoir correlation time the integrand of the Redfield master equation (2.17) vanishes. This motivates the second Markov approximation:

Second Markov approximation

The integral in the Redfield master equation (2.17) can be approximated by moving the upper integration limit to infinity.

Applying the two Markov approximations to the master equation in the Born approximation results in a Markovian equation of motion for the reduced density operator.

Master equation in the Born-Markov approximation

If the reservoir correlation time is much smaller than the time scale for the dynamics of the system S, and the hypotheses of the Born approximation are assumed to be valid, the time evolution of the reduced density operator $\rho(t)$ is governed by the (Markovian) master equation in the Born-Markov approximation,

$$\dot{\tilde{\rho}}(t) = -\frac{1}{\hbar^2}\int_0^\infty \mathrm{d}s\,\mathrm{tr}_R\left\{\left[\tilde{H}_{SR}(t),\left[\tilde{H}_{SR}(t-s),R_0\tilde{\rho}(t)\right]\right]\right\}\ . \tag{2.18}$$

It describes only effects on a time scale smaller than the relaxation time of the system and much longer than the reservoir correlation time.

Even though the master equation in the Born-Markov approximation is a useful and solvable equation, there is a problem with it. The matrix elements $\langle\Psi(t)|\rho(t)|\Psi(t)\rangle$ for the density operator $\rho(t)$ of the system are occupation probabilities, and they should be non-negative for any state $|\Psi(t)\rangle$. But it is known that for some initial densities the Redfield master equation and the master equation in the Born-Markov approximation produce time-evolving densities violating this non-negativity [37]. It is therefore common to adopt another approximation to ensure $\rho(t)$ keeps the characteristic properties of a density operator at all times.

2.1.5 General Lindblad master equation

As a first step toward the next approximation we expand the interaction Hamiltonian in terms of eigenoperators of the system Hamiltonian:

$$H_{SR} = \hbar \sum_{i,j,k} \kappa_{ijk} \hat{A}_{ij} \hat{\Gamma}_k \ , \tag{2.19}$$

where $\hat{\Gamma}_k$ are independent reservoir operators and $\hat{A}_{ij}$ are degenerate eigenoperators of H_S, such that

$$[\hat{A}_{ij}, H_S] = \hbar \omega_i \hat{A}_{ij} \ , \tag{2.20}$$

with eigenfrequencies $\omega_i \neq \omega_{i'}$ for $i \neq i'$, and j labels the degeneracy. Note that in this notation, $\hat{A}_{ij}$ is any system operator including lowering and raising operators; this has to be kept in mind when applying this approach to specific examples in Chapter 3. The interaction Hamiltonian in the interaction picture is

$$\begin{aligned} \tilde{H}_{SR} &= e^{(\mathrm{i}/\hbar)(H_S+H_R)t} \left(\hbar \sum_{i,j,k} \kappa_{ijk} \hat{A}_{ij} \hat{\Gamma}_k \right) e^{-(\mathrm{i}/\hbar)(H_S+H_R)t} \\ &= \hbar \sum_{i,j,k} \kappa_{ijk} \left(e^{(\mathrm{i}/\hbar)H_S t} \hat{A}_{ij} e^{-(\mathrm{i}/\hbar)H_S t} \right) \left(e^{(\mathrm{i}/\hbar)H_R t} \hat{\Gamma}_k e^{-(\mathrm{i}/\hbar)H_R t} \right) \\ &= \hbar \sum_{i,j,k} \kappa_{ijk} \tilde{A}_{ij}(t) \tilde{\Gamma}_k(t) \ . \end{aligned} \tag{2.21}$$

Note 2.4 In the interaction picture the time evolution of eigenoperators is governed by the Heisenberg equation of motion, and we find

$$\dot{\tilde{A}}_{ij} = \frac{1}{\mathrm{i}\hbar} e^{-(\mathrm{i}/\hbar)H_S t} [\hat{A}_{ij}, H_S] e^{+(\mathrm{i}/\hbar)H_S t} = -\mathrm{i}\omega_i \tilde{A}_{ij} \tag{2.22}$$

with solution

$$\tilde{A}_{ij}(t) = \tilde{A}_{ij}(0) e^{-\mathrm{i}\omega_i t} = \hat{A}_{ij} e^{-\mathrm{i}\omega_i t} \ . \tag{2.23}$$

◀

We substitute the interaction Hamiltonian (2.21) into the master equation in the Born-Markov approximation, and after evaluating the commutators we formally replace some of the Hermitian $\tilde{H}_{SR}$-terms by their adjoints; this will allow notational

simplifications later on:

$$\begin{aligned}\dot{\tilde{\rho}}(t) = &-\int_0^\infty ds\,\mathrm{tr}_R\Big\{\sum_{i,j,k}\big[\kappa_{ijk}\tilde{A}_{ij}(t)\tilde{\Gamma}_k(t),\\ &\qquad\qquad\sum_{l,m,n}\big[\kappa_{lmn}\tilde{A}_{lm}(t-s)\tilde{\Gamma}_n(t-s),R_0\tilde{\rho}(t)\big]\big]\Big\}\\ = &-\sum_{\substack{i,j,k,\\ l,m,n}}\int_0^\infty ds\,\mathrm{tr}_R\Big\{\big(\kappa_{ijk}\tilde{A}_{ij}(t)\tilde{\Gamma}_k(t)\big)^\dagger\kappa_{lmn}\tilde{A}_{lm}(t-s)\tilde{\Gamma}_n(t-s)R_0\tilde{\rho}(t)\\ &\qquad-\kappa_{ijk}\tilde{A}_{ij}(t)\tilde{\Gamma}_k(t)R_0\tilde{\rho}(t)\big(\kappa_{lmn}\tilde{A}_{lm}(t-s)\tilde{\Gamma}_n(t-s)\big)^\dagger\\ &\qquad-\kappa_{lmn}\tilde{A}_{lm}(t-s)\tilde{\Gamma}_n(t-s)R_0\tilde{\rho}(t)\big(\kappa_{ijk}\tilde{A}_{ij}(t)\tilde{\Gamma}_k(t)\big)^\dagger\\ &\qquad+R_0\tilde{\rho}(t)\big(\kappa_{lmn}\tilde{A}_{lm}(t-s)\tilde{\Gamma}_n(t-s)\big)^\dagger\kappa_{ijk}\tilde{A}_{ij}(t)\tilde{\Gamma}_k(t)\Big\}\ .\end{aligned} \tag{2.24}$$

Using the relation (2.23), the eigenoperators of the system can be expressed in terms of the corresponding operators in the Schrödinger picture:

$$\begin{aligned}\dot{\tilde{\rho}}(t) = -\sum_{\substack{i,j,k,\\ l,m,n}}\int_0^\infty ds\Big(&\hat{A}_{ij}^\dagger\hat{A}_{lm}\tilde{\rho}(t)\kappa_{ijk}^*\kappa_{lmn}\mathrm{tr}_R\big\{\tilde{\Gamma}_{ij}^\dagger(t)\tilde{\Gamma}_{kl}(t-s)R_0\big\}e^{+\mathrm{i}(\omega_i-\omega_l)t}e^{+\mathrm{i}\omega_l s}\\ &-\hat{A}_{ij}\tilde{\rho}(t)\hat{A}_{lm}^\dagger\kappa_{ijk}\kappa_{lmn}^*\mathrm{tr}_R\big\{\tilde{\Gamma}_{kl}^\dagger(t-s)\tilde{\Gamma}_{ij}(t)R_0\big\}e^{-\mathrm{i}(\omega_i-\omega_l)t}e^{-\mathrm{i}\omega_l s}\\ &-\hat{A}_{lm}\tilde{\rho}(t)\hat{A}_{ij}^\dagger\kappa_{ijk}^*\kappa_{lmn}\mathrm{tr}_R\big\{\tilde{\Gamma}_{ij}^\dagger(t)\tilde{\Gamma}_{kl}(t-s)R_0\big\}e^{+\mathrm{i}(\omega_i-\omega_l)t}e^{+\mathrm{i}\omega_l s}\\ &+\tilde{\rho}(t)\hat{A}_{lm}^\dagger\hat{A}_{ij}\kappa_{ijk}\kappa_{lmn}^*\mathrm{tr}_R\big\{\tilde{\Gamma}_{kl}^\dagger(t-s)\tilde{\Gamma}_{ij}(t)R_0\big\}e^{-\mathrm{i}(\omega_i-\omega_l)t}e^{-\mathrm{i}\omega_l s}\Big)\ ,\end{aligned} \tag{2.25}$$

where we have used the cyclic property of the trace and the fact that the trace over the reservoir variables does not affect system operators.

For $\omega_i \neq \omega_l$ the terms $e^{\pm\mathrm{i}(\omega_i-\omega_l)t}$ are oscillatory. In quantum optical systems these oscillations are on a much smaller time-scale than the relaxation time of the system. This allows equation (2.25) to be simplified using the following approximation.

Secular approximation

We neglect all terms with $i \neq l$ in the master equation (2.25) since they oscillate with a high frequency $|\omega_i - \omega_l|$. When the master equation is integrated over an interval that is much longer than the period of oscillation (but may still be short compared with the relaxation time of the system), these terms will tend to average out.

Adopting the secular approximation in equation (2.25) we find

$$\begin{aligned}\dot{\tilde{\rho}}(t) = -\sum_{i,j,k,m,n}\int_0^\infty ds\Big(&\hat{A}_{ij}^\dagger\hat{A}_{im}\tilde{\rho}(t)\kappa_{ijk}^*\kappa_{imn}\mathrm{tr}_R\big\{\tilde{\Gamma}_k^\dagger(t)\tilde{\Gamma}_n(t-s)R_0\big\}e^{+\mathrm{i}\omega_i s}\\ &-\hat{A}_{ij}\tilde{\rho}(t)\hat{A}_{im}^\dagger\kappa_{ijk}\kappa_{imn}^*\mathrm{tr}_R\big\{\tilde{\Gamma}_n^\dagger(t-s)\tilde{\Gamma}_k(t)R_0\big\}e^{-\mathrm{i}\omega_i s}\\ &-\hat{A}_{im}\tilde{\rho}(t)\hat{A}_{ij}^\dagger\kappa_{ijk}^*\kappa_{imn}\mathrm{tr}_R\big\{\tilde{\Gamma}_k^\dagger(t)\tilde{\Gamma}_n(t-s)R_0\big\}e^{+\mathrm{i}\omega_i s}\\ &+\tilde{\rho}(t)\hat{A}_{im}^\dagger\hat{A}_{ij}\kappa_{ijk}\kappa_{imn}^*\mathrm{tr}_R\big\{\tilde{\Gamma}_n^\dagger(t-s)\tilde{\Gamma}_k(t)R_0\big\}e^{-\mathrm{i}\omega_i s}\Big)\ .\end{aligned} \tag{2.26}$$

This can be rearranged by inserting unity four times; we find

$$\begin{aligned}\dot{\tilde{\rho}}(t) = -\frac{1}{2}\sum_{i,j,m}\Big(&\mathrm{i}\hat{A}_{ij}^\dagger\hat{A}_{im}\tilde{\rho}(t)\Delta_{ijm}(t) - \mathrm{i}\tilde{\rho}(t)\hat{A}_{im}^\dagger\hat{A}_{ij}\Delta_{ijm}(t)\\ &-\hat{A}_{ij}\tilde{\rho}(t)\hat{A}_{im}^\dagger\gamma_{ijm}(t) + \hat{A}_{ij}\tilde{\rho}(t)\hat{A}_{im}^\dagger\Delta_{ijm}(t)\\ &-\hat{A}_{im}\tilde{\rho}(t)\hat{A}_{ij}^\dagger\gamma_{ijm}(t) - \hat{A}_{im}\tilde{\rho}(t)\hat{A}_{ij}^\dagger\Delta_{ijm}(t)\\ &+\hat{A}_{ij}^\dagger\hat{A}_{im}\tilde{\rho}(t)\gamma_{ijm}(t) + \tilde{\rho}(t)\hat{A}_{im}^\dagger\hat{A}_{ij}\gamma_{ijm}(t)\Big)\ ,\end{aligned} \tag{2.27}$$

where we have defined Δ_{ijm} and the damping rates γ_{ijm}: (noting that $\mathrm{tr}_R\{\tilde{\Gamma}_k^\dagger(t)\tilde{\Gamma}_n(t-s)R_0\}$ is the complex conjugate of $\mathrm{tr}_R\{\tilde{\Gamma}_n^\dagger(t-s)\tilde{\Gamma}_k(t)R_0\}$)

$$\begin{aligned}\Delta_{ijm} &\equiv \frac{1}{\mathrm{i}}\int_0^\infty \mathrm{d}s\sum_{k,n}\Big(\kappa_{ijk}^*\kappa_{imn}\mathrm{tr}_R\big\{\tilde{\Gamma}_k^\dagger(t)\tilde{\Gamma}_n(t-s)R_0\big\}e^{+\mathrm{i}\omega_i s} - \ \mathrm{c.c.}\Big)\\ &= 2\,\mathrm{Im}\int_0^\infty \mathrm{d}s\sum_{k,n}\kappa_{ijk}^*\kappa_{imn}\,\mathrm{tr}_R\big\{\tilde{\Gamma}_k^\dagger(t)\tilde{\Gamma}_n(t-s)R_0\big\}e^{\mathrm{i}\omega_i s}\end{aligned} \tag{2.28a}$$

$$\begin{aligned}\gamma_{ijm} &\equiv \int_0^\infty \mathrm{d}s\sum_{k,n}\Big(\kappa_{ijk}^*\kappa_{imn}\mathrm{tr}_R\big\{\tilde{\Gamma}_k^\dagger(t)\tilde{\Gamma}_n(t-s)R_0\big\}e^{+\mathrm{i}\omega_i s} + \ \mathrm{c.c.}\Big)\\ &= 2\,\mathrm{Re}\int_0^\infty \mathrm{d}s\sum_{k,n}\kappa_{ijk}^*\kappa_{imn}\,\mathrm{tr}_R\big\{\tilde{\Gamma}_k^\dagger(t)\tilde{\Gamma}_n(t-s)R_0\big\}e^{\mathrm{i}\omega_i s}\ ,\end{aligned} \tag{2.28b}$$

where Im and Re denote the imaginary and real part, respectively, and c. c. denotes the complex conjugate. Finally, we transform equation (2.27) back into the Schrödinger picture to find:

$$\begin{aligned}\dot{\rho}(t) &= \frac{1}{\mathrm{i}\hbar}\left[H_S,\rho(t)\right] + e^{-(\mathrm{i}/\hbar)H_S t}\dot{\tilde{\rho}}(t)e^{(\mathrm{i}/\hbar)H_S t}\\ &= \frac{1}{\mathrm{i}\hbar}\Big(\big[H_S,\rho(t)\big] + \frac{\hbar\Delta_{ijm}}{2}\big(\hat{A}_{ij}^\dagger\hat{A}_{im}\rho(t) - \rho(t)\hat{A}_{im}^\dagger\hat{A}_{ij}\big)\Big)\\ &\quad + \frac{\Delta_{ijm}}{2}\big(\hat{A}_{im}^\dagger\rho\hat{A}_{ij} - \hat{A}_{ij}^\dagger\rho\hat{A}_{im}\big)\\ &\quad + \sum_{i,j,m}\frac{\gamma_{ijm}}{2}\Big(\hat{A}_{ij}\rho(t)\hat{A}_{im}^\dagger + \hat{A}_{im}\rho(t)\hat{A}_{ij}^\dagger - \hat{A}_{ij}^\dagger\hat{A}_{im}\rho(t) - \rho(t)\hat{A}_{im}^\dagger\hat{A}_{ij}\Big)\ .\end{aligned} \tag{2.29}$$

If all terms with $j \neq m$ vanish, this equation is said to be the *master equation in Lindblad form* or the *Lindblad equation*. In addition to the von Neumann equation $\dot{\rho}(t) = \frac{1}{\mathrm{i}\hbar}[H, \rho(t)]$, the Lindblad equation has terms of the form $\sum_i (2\hat{L}_i \rho(t) \hat{L}_i^\dagger - \hat{L}_i^\dagger \hat{L}_i \rho(t) - \rho(t) \hat{L}_i^\dagger \hat{L}_i)$ [38]. In general this can be arranged by transforming into a frame in which Δ_{ijm} and γ_{ijm} are diagonal. For our applications of the master equation in this thesis, however, there is no need for such a transformation: eigenoperators $\hat{A}_{ij}$ and $\hat{A}_{im}$ with $j \neq m$ always couple to statistically independent reservoirs, i. e. $\kappa^*_{ijk}\kappa_{imk} \neq 0$ only if $j = m$.

Master equation in Lindblad form

If the interaction Hamiltonian of the system and the reservoir is expanded in the eigenoperators $\hat{A}_i$ of the system Hamiltonian, degenerate eigenoperators couple to statistical independent reservoirs, and the secular approximation is adopted, then the master equation in the Born-Markov approximation simplifies to the master equation in Lindblad form,

$$\dot{\rho}(t) = \frac{1}{\mathrm{i}\hbar}\big[H'_S, \rho(t)\big] + \sum_i \frac{\gamma_i}{2}\left(2\hat{A}_i \rho(t) \hat{A}_i^\dagger - \hat{A}_i^\dagger \hat{A}_i \rho(t) - \rho(t) \hat{A}_i^\dagger \hat{A}_i\right) , \tag{2.30}$$

where the effective system Hamiltonian,

$$H'_S \equiv H_S + \sum_i \frac{\hbar \Delta_i}{2} \hat{A}_i^\dagger \hat{A}_i , \tag{2.31}$$

describes the coherent evolution and includes present energy shifts, and Δ_i and γ_i are defined as

$$\Delta_i \equiv 2\,\mathrm{Im} \sum_{k,n} \kappa^*_{ik}\kappa_{in} \int_0^\infty \mathrm{d}s\, \mathrm{tr}_R\big\{\tilde{\Gamma}_k^\dagger(t) \tilde{\Gamma}_n(t-s) R_0\big\} e^{\mathrm{i}\omega_i s} , \tag{2.32}$$

$$\gamma_i \equiv 2\,\mathrm{Re} \sum_{k,n} \kappa^*_{ik}\kappa_{in} \int_0^\infty \mathrm{d}s\, \mathrm{tr}_R\big\{\tilde{\Gamma}_k^\dagger(t) \tilde{\Gamma}_n(t-s) R_0\big\} e^{\mathrm{i}\omega_i s} , \tag{2.33}$$

where $\tilde{\Gamma}(t)$ are reservoir operators.

The master equation in Lindblad form ensures that $\rho(t)$ remains Hermitian, positive semi-definite and $\mathrm{tr}\{\rho(t)\} = 1$ at all times for any initially positive semi-definite, normalised density operator $\rho(0)$.

Note 2.5 The assumption that degenerate eigenoperators couple to statistical independent reservoirs holds for all the cases we are interested in. However, there are physical systems, like superradiance [39, 40], where this is not the case. Nevertheless, in this situations it is still possible to bring the master equation into Lindblad form, simply by transforming into a space where Δ_{ijl} and γ_{ijl} become diagonal. ◀

The terms $-\hat{A}_i^\dagger \hat{A}_i \rho(t)$ and $-\rho(t)\hat{A}_i^\dagger \hat{A}_i$ in the Lindblad form of the master equation describe the loss of population from the current states, whereas the terms $\hat{A}_i \rho(t) \hat{A}_i^\dagger$ describe the gain of population of the states toward which the system propagates. Therefore, $\hat{A}_i \rho \hat{A}_i^\dagger$ can be understood as the density matrix after the transition described by $\hat{A}_i$. In the next section about quantum trajectories we introduce a concept within which these transitions are interpreted as "quantum jumps".

Having derived the Lindblad form of the master equation, we have reached our goal in this section. Before introducing the quantum trajectory theory in the following section, we derive an essential formula in the next subsection that will be needed later on. In preparation for this derivation and its later use, it is useful to formally rewrite the master equation for the reduced density operator in a more abstract notation:

$$\dot{\rho}(t) = \mathcal{L}\rho(t) \ . \tag{2.34}$$

$\mathcal{L}$ is a generalised Liouvillian, sometimes called a superoperator. It is a linear operator that acts on operators rather than on vectors in the Hilbert space. For example, in the case of the master equation in Lindblad form (2.30) the action of $\mathcal{L}$ is defined by

$$\mathcal{L}\cdot \equiv \frac{1}{\mathrm{i}\hbar}\big[H'_S, \cdot\big] + \sum_i \frac{\gamma_i}{2}\left(2\hat{A}_i \cdot \hat{A}_i^\dagger - \hat{A}_i^\dagger \hat{A}_i \cdot - \cdot \hat{A}_i^\dagger \hat{A}_i\right) \ . \tag{2.35}$$

2.1.6 Quantum regression formula

So far we have seen that the master equation approach allows us to derive an explicit formula for the time dependence of the reduced density operator $\rho(t)$ which can be used to calculate the time dependence of the expectation value of any operator $\hat{O}$ in the Hilbert space of S:

$$\langle \hat{O} \rangle(t) = \mathrm{tr}_{S\otimes R}\{\hat{O}\chi(t)\} = \mathrm{tr}_S\big\{\hat{O}\,\mathrm{tr}_R\{\chi(t)\}\big\} = \mathrm{tr}_S\{\hat{O}\rho(t)\} \ . \tag{2.36}$$

But how shall we calculate two-time averages like the expectation value for the emission of a photon conditioned on another emission at an earlier time,

$$\langle \hat{a}^\dagger(t)\hat{a}^\dagger(t+\tau)\hat{a}(t+\tau)\hat{a}^\dagger(t)\rangle \quad \text{with} \quad \tau \geq 0 \ , \tag{2.37}$$

i. e. second-order correlation functions? In the Schrödinger picture—where operators are generally time independent—such an expression cannot be evaluated. And the derived master equation in the Schrödinger picture is for a start unusable. Clearly, two-time averages are well defined in the Heisenberg picture. Therefore, to evaluate a two-time average of the form

$$\langle \hat{O}_1(t)\hat{O}_2(t')\hat{O}_3(t)\rangle \quad \text{with} \quad t' - t \geq 0 \ . \tag{2.38}$$

we write the average as a trace in the Heisenberg picture and transform the trace into the Schrödinger picture. Using the cyclic property of the trace we find

$$\begin{aligned}\langle \hat{O}_1(t)\hat{O}_2(t')\hat{O}_3(t)\rangle &= \mathrm{tr}_{S\otimes R}\left\{\chi \hat{O}_1(t)\hat{O}_2(t')\hat{O}_3(t)\right\} \\ &= \mathrm{tr}_{S\otimes R}\left\{\hat{O}_2 e^{-(\mathrm{i}/\hbar)H(t'-t)}\hat{O}_3\chi(t)\hat{O}_1 e^{(\mathrm{i}/\hbar)H(t'-t)}\right\} \\ &= \mathrm{tr}_S\left\{\hat{O}_2 \mathrm{tr}_R\left\{e^{-(\mathrm{i}/\hbar)H(t'-t)}\hat{O}_3\chi(t)\hat{O}_1 e^{(\mathrm{i}/\hbar)H(t'-t)}\right\}\right\} \\ &= \mathrm{tr}_S\left\{\hat{O}_2 \mathrm{tr}_R\{\chi_{\hat{O}_3\hat{O}_1}(\tau)\}\right\} , \end{aligned} \tag{2.39}$$

where we defined

$$\chi_{\hat{O}_3\hat{O}_1}(\tau) \equiv e^{-(\mathrm{i}/\hbar)H\tau}\hat{O}_3\chi(t)O_1 e^{(\mathrm{i}/\hbar)H\tau} \quad \text{with} \quad \tau \equiv t'-t \; . \tag{2.40}$$

Since we have to evaluate the trace of $\chi_{\hat{O}_3\hat{O}_1}(\tau)$ we also define the reduced operator

$$\rho_{\hat{O}_3\hat{O}_1}(\tau) \equiv \mathrm{tr}_R\{\chi_{\hat{O}_3\hat{O}_1}(\tau)\} \; . \tag{2.41}$$

We find

$$\begin{aligned}\chi_{\hat{O}_3\hat{O}_1}(0) &= \hat{O}_3\chi(t)\hat{O}_1 = \hat{O}_3 R_0\rho(t)\hat{O}_1 = R_0\hat{O}_3\rho(t)O_1 \\ &= R_0\mathrm{tr}_R\{\hat{O}_3\chi(t)\hat{O}_1\} = R_0\mathrm{tr}_R\{\chi_{\hat{O}_3\hat{O}_1}(0)\} \\ &= R_0\rho_{\hat{O}_3\hat{O}_1}(0) \; , \end{aligned} \tag{2.42}$$

where we have used the assumption $\tilde{\chi}(t) = R_0\tilde{\rho}(t)$ discussed in subsection 2.1.3 (Born approximation). The three equations (2.41), (2.42) and the time-derivative of $\chi_{\hat{O}_3\hat{O}_1}(\tau)$ with respect to τ,

$$\frac{\mathrm{d}}{\mathrm{d}\tau}\chi_{\hat{O}_3\hat{O}_1}(\tau) = \frac{1}{\mathrm{i}\hbar}[H, \chi_{\hat{O}_3\hat{O}_1}(\tau)] \; , \tag{2.43}$$

are respectively equivalent to the definition of the reduced density operator $\rho(t)$, equation (2.14) and the von-Neumann equation for $\chi(t)$—our three starting equations for the derivation of the master equation in the Born approximation. Since the von-Neumann equation for $\chi(t)$ and equation (2.43) share the same Hamiltonian, we can derive the equation of motion for $\rho_{\hat{O}_3\hat{O}_1}(\tau)$ in the same fashion as we derived the master equation for $\rho(t)$, and find

$$\frac{\mathrm{d}}{\mathrm{d}\tau}\rho_{\hat{O}_3\hat{O}_1}(\tau) = \mathcal{L}\rho_{\hat{O}_3\hat{O}_1}(\tau) \; , \tag{2.44}$$

with the formal solution

$$\rho_{\hat{O}_3\hat{O}_1}(\tau) = e^{\mathcal{L}\tau}\big(\rho_{\hat{O}_3\hat{O}_1}(0)\big) = e^{\mathcal{L}\tau}\big(\hat{O}_3\rho(t)\hat{O}_1\big) \; . \tag{2.45}$$

This relation simplifies equation (2.39).

Quantum regression formula

Adopting the formal assumptions for the master equation in the Born approximation, the two-time average $\langle \hat{O}_1(t)\hat{O}_2(t+\tau)\hat{O}_3(t)\rangle$, $\tau \geq 0$, for any three system operators $\hat{O}_1$, $\hat{O}_2$ and $\hat{O}_3$ is given by the quantum regression formula,

$$\langle O_1(t)O_2(t+\tau)O_3(t)\rangle = \mathrm{tr}_S\Big\{\hat{O}_2 e^{\mathcal{L}\tau}\big(\hat{O}_3\rho(t)\hat{O}_1\big)\Big\}\ , \tag{2.46}$$

where $\rho(t)$ is the reduced density operator fulfilling the master equation $\dot{\rho}(t) = \mathcal{L}\rho(t)$.

Our main application of this formula is in chapters 4 and 5 where we calculate steady state second-order photon correlation functions.

2.2 Quantum trajectories

In this section we introduce an alternative method for describing the dynamics of a quantum system coupled to its environment. This method is equivalent to the master equation approach. The presentation in this section follows closely the ideas of lecture 7 in [28], which, along with [41], should be consulted for a more fundamental introduction and a broader discussion of the quantum trajectory theory. This would go beyond the needs of our presentation and we are content with unravelling the master equation in Lindblad form that will allow us to put the dynamics of the system in another perspective.

2.2.1 Unravelling the master equation

For the unravelling of the master equation in Lindblad form we write the Liouvillian $\mathcal{L}$ as a sum of an unperturbed part $\mathcal{L}_0$ and a small perturbation $\mathcal{S}$,

$$\dot{\rho}(t) = (\mathcal{L}_0 + \mathcal{S})\,\rho(t) \tag{2.47}$$

with

$$\mathcal{L}_0 \equiv \mathcal{L} - \mathcal{S}\ . \tag{2.48}$$

The formal solution of equation (2.47) is

$$\rho(t) = e^{(\mathcal{L}_0+\mathcal{S})t}\rho(0) \tag{2.49}$$

provided that $(\mathcal{L}_0 + \mathcal{S})$ is not explicitly time-dependent. Our aim is to recast this solution in a more descriptive form which allows a clear interpretation. As a first step we define an auxiliary density operator $\rho'(t)$,

$$\rho'(t) \equiv e^{-\mathcal{L}_0 t}\rho(t)\ . \tag{2.50}$$

Taking the time-derivative of equation (2.50) and applying equation (2.47) leads to the equation of motion for $\rho'(t)$,

$$\begin{aligned}\dot{\rho}'(t) &= -e^{-\mathcal{L}_0 t}\mathcal{L}_0\rho(t) + e^{-\mathcal{L}_0 t}(\mathcal{L}_0+\mathcal{S})\rho(t) \\ &= e^{-\mathcal{L}_0 t}\mathcal{S}e^{\mathcal{L}_0 t}\rho'(t)\ . \end{aligned} \tag{2.51}$$

If we formally integrate this equation, apply equation (2.50), and multiply with $e^{\mathcal{L}_0 t}$ from the right, we obtain

$$\rho(t) = \rho(0) + \int_0^t \mathrm{d}s\, e^{\mathcal{L}_0(t-s)}\mathcal{S}e^{\mathcal{L}_0 s}\rho'(s)\ . \tag{2.52}$$

Iterating this solution results in Dyson's expansion,

$$\rho(t) = \sum_{m=0}^{\infty}\int_0^t \mathrm{d}t_m \int_0^{t_m}\mathrm{d}t_{m-1}\cdots\int_0^{t_2}\mathrm{d}t_1 e^{\mathcal{L}_0(t-t_m)}\mathcal{S}e^{\mathcal{L}_0(t_m-t_{m-1})}\mathcal{S}\cdots\mathcal{S}e^{\mathcal{L}_0 t_1}\rho(0)\ , \tag{2.53}$$

where (t_m) is a monotonic increasing sequence. The integration kernel describes a *quantum trajectory* of the initial state $\rho(0)$; where the reason for the name "quantum trajectory" becomes clear later on (note 2.7). The terms $e^{\mathcal{L}_0(t_m-t_{m-1})}$ represent a continuous time-evolution in the time-intervals $[t_m, t_{m-1}]$, and $\mathcal{S}$ represents discontinuous collapses ("jumps") at the times $t_1, t_2, \ldots, t_m$. Equation (2.53) is simply the sum over all possible numbers of collapses, $m = 0, \ldots, \infty$, and an integration over all possible separation times of these emissions within the interval $[0, t]$.

We now want to take distinguishable perturbations into account each causing the system to collapse at different times. If we consider a second perturbation $\mathcal{S}_1$ in addition to $\mathcal{S}$ in the master equation (2.47), each initially free evolution in the time-intervals $[t_m, t_{m-1}]$ in the Dyson expansion (2.53) will be interrupted by a certain number of collapses due to $\mathcal{S}_1$. Thus, we have to replace each free evolution term by its own Dyson expansion

$$\begin{aligned}e^{\mathcal{L}_0(t_m-t_{m-1})} = \sum_{n=0}^{\infty}\int_{t_{m-1}}^{t_m}\mathrm{d}t_n\int_{t_{m-1}}^{t_n}\mathrm{d}t_{n-1}\cdots\int_{t_{m-1}}^{t_2}\mathrm{d}t_1 e^{\mathcal{L}_0(t-t_n)}\mathcal{S}_1 \\ \times e^{\mathcal{L}_0(t_n-t_{n-1})}\mathcal{S}_1\cdots\mathcal{S}_1 e^{\mathcal{L}t_1}\ . \end{aligned} \tag{2.54}$$

Instead of substituting the expansion for every free time-evolution in equation (2.53) we redefine m as the total number of collapses of both $\mathcal{S}$ and $\mathcal{S}_1$, and sum at each collapse over the two possibilities,

$$\begin{aligned}\rho(t) = \sum_{m=0}^{\infty}\sum_{\nu_1=1}^{2}\sum_{\nu_2=1}^{2}\cdots\sum_{\nu_m=1}^{2}\int_0^t\mathrm{d}t_m\int_0^{t_m}\mathrm{d}t_{m-1}\cdots\int_0^{t_2}\mathrm{d}t_1 e^{\mathcal{L}_0(t-t_m)}\mathcal{S}_{\nu_m} \\ \times e^{\mathcal{L}_0(t_m-t_{m-1})}\mathcal{S}_{\nu_{m-1}}\cdots\mathcal{S}_{\nu_1}e^{\mathcal{L}_0 t_1}\rho(0)\ . \end{aligned} \tag{2.55}$$

For more than two distinguishable perturbations we can iterate this procedure.

Quantum trajectories of the density operator

The solution of the the master equation

$$\dot{\rho}(t) = (\mathcal{L}_0 + \mathcal{S})\,\rho(t) \qquad \text{with} \qquad \mathcal{S} = \sum_{i=1}^{I} \mathcal{S}_i \ , \tag{2.56}$$

where $\mathcal{S}$ is a small perturbation of $\mathcal{L}_0$, is

$$\begin{aligned}\rho(t) = \sum_{m=0}^{\infty} \sum_{\nu_1=1}^{I} \sum_{\nu_2=1}^{I} \cdots \sum_{\nu_m=1}^{I} \int_0^t \mathrm{d}t_m \int_0^{t_m} \mathrm{d}t_{m-1} \cdots \int_0^{t_2} \mathrm{d}t_1 e^{\mathcal{L}_0(t-t_m)} \mathcal{S}_{\nu_m} \\ \times e^{\mathcal{L}_0(t_m - t_{m-1})} \mathcal{S}_{\nu_{m-1}} \cdots \mathcal{S}_{\nu_1} e^{\mathcal{L}_0 t_1} \rho(0) \ ,\end{aligned} \tag{2.57}$$

where (t_m) is a monotonic increasing sequence. The integration kernel describes a quantum trajectory of the initial state $\rho(0)$, and equation (2.57) is simply the summation over all possible trajectories.

For later use we introduce the *conditioned reduced density operator* $\rho_c(t)$ describing the system at time t with initial state $\rho(0)$ and a particular sequence of collapse times in the interval $[0, t]$,

$$\rho_c(t) \equiv \frac{\bar{\rho}_c(t)}{\mathrm{tr}\{\bar{\rho}_c(t)\}} \ , \tag{2.58}$$

where $\bar{\rho}_c(t)$ is the unnormalised operator

$$\bar{\rho}_c(t) \equiv e^{\mathcal{L}_0(t-t_m)} \mathcal{S}_{\nu_m} e^{\mathcal{L}_0(t_m - t_{m-1})} \mathcal{S}_{\nu_{m-1}} \cdots \mathcal{S}_{\nu_1} e^{\mathcal{L}_0 t_1} \rho(0) \ . \tag{2.59}$$

Up to this point our derivation is quite general and holds for all choices of $\mathcal{L}_0 + \mathcal{S} = \mathcal{L}$ as long as $\mathcal{S}$ can be considered as a small perturbation. In the next subsection we present a specific unravelling of the master equation in Lindblad form.

2.2.2 Stochastic wavefunctions

As mentioned at the end of subsection 2.1.5, certain decay terms of the master equation in Lindblad form can be identified as transitions between system states. This suggests an unravelling where the transition terms are interpreted as the cause for the collapses in the trajectories of the reduced density operator of the system, and the remaining terms as a modified coherent time-evolution operator. Having this in mind we rewrite the master equation in Lindblad form,

$$\dot{\rho}(t) = (\mathcal{L}_0 + \mathcal{S})\,\rho \qquad \text{with} \qquad \mathcal{S} = \sum_{i} \mathcal{S}_i \tag{2.60a}$$

and

$$\mathcal{L}_0\rho \equiv \frac{1}{\mathrm{i}\hbar}\left[H'_S,\rho\right] - \sum_i \frac{\gamma_i}{2}\left(A_i^\dagger A_i\rho + \rho A_i^\dagger A_i\right) = \frac{1}{\mathrm{i}\hbar}\left(H_{\mathrm{eff}}\rho - \rho H_{\mathrm{eff}}^\dagger\right) \ , \tag{2.60b}$$

$$\mathcal{S}_i\rho \equiv \gamma_i A_i \rho A_i^\dagger = C_i \rho C_i^\dagger \ , \tag{2.60c}$$

where we have introduced the *collapse operators*

$$C_i \equiv \sqrt{\gamma_i} A_i \ , \tag{2.61}$$

and H_{eff} is an *effective, non-Hermitian Hamiltonian* defined as

$$H_{\mathrm{eff}} \equiv H'_S - \sum_i \gamma_i A_i \rho A_i^\dagger \ . \tag{2.62}$$

Note 2.6 This choice of $\mathcal{L}_0$ and $\mathcal{S}_i$ corresponds to a direct detection of the collapses, e. g. the direct photoelectric detection of the light leaking out of a cavity. A different detection set-up (e. g. homodyne detection) might suggest a different unravelling of the master equation with another choice of $\mathcal{L}_0$ and $\mathcal{S}_i$. This way the quantum trajectory approach enables us to take different possible detection set-ups into account, a property the master equation cannot provide (see note 2.1). ◀

Often the conditioned density operator can be factorised in a pure state at time t,

$$\rho_c(t) = |\psi_c(t)\rangle\langle\psi_c(t)| \ , \qquad \bar{\rho}_c(t) = \left|\bar{\psi}_c(t)\right\rangle\left\langle\bar{\psi}_c(t)\right| \ . \tag{2.63}$$

In this situation we can replace the coherent time-evolution operator $e^{\mathcal{L}_0\Delta t}$ for the density operator by a time-evolution operator for the state $|\bar{\psi}_c(t)\rangle$, i. e.

$$\left|\bar{\psi}_c(t+\Delta t)\right\rangle = e^{-(\mathrm{i}/\hbar)H_{\mathrm{eff}}\Delta t}\left|\bar{\psi}_c(t)\right\rangle \ , \tag{2.64}$$

and at times of collapses we have

$$\left|\bar{\psi}_c\right\rangle \to \hat{C}_i\left|\bar{\psi}_c\right\rangle \ . \tag{2.65}$$

Note 2.7 This way of unravelling the master equation has as a consequence that if the conditioned density operator factorises initially in a pure state then it does so for all times. Thus, we can follow the state of the system through its Hilbert space in the same way as we can follow the classical trajectory of a particle. This motivates the name "quantum trajectory theory". ◀

There is one thing missing. The collapses of a quantum mechanical system, e. g. due to the emission of a photon into the reservoir, are not deterministic. Actually, they appear at random times. Thus the times $(t_m - t_{m-1})$ in the exponentials of

equation (2.57) characterising the time intervals between two consecutive collapses have to follow quantum mechanical randomness. The probability for a collapse in the time interval $[t, t + \Delta t]$ is given by the collapse probability at time t multiplied by the length Δt of the time interval:

$$p_c(t) = \mathrm{tr}\{\mathcal{S}\rho_c(t)\}\Delta t \ , \qquad p_{c,i}(t) = \mathrm{tr}\{\mathcal{S}_i\rho_c(t)\}\Delta t \ , \tag{2.66}$$

where $p_{c,i}(t)$ is the probability of a collapse due to $\mathcal{S}_i$ and $p_c(t)$ the probability to find at least one collapse in the time interval $[t, t + \Delta t]$, i. e. $p_c(t) = \sum_i p_{c,i}(t)$. The theory has to take account of this randomness in a statistically correct way. We simply claim that the quantum trajectories generated by the following Monte-Carlo algorithm are statistically equivalent to the solution of the master equation and refer to [28, 41] and the references within them for a more mathematical justification.

Algorithm to determine the time-evolution of the system wavefunction

The quantum trajectory of the system wavefunction can be simulated by using a Monte-Carlo algorithm. In the simulation, time is discrete with a time step Δt. For the wave-function ψ_c at time t_n the wave-function at time $t_{n+1} = t_n + \Delta t$ is determined by the following algorithm:

1. Calculate the probabilities $p_{c,i}(t_n)$ for a collapse in the interval $[t_n, t_n + \Delta t]$:

$$p_{c,i}(t_n) = \langle\psi_c(t_n)|\hat{C}_i^\dagger\hat{C}_i|\psi_c(t_n)\rangle\Delta t \ . \tag{2.67}$$

2. Draw a uniformly distributed random number r_n from the interval $[0, 1]$.

3. Compare the collapse probability $p_c(t_n) = \sum_i p_{c,i}(t_n)$ with the random number r_n and determine the unnormalised state at time t_{n+1} according to:

   If ($p_c(t_n) \geq r_n$) **then**

   a) Draw a uniformly distributed random number r_n' from the interval $[0, 1]$.

   b) Divide a unit interval into i sub-intervals according to the probabilities $p_{c,i}(t_n)$.

   c) Choose the interval j out of the i sub-intervals in which the random number r_n' falls, and calculate

$$|\bar{\psi}_c(t_{n+1})\rangle \equiv \hat{C}_j|\psi_c(t_n)\rangle \ . \tag{2.68}$$

   else calculate

$$|\bar{\psi}_c(t_{n+1})\rangle \equiv e^{-(\mathrm{i}/\hbar)H_{\mathrm{eff}}\Delta t}|\psi_c(t_n)\rangle \ . \tag{2.69}$$

4. Normalise the new state:

$$|\psi_c(t_{n+1})\rangle = \frac{|\bar{\psi}_c(t_{n+1})\rangle}{\sqrt{\langle\bar{\psi}_c(t_{n+1})|\bar{\psi}_c(t_{n+1})\rangle}} \,. \tag{2.70}$$

It is important to remember that our derivation of Dyson's expansion of the reduced density operator relies on the fact that $\mathcal{S}$ (representing the collapses) is a small perturbation of $\mathcal{L}_0$ (representing the free time-evolution). Thus, jumps should occur only very seldom. In our Monte-Carlo simulation we have to take this into account by choosing the size of the time step Δt small enough such that the probability for a jump is small and most of the time the system evolves coherently. If so, the times t_m at which the collapses occur are separated by many time steps $\Delta t \ll (t_m - t_{m-1})$ and the Monte-Carlo algorithm provides a stochastic quantum mapping between them:

$$|\psi_c(t_{m+1})\rangle = \frac{\hat{C}e^{-(\mathrm{i}/\hbar)H_{\mathrm{eff}}(t_{m+1}-t_m)}|\psi_c(t_m)\rangle}{\sqrt{\langle\psi_c(t_m)|e^{(\mathrm{i}/\hbar)H_{\mathrm{eff}}^\dagger(t_{m+1}-t_m)}\hat{C}^\dagger\hat{C}e^{-(\mathrm{i}/\hbar)H_{\mathrm{eff}}(t_{m+1}-t_m)}|\psi_c(t_m)\rangle}} \,. \tag{2.71}$$

Note 2.8 The times $(t_{m+1} - t_m)$ between two collapses are random and depend on the wavefunction itself through the collapse probabilities (2.67). Our Monte-Carlo algorithm provides the statistics for the collapse times on run-time by basing its decision, whether a collapse or a time evolution of the wavefunction occurs, on these collapse probabilities. We do not need to embed an explicit distribution of the collapse times in our simulation. ◀

Note 2.9 Unlike in the master equation approach, where the system evolves eventually towards a steady state with a density operator constant in time, the wavefunction in the quantum trajectory will never do so; it retains its stochastic evolution for all times. However, in a statistical sense the wavefunction becomes eventually stationary. Thus, an ensemble average in the steady state within the master equation approach gives the same results as a (long) time average in the statistically stationary regime within the quantum trajectory approach. ◀

The quantum trajectory formalism is attractive for computer simulations (chapter 6), especially for modelling systems with a large number N of possible states The computational advantage of the Monte-Carlo algorithm is that the time evolution of the system involves solving a set of only $\mathcal{O}(N)$ differential equations—compared to $\mathcal{O}(N^2)$ when solving the master equation directly. The quantum trajectory theory can also be used for analytic investigations in the weak-excitation limit (chapter 4).

Chapter 3

Cavity Quantum Electrodynamics

When atoms interact with the modes of a cavity, this is the domain of *cavity quantum electrodynamics* (cavity QED). The simplest example is a single two-level atom coupled to a single cavity mode, and was first analysed in detail by E. T. Jaynes and F. W. Cummings in 1963 [42]; it is therefore called the *Jaynes-Cummings model*. In the first section of this chapter we give a very brief introduction into this model to familiarise the reader with some terminologies and a few key properties that are helpful to understand results presented in Chapters 4–6.

As we mentioned in the first chapter, measurements on a cavity QED system are performed by detecting light that leaks from the system; and therefore, the interaction of the system with its surrounding reservoir is essential. There are two parts of a cavity QED system that interact with the reservoir: (a) photons of the cavity modes leave the cavity through the high reflective but not perfect mirrors; (b) the atom emits photons by spontaneous emission out of the side of the cavity. Adopting the master equation formalism of Chapter 2, we discuss these interactions in the second and third sections, respectively.

In the final section we put together our knowledge acquired in the previous section to find the master equation for the single-atom two-mode cavity QED system that we aim to model. We present the master equation for both models, one with a two-level atom, and the other with a two-level atom with Zeeman sub-structure.

3.1 The Jaynes-Cummings model

The simplest example for cavity QED is the interaction of a two-level atom with a resonant cavity mode; it is described by the so-called *Jaynes-Cummings Hamiltonian*, which is simply the Hamiltonian in equation (1.33) reduced to a single field mode,

$$H_{\text{Jaynes-Cummings}} = \hbar\omega\hat{\sigma}_+\hat{\sigma}_- + \hbar\omega\hat{a}^\dagger\hat{a} + \mathrm{i}\hbar g\left(\hat{a}^\dagger\hat{\sigma}_- - \hat{a}\hat{\sigma}_+\right) \ , \tag{3.1}$$

with dipole coupling strength

$$g = \sqrt{\frac{2\pi\omega|\boldsymbol{d}_{ge}|^2}{\hbar V_a}} \ , \tag{3.2}$$

where V_a is the cavity-mode volume.

If the interaction was switched off, all system eigenstates except the ground state $|g\rangle|0\rangle$ would be doubly degenerate (for example, $|e\rangle|0\rangle$ and $|g\rangle|1\rangle$ would have the same energy). The interaction between the atom and the cavity mode lifts this degeneracy; the resulting energy eigenstates are called *dressed states*, and the energy eigenvalues are referred as the *Jaynes-Cummings ladder* (see figure 3.1). The splitting of the first rung of the ladder is called the *vacuum Rabi splitting*, and its magnitude is determined by the dipole coupling strength [43]:

$$\Delta E_{\text{vacuum Rabi splitting}} = 2\hbar g \ . \tag{3.3}$$

The atom and the cavity mode are both coupled to the free space modes of the environment; the cavity mode decays through the cavity mirrors, and spontaneous emission from the atom exits out the side of the cavity. These interactions are subjects of the following sections.

3.2 The damped electromagnetic cavity field

3.2.1 The master equation for the non-driven multi-mode cavity

In this subsection we determine the master equation in Lindblad form for the damped electromagnetic cavity field. For the derivation we do not have to start from scratch; rather, we set up the formal description of the multi-mode cavity such that the equivalence to the conditions for the derivation of the Lindblad form are obvious, and adopt the results.

We consider a system S comprised of a collection of uncoupled harmonic oscillators, each oscillator representing a single cavity mode. If we refer the energy of the ith oscillator to its corresponding ground state, the system Hamiltonian can be written as

$$H_S = \sum_i \hbar\omega_i\hat{s}_i^\dagger\hat{s}_i \ , \tag{3.4}$$

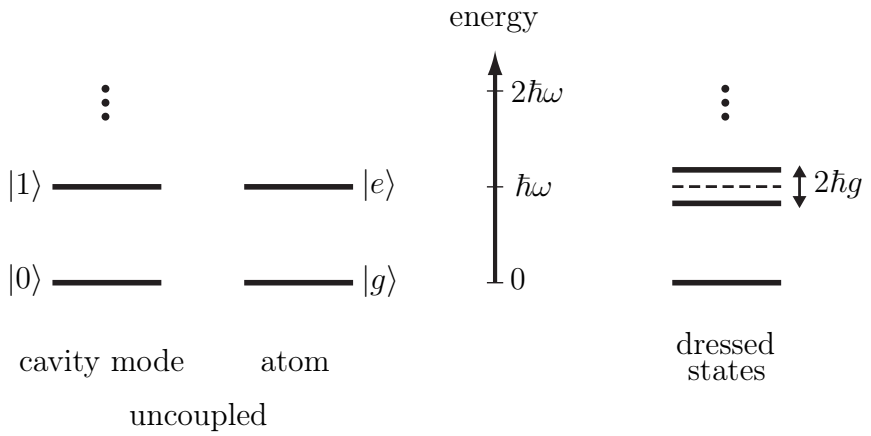

Figure 3.1 Left: energy eigenstates of the cavity mode and the two-level atom. Right: the Jaynes-Cummings ladder, i. e. energy eigenstates of the coupled atom-cavity system, up to one-quantum states. The splitting of the one-quantum energy eigenstates is referred to as the vacuum Rabi splitting.

where $\hat{s}_i^\dagger$ and $\hat{s}_i$ are the bosonic creation and annihilation operator of an harmonic oscillator with frequency ω_i.

The reservoir is modelled as a collection of harmonic oscillators, and is taken to be in the vacuum state [44]. Its density operator is written as

$$R_0 = |0\rangle\langle 0| \ , \tag{3.5}$$

and the reservoir Hamiltonian reads as

$$H_R = \sum_j \hbar\omega_j \hat{r}_j^\dagger \hat{r}_j \ , \tag{3.6}$$

where $\hat{r}_j^\dagger$ and $\hat{r}_j$ are the ladder operators of the jth reservoir oscillator with frequency ω_j.

The system Hamiltonian H_S has two non-degenerate eigenoperators [45] for each oscillator, namely $\hat{s}_i$ and $\hat{s}_i^\dagger$, with eigenfrequencies $-\omega_i$ and $+\omega_i$, respectively. Just like in the first chapter, where we discussed the interaction of a driving field with the cavity, we assume a linear coupling between the cavity and reservoir modes. The interaction Hamiltonian expanded in terms of system eigenoperators, and written in the rotating-wave approximation is

$$H_{SR} = \sum_{i,j} \hbar \left(\kappa_{i,j}^* \hat{s}_i \hat{r}_j^\dagger + \kappa_{ij} \hat{s}_i^\dagger \hat{r}_j \right) \ , \tag{3.7}$$

where the coupling constant κ_{ij} characterises the strength of the interaction between the ith system oscillator and the jth reservoir oscillator.

Equation (3.7) is a special case of equation (2.19). If we assume that different $\hat{s}_i$ couple to statistically independent reservoir modes, the master equation in Lindblad form (2.30) is immediately adapted. For the non-driven multi-mode cavity in a vacuum reservoir, we find

$$\begin{aligned}\dot{\rho}(t) = \frac{1}{\mathrm{i}\hbar}\big[H'_S, \rho(t)\big] &+ \sum_i \frac{\gamma_{\hat{s}_i}}{2}\Big(2\hat{s}_i\rho(t)\hat{s}_i^\dagger - \hat{s}_i^\dagger\hat{s}_i\rho(t) - \rho(t)\hat{s}_i^\dagger\hat{s}_i\Big) \\ &+ \sum_i \frac{\gamma_{\hat{s}_i^\dagger}}{2}\Big(2\hat{s}_i^\dagger\rho(t)\hat{s}_i - \hat{s}_i\hat{s}_i^\dagger\rho(t) - \rho(t)\hat{s}_i\hat{s}_i^\dagger\Big) \ ,\end{aligned} \tag{3.8}$$

where

$$H'_S \equiv H_S + \sum_i \frac{\hbar\Delta_{s_i}}{2}\hat{s}_i^\dagger\hat{s}_i + \sum_i \frac{\hbar\Delta_{s_i^\dagger}}{2}\hat{s}_i\hat{s}_i^\dagger \ , \tag{3.9}$$

and

$$\begin{aligned}\gamma_{s_i} &\equiv 2\mathrm{Re}\sum_{j,j'}\kappa_{ij}^*\kappa_{ij'}\int_0^\infty \mathrm{d}s\,\mathrm{tr}_R\big\{\tilde{\Gamma}_j(t)\tilde{\Gamma}_{j'}^\dagger(t-s)R_0\big\}e^{\mathrm{i}\omega_i s} \ , \\ \Delta_{s_i} &\equiv 2\mathrm{Im}\sum_{j,j'}\kappa_{ij}^*\kappa_{ij'}\int_0^\infty \mathrm{d}s\,\mathrm{tr}_R\big\{\tilde{\Gamma}_j(t)\tilde{\Gamma}_{j'}^\dagger(t-s)R_0\big\}e^{\mathrm{i}\omega_i s} \ ,\end{aligned} \tag{3.10a}$$

$$\begin{aligned}\gamma_{s_i^\dagger} &\equiv 2\mathrm{Re}\sum_{j,j'}\kappa_{ij}^*\kappa_{ij'}\int_0^\infty \mathrm{d}s\,\mathrm{tr}_R\big\{\tilde{\Gamma}_j^\dagger(t)\tilde{\Gamma}_{j'}(t-s)R_0\big\}e^{\mathrm{i}\omega_i s} \ , \\ \Delta_{s_i^\dagger} &\equiv 2\mathrm{Im}\sum_{j,j'}\kappa_{ij}^*\kappa_{ij'}\int_0^\infty \mathrm{d}s\,\mathrm{tr}_R\big\{\tilde{\Gamma}_j^\dagger(t)\tilde{\Gamma}_{j'}(t-s)R_0\big\}e^{\mathrm{i}\omega_i s} \ .\end{aligned} \tag{3.10b}$$

All we are left with to obtain the master equation in Lindblad form is to solve the integrals in equation (3.10).

Since we take the reservoir to be in the vacuum state, the traces (and therefore the integrals) in equation (3.10b) vanish. For the integral in equation (3.10a), we find

$$\begin{aligned}&2\sum_{j,j'}\kappa_{ij}^*\kappa_{ij'}\int_0^\infty \mathrm{d}s\,\mathrm{tr}_R\big\{\tilde{\Gamma}_j(t)\tilde{\Gamma}_{j'}^\dagger(t-s)R_0\big\}e^{\mathrm{i}\omega_i s} \\ =&\,2\sum_{j,j'}\kappa_{ij}^*\kappa_{ij'}\int_0^\infty \mathrm{d}s\,e^{-\mathrm{i}\omega_j t}e^{\mathrm{i}\omega_{j'}(t-s)}\,\mathrm{tr}_R\big\{\hat{\Gamma}_j\hat{\Gamma}_{j'}^\dagger R_0\big\}e^{\mathrm{i}\omega_i s} \\ =&\,2\sum_j|\kappa_{ij}|^2\int_0^\infty \mathrm{d}s\,e^{-\mathrm{i}(\omega_j-\omega_i)s} \ ,\end{aligned} \tag{3.11}$$

where we have used that $\hat{\Gamma}_j$ and $\hat{\Gamma}_{j'}$ are statistically independent for $j \neq j'$. Expression (3.11) involves a summation over the reservoir oscillators, which we are going to change to an integration. Since the electromagnetic radiation field is the reservoir, the

reservoir modes form a continuum. Hence, the summation over the reservoir modes has to be changed into an integration over a density of states $g(\omega)$; that is, there are $g(\omega)\mathrm{d}\omega$ oscillators with frequencies in the interval $(\omega, \omega + d\omega)$. With this change, expression (3.11) becomes

$$\begin{aligned} & 2\sum_j \left|\kappa_{ij}\right|^2 \int_0^\infty \mathrm{d}s\, e^{-\mathrm{i}(\omega_j-\omega_i)s} \\ &= 2\int_0^\infty \mathrm{d}\omega\, g(\omega)\left|\kappa_i\right|^2 \int_0^\infty \mathrm{d}s\, e^{-\mathrm{i}(\omega-\omega_i)s} \\ &= 2\pi g(\omega_i)\left|\kappa_i\right|^2 - 2\mathrm{i}P[\int_0^\infty \mathrm{d}\omega\, \frac{g(\omega)|\kappa_i(\omega_i)|^2}{\omega_i-\omega}] \,, \end{aligned} \tag{3.12}$$

where $P[\cdot]$ denotes the Cauchy principle value defined by

$$P[\int_a^b \frac{f(\omega)}{\omega-\omega_0}\mathrm{d}\omega] \equiv \lim_{\varepsilon\to 0}\left(\int_a^{\omega_0-\varepsilon} \frac{f(\omega)}{\omega-\omega_0}\mathrm{d}\omega + \int_{\omega_0+\varepsilon}^b \frac{f(\omega)}{\omega-\omega_0}\mathrm{d}\omega\right) \,. \tag{3.13}$$

The real and imaginary parts of equation (3.12) are γ_{s_i} and Δ_{s_i}, respectively.

Master equation for the damped electromagnetic cavity field

The master equation for a collection of damped harmonic oscillators in a vacuum reservoir is

$$\dot{\rho} = \frac{1}{\mathrm{i}\hbar}\Big[\sum_i \hbar\omega_i' s_i^\dagger s_i, \rho\Big] + \sum_i \frac{\gamma_i}{2}\left(2s_i\rho s_i^\dagger - s_i^\dagger s_i\rho - \rho s_i^\dagger s_i\right) \,, \tag{3.14}$$

with

$$\omega_i' \equiv \omega_i + \Delta_i \,, \tag{3.15}$$

and

$$\Delta_i \equiv P[\int_0^\infty \frac{g(\omega)|\kappa_i(\omega_i)|^2}{\omega_i-\omega}\mathrm{d}\omega] \,, \qquad \gamma_i \equiv 2\pi\left|\kappa_i(\omega_i)\right|^2 g(\omega_i) \,, \tag{3.16}$$

where $P[\cdot]$ denotes the Cauchy principle value. This master equation may represent the damped electromagnetic cavity field modes.

3.2.2 The single-mode cavity

For a single mode a of the cavity there is loss through both cavity mirrors; the cavity mode couples to two reservoir modes. Adopting equation (3.14), written in a frame rotating with frequency ω', we find

$$\dot{\rho}(t) = \frac{\gamma_{a1}+\gamma_{a2}}{2}\left(2\hat{a}\rho(t)\hat{a}^\dagger - \hat{a}^\dagger\hat{a}\rho(t) - \rho(t)\hat{a}^\dagger\hat{a}\right) \,, \tag{3.17}$$

where γ_{a1} and γ_{a2} are the damping rates associate with the two mirrors.

Due to the interaction with the vacuum reservoir, any initially present mean amplitude of the cavity mode decays. This can be seen by calculating the time dependence of the mean amplitude from the master equation: by multiplying equation (3.17) from the left with $\hat{a}$ and taking the trace, we find

$$\begin{aligned}\frac{\mathrm{d}}{\mathrm{d}t}\langle\hat{a}\rangle &= \tfrac{1}{2}(\gamma_{a1}+\gamma_{a2})\,\mathrm{tr}\left\{2\hat{a}\hat{a}\rho(t)\hat{a}^\dagger - \hat{a}\hat{a}^\dagger\hat{a}\rho(t) - \hat{a}\rho(t)\hat{a}^\dagger\hat{a}\right\}\\ &= \tfrac{1}{2}(\gamma_{a1}+\gamma_{a2})\,\mathrm{tr}\left\{(\hat{a}^\dagger\hat{a} - \hat{a}\hat{a}^\dagger)\hat{a}\rho(t)\right\}\\ &= -\tfrac{1}{2}(\gamma_{a1}+\gamma_{a2})\,\langle\hat{a}\rangle\ . \end{aligned} \tag{3.18}$$

It is common to introduce the *cavity mode damping rate*

$$\kappa \equiv \tfrac{1}{2}(\gamma_{a1}+\gamma_{a2})\ . \tag{3.19}$$

A non-driven cavity in a vacuum reservoir is not spectacular at all. As time goes by the cavity field decays and finally ends up in the vacuum state as well. For atom-cavity experiments we have to provide the cavity from the outside with photons. A common realisation is to drive the cavity with an external laser through one of the mirrors.

3.2.3 The coherently-driven single-mode cavity

We consider a single-mode cavity that is driven on-axis by a laser. A driving laser constantly provides the cavity with energy in the form of photons; the driving mode is distinguished from all the other reservoir modes that do not provide energy since the amplitude of the driving mode has a non-zero mean. But in the derivation of the master equation in Lindblad form in the previous chapter, the assumption of a zero mean amplitude of the reservoir modes was used. To ensure this assumption, we include the driving laser mode in the system S, such that the reservoir is again in the vacuum state.

System Hamiltonian and Master equation

The system Hamiltonian for a coherently driven cavity is given in equation (1.61). If we transform into a frame rotating at the laser frequency, and specifying the laser and cavity-mode frequencies to be resonant, the system Hamiltonian reads as

$$H_S = \mathrm{i}\hbar\mathcal{E}(\hat{a}^\dagger - \hat{a})\ . \tag{3.20}$$

Master equation for the resonantly driven, damped single-mode cavity

In a frame rotating at the laser frequency the master equation for a resonantly driven, damped single-mode cavity in a vacuum reservoir is

$$\dot{\rho} = \frac{1}{\mathrm{i}\hbar}\Big[H_S, \rho\Big] + \kappa\left(2\hat{a}\rho\hat{a}^\dagger - \hat{a}^\dagger\hat{a}\rho - \rho\hat{a}^\dagger\hat{a}\right) \tag{3.21}$$

with the cavity-mode damping rate κ, and the system Hamiltonian

$$H_S = \mathrm{i}\hbar\mathcal{E}(\hat{a}^\dagger - \hat{a}) \ , \tag{3.22}$$

where $\mathcal{E}$ denotes the laser-cavity coupling strength.

Since the driving laser constantly provides photons to the cavity, the photon input will balance the photons leaking out of the cavity, and the cavity field will eventually become steady with a finite mean photon number.

Mean photon number

To calculate the mean photon number $\langle\hat{a}^\dagger\hat{a}\rangle = \mathrm{tr}\{\hat{a}^\dagger\hat{a}\rho(t)\}$ in the resonantly driven cavity mode, we multiply the master equation (3.21) from the left hand side with $\hat{a}^\dagger\hat{a}$:

$$\begin{aligned}\frac{\mathrm{d}}{\mathrm{d}t}\langle\hat{a}^\dagger\hat{a}\rangle &= \mathrm{tr}\big\{\hat{a}^\dagger\hat{a}\big[\mathcal{E}(\hat{a}^\dagger - \hat{a}), \rho(t)\big] + \kappa\hat{a}^\dagger\hat{a}\big(2\hat{a}\rho(t)\hat{a}^\dagger - \hat{a}^\dagger\hat{a}\rho(t) - \rho(t)\hat{a}^\dagger\hat{a}\big)\big\} \\ &= \mathcal{E}\mathrm{tr}\big\{\hat{a}^\dagger(\hat{a}\hat{a}^\dagger - \hat{a}^\dagger\hat{a})\rho(t) + (\hat{a}\hat{a}^\dagger - \hat{a}^\dagger\hat{a})\hat{a}\rho(t)\big\} \\ &\quad - 2\kappa\mathrm{tr}\big\{\hat{a}^\dagger(\hat{a}\hat{a}^\dagger - \hat{a}^\dagger\hat{a})\hat{a}\rho(t)\big\} \\ &= \mathcal{E}\big(\langle\hat{a}\rangle + \langle\hat{a}^\dagger\rangle\big) - 2\kappa\langle\hat{a}^\dagger\hat{a}\rangle \ ,\end{aligned} \tag{3.23}$$

where we have used the cyclic property of the trace, and the boson commutation relation. The mean photon number remains constant in time when the system is in the steady state. Hence, we find

$$\langle\hat{a}^\dagger\hat{a}\rangle_{ss} = \frac{\mathcal{E}}{2\kappa}\big(\langle\hat{a}\rangle_{ss} + \langle\hat{a}^\dagger\rangle_{ss}\big) \ . \tag{3.24}$$

Similarly, one derives

$$\langle\hat{a}\rangle_{ss} = \langle\hat{a}^\dagger\rangle_{ss} = \frac{\mathcal{E}}{\kappa} \ , \tag{3.25}$$

which can be substituted into equation (3.24):

Mean photon number of a resonantly driven single-mode cavity in a vacuum reservoir

The mean photon number of a resonantly driven single-mode cavity in a vacuum reservoir is

$$\langle \hat{a}^\dagger \hat{a} \rangle = \left(\frac{\mathcal{E}}{\kappa} \right)^2 \ . \tag{3.26}$$

Amplitude of the driving laser

Consider the laser mode with amplitude $\mathcal{A}$ that resonantly drives the cavity mode a. Due to the resonance condition all light gets transmitted through the cavity. The photon flux out of the cavity is determined by the mean photon number in the cavity mode and the cavity mode decay rate:

$$\kappa \langle \hat{a}^\dagger \hat{a} \rangle_{ss} = \kappa (\mathcal{E}/\kappa)^2 = \mathcal{E}^2/\kappa \ . \tag{3.27}$$

Thus, photon flux conservation requires for the *amplitude of the driving field*

$$\mathcal{A} = \frac{\mathcal{E}}{\sqrt{\kappa}} \ , \tag{3.28}$$

which is written in units of the square root of photon flux.

The last step before considering a full atom-cavity system is the damping of an atom due to the interaction with the vacuum radiation field; in the atom-cavity system this interaction takes place through the sides of the cavity.

3.3 The radiatively damped two-level atom

In this section we derive the master equation in Lindblad form for the radiatively damped two-level atom. The Hamiltonian of the two-level atom is

$$H_S = \hbar \omega_A \hat{\sigma}_+ \hat{\sigma}_- \tag{3.29}$$

where $\hat{\sigma}_+$ and $\hat{\sigma}_-$ are the atomic raising and lowering operators of a non-degenerate two-level atom with energy difference $\hbar\omega_A$ between its ground and excited states (see subsection 1.3.1). Like in the previous section, the reservoir is in the vacuum state, and is modelled as a collection of harmonic oscillators. Taking different wave vectors $\boldsymbol{k}$ and polarisations λ of the reservoir modes into account, the reservoir Hamiltonian reads as

$$H_R = \sum_{\boldsymbol{k},\lambda} \hbar \omega_k \hat{r}^\dagger_{\boldsymbol{k},\lambda} \hat{r}_{\boldsymbol{k},\lambda} \ . \tag{3.30}$$

In this notation, the interaction Hamiltonian in the rotating-wave and dipole approximations (equation (1.35)) is given by

$$H_{SR} = \sum_{\boldsymbol{k},\lambda} \hbar \left(\kappa^*_{\boldsymbol{k},\lambda} \hat{\sigma}_- \hat{r}^\dagger_{\boldsymbol{k},\lambda} + \kappa_{\boldsymbol{k},\lambda} \hat{\sigma}_+ \hat{r}_{\boldsymbol{k},\lambda} \right) \tag{3.31}$$

with

$$\kappa_{\boldsymbol{k},\lambda} = e^{-\mathrm{i}\boldsymbol{k}\cdot\boldsymbol{r}_A} \sqrt{\frac{2\pi\omega_k}{\hbar L^3}}\ \boldsymbol{\pi}_{\boldsymbol{k},\lambda} \cdot \boldsymbol{d}^*_{ge}\ . \tag{3.32}$$

To find the master equation in Lindblad from we have to go through a similar calculation as in the previous section; with the only difference that in the integrals in equation (3.10) the summation over the reservoir oscillators has to be changed into a summation over wave vector directions and polarisation states. Going again through the calculation does not give any new insights; thus, we skip all intermediate steps, and simply state the result:

$$\gamma \equiv 2\pi \sum_\lambda \int \mathrm{d}^3k\, g(\boldsymbol{k}) |\kappa(\boldsymbol{k},\lambda)|^2 \delta(\omega_k - \omega_A)\ , \tag{3.33}$$

$$\Delta \equiv \sum_\lambda P[\int \mathrm{d}^3k\, \frac{g(\boldsymbol{k})|\kappa(\boldsymbol{k},\lambda)|^2}{\omega_A - \omega_k}]\ , \tag{3.34}$$

where $\omega_k = kc$. These two expressions can be further evaluated; in the following paragraph we draft this evaluation.

The electromagnetic field is quantised by fitting plane waves into a cube of length L with periodic boundary conditions. Thus, the plane waves that fit into the cube have wave numbers $\boldsymbol{k} = 2\pi(n_x, n_y, n_z)/L$ with integers n_x, n_y and n_z, and the density of possible wave vectors is

$$g(\boldsymbol{k}) = \left(\frac{L}{2\pi}\right)^3\ . \tag{3.35}$$

Using this equation and transforming into spherical coordinates, we have

$$g(\boldsymbol{k})\mathrm{d}^3k = \left(\frac{L}{2\pi}\right)^3 k^2 \mathrm{d}k \sin(\theta)\mathrm{d}\theta\mathrm{d}\phi = \frac{\omega_k^2 L^3}{8\pi^3 c^3} \mathrm{d}\omega_k \sin(\theta)\mathrm{d}\theta\mathrm{d}\phi\ . \tag{3.36}$$

We choose the k_z-axis parallel to $\boldsymbol{d}_{21}$, and for each $\boldsymbol{k}$, polarisation states λ_1 and λ_2 such that $\boldsymbol{\pi}_{\boldsymbol{k},\lambda_1} \cdot \boldsymbol{d}^*_{ge} = 0$. With this choice and equations (3.32, 3.36), the evaluation of the integral (3.33) is straight forward. We obtain

$$\gamma = \frac{4\omega_A^3 |\boldsymbol{d}_{ge}|^2}{3\hbar c^3}\ , \tag{3.37}$$

$$\Delta = \frac{2|\boldsymbol{d}_{ge}|^2}{3\hbar\pi c^3} P[\int_0^\infty \mathrm{d}\omega\, \frac{\omega^3}{\omega_A - \omega}]\ . \tag{3.38}$$

The damping constant γ is the atomic decay rate due to spontaneous emission. The obtained γ agrees with the *Einstein A coefficient* from the Wigner-Weisskopf theory of natural linewidth [46].

Δ represents a frequency shift of the free atomic transition frequency to an effective resonance frequency ω'_A. The Δ we observed in equation (3.38) diverges, our model is unrealistic in this point. Only a fully relativistic Hamiltonian and QED renormalisation make this shift finite—experimentally observed as the *Lamb shift*. The Lamb shift is normally much smaller than the free atomic transition frequency and can be neglected; or at least absorbed into the definition of the atomic transition frequency.

Master equation for the radiatively damped two-level atom

The master equation for a radiatively damped two-level atom in a vacuum reservoir is

$$\dot{\rho}(t) = \frac{1}{\mathrm{i}\hbar}[\hbar\omega'_A\hat{\sigma}_+\hat{\sigma}_-, \rho(t)] + \frac{\gamma}{2}\left(2\hat{\sigma}_-\rho(t)\hat{\sigma}_+ - \hat{\sigma}_+\hat{\sigma}_-\rho(t) - \rho(t)\hat{\sigma}_+\hat{\sigma}_-\right) \tag{3.39}$$

with an effective atomic resonance frequency ω'_A including the Lamb shift, and the atomic decay rate

$$\gamma = \frac{4\omega_A^3|\boldsymbol{d}_{ge}|^2}{3\hbar c^3}\ . \tag{3.40}$$

We are now in the position to put all the atom-cavity, atom-reservoir, and cavity-reservoir interactions together and to describe a driven atom-cavity system in the following section.

3.4 The driven single-atom two-mode cavity QED system

We are now in a position to model fully the cavity QED experiment introduced in section 1.1, where two optical cavity modes interact on resonance with a single atom that is localised in the centre of the cavity. The atom and the cavity modes are both coupled to the electromagnetic radiation field of the environment: the cavity modes decay due to loss through the mirrors, and the atom spontaneously emits photons that exit out the sides of the cavity. We denote the cavity mode decay rate as κ. For the spontaneous emission rate γ we use the full Einstein A coefficient, which is a good approximation if the solid angle subtended by the cavity modes is very small. A cavity of this type is used in the experimental realisation of two-mode cavity QED [21].

As mentioned in the derivation of the system Hamiltonian in section 1.4, we investigate two models that differ in the atomic level structure. In the simple model

we consider a simple two-level atom that couples to the two cavity modes, and in a more precise model we take the degeneracy of the atomic levels into account.

3.4.1 Two-level atom

For a simple two-level atom, we do not account for different polarisations of the light from spontaneous emission events that exits out the side of the cavity. Thus, there are three decay channels: one for each mode and one for spontaneous emission.

Master equation for the two-level atom two-mode cavity QED system

In a frame rotating at the frequency of the driving laser, the master equation for the two-level atom two-mode cavity QED is

$$\begin{aligned}\dot{\rho}(t) = \frac{1}{\mathrm{i}\hbar}[H_S, \rho(t)] &+ \kappa\left(2\hat{a}\rho(t)\hat{a}^\dagger - \hat{a}^\dagger\hat{a}\rho(t) - \rho(t)\hat{a}^\dagger\hat{a}\right) \\ &+ \kappa\left(2\hat{b}\rho(t)\hat{b}^\dagger - \hat{b}^\dagger\hat{b}\rho(t) - \rho(t)\hat{b}^\dagger\hat{b}\right) \\ &+ \frac{\gamma}{2}\left(2\hat{\sigma}_-\rho(t)\hat{\sigma}_+ - \hat{\sigma}_+\hat{\sigma}_-\rho(t) - \rho(t)\hat{\sigma}_+\hat{\sigma}_-\right) \ ,\end{aligned} \tag{3.41}$$

where κ and γ denote the cavity mode and atomic decay rates respectively, and the system Hamiltonian is given by

$$H_S = \mathrm{i}\hbar\mathcal{E}(\hat{a}^\dagger - \hat{a}) + \mathrm{i}\hbar g_a\left(\hat{a}^\dagger\hat{\sigma}_- - \hat{a}\hat{\sigma}_+\right) + \mathrm{i}\hbar g_b\left(\hat{b}^\dagger\hat{\sigma}_- - \hat{b}\hat{\sigma}_+\right) \ . \tag{3.42}$$

3.4.2 Two-level atom with Zeeman sub-structure

If we include the degeneracy of the atomic levels in our model, we also have to take into account the polarisation of the light that exits out the side of the cavity. Atomic dipole transitions with different Δm_F refer to light with different polarisation, and couple to statistically independent reservoirs. Thus, the master equation comprises five decay channels: one for each of the two cavity modes, and three for spontaneous emission events of the atom, that is, one for each of $\Delta m_F = -1, 0, 1$ transitions.

Master equation for the Zeeman sub-structured two-level atom, two-mode cavity QED system

In a frame rotating at the frequency of the driving laser the master equation for a

Zeeman sub-structured two-level atom, two-mode cavity QED system is

$$\begin{aligned}\dot{\rho}(t) = \frac{1}{\mathrm{i}\hbar}[H_S, \rho(t)] &+ \kappa\left(2\hat{a}\rho(t)\hat{a}^\dagger - \hat{a}^\dagger\hat{a}\rho(t) - \rho(t)\hat{a}^\dagger\hat{a}\right) \\ &+ \kappa\left(2\hat{b}\rho(t)\hat{b}^\dagger - \hat{b}^\dagger\hat{b}\rho(t) - \rho(t)\hat{b}^\dagger\hat{b}\right) \\ &+ \frac{\gamma}{2}\sum_{p=0,\pm1}\left(2\hat{\Sigma}_p\rho(t)\hat{\Sigma}_p^\dagger - \hat{\Sigma}_p^\dagger\hat{\Sigma}_p\rho(t) - \rho(t)\hat{\Sigma}_p^\dagger\hat{\Sigma}_p\right)\end{aligned} \tag{3.43}$$

where κ and γ denote the cavity mode and atomic decay rates respectively, and the system Hamiltonian is given by

$$\begin{aligned}H_S = \mathrm{i}\hbar\mathcal{E}_L(\hat{a}^\dagger - \hat{a}) &+ \mathrm{i}\hbar g\left(\hat{a}^\dagger\hat{\Sigma}_0 - \hat{a}\hat{\Sigma}_0^\dagger\right) \\ &+ \mathrm{i}\hbar g\left(\hat{b}^\dagger\left(\frac{\hat{\Sigma}_{-1} + \hat{\Sigma}_{+1}}{\sqrt{2}}\right) - \hat{b}\left(\frac{\hat{\Sigma}_{-1}^\dagger + \hat{\Sigma}_{+1}^\dagger}{\sqrt{2}}\right)\right).\end{aligned} \tag{3.44}$$

The atomic operators Σ_p have expansion in terms of atomic states and appropriate Clebsch-Gordan coefficients; for an $F = 3$ to $F' = 4$ transition, they are given in equation (1.73a).

In the next chapter we investigate these two models using an analytic approach based on quantum trajectory theory.

Chapter 4

Two-Mode Cavity Quantum Electrodynamics I: Analytic Investigations

Having seen how to describe the interaction of a cavity QED system with its environment, we are now in a position to analyse the particular two-mode cavity QED system introduced in the first section of Chapter 1.

The first objective of our analysis is to characterise the QED system in the weak-excitation limit; this forms the content of Chapter 4. 'Weak excitation' means that the average photon number in the cavity is very small—or equivalently, that the driving field strength is weak. To ensure that the average photon number is small enough, most of the time there are no photons in the cavity at all. This enables the assumption that, once a photon is emitted from the cavity, we can neglect the possibility of any further photon emissions while the system relaxes to its steady state. The formulation of this approximation is presented in the first section.

In the second section, we adopt this approximation method for our two-mode cavity QED model with a non-degenerate two-level atom. We calculate analytic expressions for steady state properties, similar to the work of Eleuch *et al* [47], including second-order photon correlation functions.

In the final section, we consider a model with the full atomic level structure. We identify an additional time scale of the correlations from the possible system states. Even though an analytic calculation would be possible in principle, we refrain from doing so due to its complexity—the corresponding steady state properties and photon correlation functions are numerically calculated in the next chapter.

4.1 Method

We investigate the weak-excitation limit, where two approximations can be made. The combination of these approximations results in a method that makes use of a perturbation expansion in the driving field strength $\mathcal{E}$. This enables us to find analytic solutions for some system properties in the following sections.

4.1.1 Pure-state factorisation

Under the weak-excitation condition, we aim to simplify the master equation

$$\dot{\rho} = \mathcal{L}\rho \ , \tag{4.1}$$

where the Liouvillian is defined by

$$\mathcal{L}\cdot \equiv \frac{1}{\mathrm{i}\hbar}\big[H_S', \cdot\big] + \sum_i \frac{\gamma_i}{2}\left(2\hat{A}_i \cdot \hat{A}_i^\dagger - \hat{A}_i^\dagger \hat{A}_i \cdot - \cdot \hat{A}_i^\dagger \hat{A}_i\right) \ . \tag{4.2}$$

Within the quantum trajectory theory in section 2.2, we identified collapses of the system that are related to the interaction of the system with its environment. These collapses are represented by the terms $2\hat{A}_i \cdot \hat{A}_i^\dagger$ in the Liouvillian, and give a mixed-state character to the density operator.

If we assume a very weak excitation of the system, the probability of an interaction with the environment through a photon emission is very small. In this situation the coherent time-evolution is seldom interrupted and the system undergoes, at least to a good approximation, a pure state evolution during relaxation. This approximation of the evolution is equivalent to neglecting the terms $2\hat{A}_i \cdot \hat{A}_i^\dagger$ in the Liouvillian:

$$\mathcal{L}\cdot \approx \frac{1}{\mathrm{i}\hbar}\big[H_S', \cdot\big] - \sum_i \frac{\gamma_i}{2}\big[\hat{A}_i^\dagger \hat{A}_i, \cdot\big]_+ \ , \tag{4.3}$$

where $[\cdot,\cdot]_+$ denotes the anti-commutator. Since the approximate Liouvillian consists only of commutators and anti-commutators, the density matrix factorises into a pure state whose relaxation toward a stationary state is described by the non-unitary Schrödinger equation,

$$|\dot{\Psi}(t)\rangle = \frac{1}{\mathrm{i}\hbar} H_{\mathrm{eff}} |\Psi(t)\rangle \ , \tag{4.4}$$

with the non-Hermitian effective Hamiltonian

$$H_{\mathrm{eff}} \equiv H_S' - \mathrm{i}\hbar \sum_i \frac{\gamma_i}{2} \hat{A}_i^\dagger \hat{A}_i \ . \tag{4.5}$$

Note that the Schrödinger equation (4.4) describes a coherent relaxation of the system. Therefore, we have to explicitly "force" photon emissions by hand if we want to calculate correlation functions. Thus, our strategy is to find the steady state of the system first, annihilate a photon from this steady state to simulate a photon emission, then finally observe the dynamics—especially the emission probability for a second photon—while the system relaxes back to the steady state.

4.1.2 Expansion of the density operator

The second approximation we want to introduce is in fact more a conseqence of the pure-state factorisation than an independent concept. Since the density operator factorises into a pure state, we can write any system state $|\Psi(t)\rangle$ as a linear combination of basis states. In our two-mode cavity QED system, each basis state might label the internal state of the atom and the photon number state of each cavity mode.

In the weak excitation regime the cavity contains no photons most of the time, very seldom one photon is present, and barely ever two or more photons. Thus, states with more than two photons in the cavity can be neglected. This allows us to tackle the dynamics of our system analytically by truncating the infinitely large Hilbert space, and expanding $|\Psi(t)\rangle$ in a two-quanta basis. In this two-quanta basis the atom is either in the ground state and up to two photons in the cavity, or the atom is excited and at most one photon is in the cavity.

To calculate second-order photon correlation functions the inclusion of the two-quanta states in the truncation of the Hilbert space is essential. If we were only interested in the mean photon number or mode amplitudes, then an expansion in a one-quantum basis would be sufficient.

4.2 Non-degenerate two-level atom

The Hamiltonian and the master equation for a non-degenerate two-level atom in a driven two-mode cavity is given by equations (3.41) and (3.42). For our purposes, in this section we modify the Hamiltonian slightly:

$$H = \mathrm{i}\hbar g\big(\hat{a}^\dagger\hat{\sigma}^+ - \hat{a}\hat{\sigma}^-\big) + \mathrm{i}\hbar\eta g\big(\hat{b}^\dagger\sigma^+ - \hat{b}\sigma^-\big) + \mathrm{i}\hbar\mathcal{E}\hat{a}^\dagger \ , \tag{4.6}$$

where we have defined the *ratio factor of the coupling constants* $\eta \equiv \frac{g_b}{g_a}$, which takes into account the Clebsch-Gordan coefficients of the electric dipole transitions that link the two levels. Furthermore, we have neglected the term $\mathrm{i}\hbar\mathcal{E}\hat{a}$, since it gives a contribution only at higher order in $\mathcal{E}$. Using the approximated Liouvillian of equation (4.3), the *master equation for a single non-degenerate two-level atom, two-mode cavity QED system in the weak-excitation limit* is

$$\dot{\rho}(t) = \frac{1}{\mathrm{i}\hbar}[H,\rho(t)] + \kappa[\hat{a}^\dagger\hat{a},\rho(t)]_+ + \kappa[\hat{b}^\dagger\hat{b},\rho(t)]_+ + \frac{\gamma}{2}[\hat{\sigma}^+\hat{\sigma}^-,\rho(t)]_+ \ . \tag{4.7}$$

Thus, the non-unitary Schrödinger equation

$$|\dot{\Psi}(t)\rangle = \frac{1}{\mathrm{i}\hbar}\bigg(H - \mathrm{i}\hbar\Big(\kappa\big(\hat{a}^\dagger\hat{a} + \hat{b}^\dagger\hat{b}\big) + \frac{\gamma}{2}\hat{\sigma}^+\hat{\sigma}^-\Big)\bigg)|\Psi(t)\rangle \tag{4.8}$$

describes the coherent time-evolution between successive photon emissions.

The *two-quanta basis for a single non-degenerate two-level atom in a two-mode cavity* is

$$\Big\{|g00\rangle, |e00\rangle, |g10\rangle, |g01\rangle, |e10\rangle, |e01\rangle, |g11\rangle, |g20\rangle, |g02\rangle\Big\} \,, \tag{4.9}$$

which may be written as $|ijk\rangle$, where $i = \{g, e\}$ labels the atomic ground and excited state, and j and k are the numbers of photons in the driven and non-driven modes, respectively. We expand a general system state $|\Psi(t)\rangle$ in this basis:

$$\begin{aligned} |\Psi(t)\rangle = |g00\rangle &+ A_{e00}(t)|e00\rangle + A_{g10}(t)|g10\rangle + A_{g01}(t)|g01\rangle \\ &+ B_{e10}(t)|e10\rangle + B_{e01}(t)|e01\rangle + B_{g11}(t)|g11\rangle \\ &+ B_{g20}(t)|g20\rangle + B_{g02}(t)|g02\rangle \,, \end{aligned} \tag{4.10}$$

where the time-evolution of the general system state is described by the time-dependence of the state amplitudes. The normalisation is chosen such that the state amplitude of $|g00\rangle$ is unity at all times. This is certainly only an approximation, because the amplitudes of the other states contribute to the norm as well. But, since all excitations originate from the (weak) driving field in the first place, this approximation is well-founded, at least to leading order in $\mathcal{E}$.

Substituting the expanded state of equation (4.10) into the Schrödinger equation (4.8) results in two sets of coupled differential equations for the time-varying state amplitudes. These differential equations are the *equations of motion in the two-quanta truncation of the master equation for a single non-degenerate two-level atom in two-mode cavity QED*:

$$\dot{A}(t) = D_A A(t) + d_A \tag{4.11a}$$

$$\dot{B}(t) = D_B B(t) + d_B(t) \tag{4.11b}$$

with

$$A(t) \equiv \begin{pmatrix} A_{e00}(t) \\ A_{g10}(t) \\ A_{g01}(t) \end{pmatrix} \,, \quad d_A \equiv \begin{pmatrix} 0 \\ \mathcal{E} \\ 0 \end{pmatrix} \,, \quad D_A \equiv \begin{pmatrix} -\frac{\gamma}{2} & -g & -\eta g \\ g & -\kappa & 0 \\ \eta g & 0 & -\kappa \end{pmatrix} \,, \tag{4.12a}$$

$$B(t) \equiv \begin{pmatrix} B_{e10}(t) \\ B_{e01}(t) \\ B_{g11}(t) \\ B_{g20}(t) \\ B_{g02}(t) \end{pmatrix} \,, \qquad d_B(t) \equiv \begin{pmatrix} \mathcal{E} A_{e00}(t) \\ 0 \\ \mathcal{E} A_{g01}(t) \\ \sqrt{2}\mathcal{E} A_{g10}(t) \\ 0 \end{pmatrix} \,, \tag{4.12b}$$

$$D_B \equiv \begin{pmatrix} -\left(\frac{\gamma}{2}+\kappa\right) & 0 & -\eta g & -\sqrt{2}g & 0 \\ 0 & -\left(\frac{\gamma}{2}+\kappa\right) & -g & 0 & -\sqrt{2}\eta g \\ \eta g & g & -2\kappa & 0 & 0 \\ \sqrt{2}g & 0 & & -2\kappa & 0 \\ 0 & \sqrt{2}\eta g & 0 & 0 & -2\kappa \end{pmatrix} \,. \tag{4.12c}$$

Note 4.1 Within each differential equation, all coefficients are from states of the same order in $\mathcal{E}$. This must be the case for consistency, and is the underlying reason for dropping the term $i\hbar\mathcal{E}\hat{a}$ in the Hamiltonian earlier in this subsection. ◀

From the dynamics of the state amplitudes we can deduce the steady state and photon correlation functions; this is subject of the next two subsections.

4.2.1 Steady state

In the steady state regime the state coefficients are stationary in time:

$$A(t) \to A_{ss} \qquad \text{with} \qquad \dot{A}_{ss}(t) = 0 \tag{4.13a}$$

$$B(t) \to B_{ss} \qquad \text{with} \qquad \dot{B}_{ss}(t) = 0 \ . \tag{4.13b}$$

Thus, setting the time-derivative in equation (4.11a) to zero results in

$$A_{ss} = -D_A^{-1} d_A \ , \tag{4.14}$$

with

$$(A_{e00})_{ss} = -\frac{C\kappa}{(C'+1)g}\left(\frac{\mathcal{E}}{\kappa}\right) \tag{4.15a}$$

$$(A_{g10})_{ss} = \frac{(1+\eta^2 C)}{(C'+1)}\left(\frac{\mathcal{E}}{\kappa}\right) \tag{4.15b}$$

$$(A_{g01})_{ss} = \frac{\eta g}{\kappa}(A_{e00})_{ss} \ , \tag{4.15c}$$

where we have defined the *atomic cooperativity* by

$$C \equiv \frac{2g^2}{\kappa\gamma} \ , \tag{4.16}$$

and the *2-mode atomic cooperativity* by

$$C' \equiv \left(1+\eta^2\right) C \ . \tag{4.17}$$

The steady state coefficients $(B_{ijk})_{ss}$ are given by

$$\dot{B}_{ss}(t) = 0 \quad \Rightarrow \quad B_{ss} = -D_B^{-1} d_{B,ss} \tag{4.18}$$

and read explicitly:

$$(B_{e10})_{ss} = -\frac{fg(2+f+2C\eta^2)}{2\kappa(1+C')(2+f+2C')}\left(\frac{\mathcal{E}}{\kappa}\right)^2 \ , \tag{4.19a}$$

$$(B_{e01})_{ss} = \frac{Cf\eta g}{\kappa(1+C')(2+f+2C')}\left(\frac{\mathcal{E}}{\kappa}\right)^2 \ , \tag{4.19b}$$

$$(B_{g11})_{ss} = \frac{\eta g}{\kappa}(B_{e10})_{ss} \ , \tag{4.19c}$$

$$(B_{g20})_{ss} = \frac{2(1+C\eta^2)^2 + f(1+C(\eta^2-1))}{\sqrt{2}(1+C')(2+f+2C')}\left(\frac{\mathcal{E}}{\kappa}\right)^2 \ , \tag{4.19d}$$

$$(B_{g02})_{ss} = \frac{\eta g}{\sqrt{2}\kappa}(B_{e01})_{ss} \ , \tag{4.19e}$$

where $f \equiv \frac{4\kappa}{\gamma}$ is the ratio of the cavity-mode and the atomic decay rates.

We use this steady state to calculate the photon correlation functions in the next subsection.

4.2.2 Steady state photon correlation functions

The steady state second-order photon correlation functions are defined as

$$g^{(2)}_{\mu\nu}(\tau) = \frac{\langle \mu^\dagger(0)\nu^\dagger(\tau)\nu(\tau)\mu(0)\rangle_{ss}}{\langle \mu^\dagger\mu\rangle_{ss}\langle \nu^\dagger\nu\rangle_{ss}} \ , \qquad \tau \geq 0 \ , \tag{4.20}$$

for $\mu\nu = aa$, ab, ba and bb. The subscript ss indicates that we take the system to be in the steady state regime at time $\tau = 0$, when a photon of the driven or non-driven mode is emitted through the cavity mirrors. With this photon emission the steady state wavefunction collapses to the *reduced wavefunction* $\Psi^{(ca)}(0)$ or $\Psi^{(cb)}(0)$ depending on whether the emitted photon is from the driven or non-driven mode, respectively.

With the initial wavefunction expanded in the two-quanta basis, the reduced wavefunction can be expanded in the one-quanta basis:

$$|\Psi^{(ca)}(\tau)\rangle = |g00\rangle + A^{(ca)}_{e00}(t)|e00\rangle + A^{(ca)}_{g10}(t)|g10\rangle + A^{(ca)}_{g01}(t)|g01\rangle \ , \tag{4.21a}$$

$$|\Psi^{(cb)}(\tau)\rangle = |g00\rangle + A^{(cb)}_{e00}(t)|e00\rangle + A^{(cb)}_{g10}(t)|g10\rangle + A^{(cb)}_{g01}(t)|g01\rangle \ , \tag{4.21b}$$

with initial conditions

$$|\Psi^{(ca)}(0)\rangle = \frac{a|\Psi\rangle_{ss}}{\sqrt{\langle a^\dagger a\rangle_{ss}}} \qquad \text{and} \qquad |\Psi^{(cb)}(0)\rangle = \frac{b|\Psi\rangle_{ss}}{\sqrt{\langle b^\dagger b\rangle_{ss}}} \ , \tag{4.22a}$$

where

$$A^{(ca)}_{e00}(0) = \frac{(B_{e10})_{ss}}{(A_{g10})_{ss}} \ , \qquad A^{(cb)}_{e00}(0) = \frac{(B_{e01})_{ss}}{(A_{g01})_{ss}} \ , \tag{4.22b}$$

$$A^{(ca)}_{g10}(0) = \frac{\sqrt{2}(C_{g20})_{ss}}{(A_{g10})_{ss}} \ , \qquad A^{(cb)}_{g10}(0) = \frac{(B_{g11})_{ss}}{(A_{g01})_{ss}} \ , \tag{4.22c}$$

$$A^{(ca)}_{g01}(0) = \frac{(B_{g11})_{ss}}{(A_{g10})_{ss}} \ , \qquad A^{(cb)}_{g01}(0) = \frac{\sqrt{2}(C_{g02})_{ss}}{(A_{g01})_{ss}} \ . \tag{4.22d}$$

The reduced wavefunctions are renormalised such that the basis states of highest order in $\mathcal{E}$ have a unit amplitude. Thus, the correlation functions (4.20) become

$$g^{(2)}_{aa}(\tau) = \frac{\langle \Psi^{(ca)}(\tau)|a^\dagger a|\Psi^{(ca)}(\tau)\rangle}{\langle a^\dagger a\rangle_{ss}} = \frac{|A^{(ca)}_{g10}(\tau)|^2}{|(A_{g10})_{ss}|^2} \ , \tag{4.23a}$$

and

$$g^{(2)}_{ab}(\tau) = \frac{|A^{(ca)}_{g01}(\tau)|^2}{|(A_{g01})_{ss}|^2} \ , \quad g^{(2)}_{ba}(\tau) = \frac{|A^{(cb)}_{g10}(\tau)|^2}{|(A_{g10})_{ss}|^2} \ , \quad g^{(2)}_{bb}(\tau) = \frac{|A^{(cb)}_{g01}(\tau)|^2}{|(A_{g01})_{ss}|^2} \ . \tag{4.23b}$$

Evidently, the dynamics of the state coefficients of the reduced wavefunctions determine the correlation functions. After the photon emission, the reduced wavefunction undergoes a pure state evolution governed by the Schrödinger equation (4.8). Thus, aside from the notational difference in the superscripts, equation (4.11a) is the equation of motion for the coefficients of the reduced wavefunctions, which we have to solve.

For a general solution of equation (4.11a) we transform into a coordinate system in which D_A becomes diagonal. If T is the matrix whose columns are the right eigenvectors of D_A, then $\Lambda \equiv T^{-1} D_A T$ is a diagonal matrix with the right eigenvalues of D_A on the diagonal, i. e.,

$$T = \begin{pmatrix} 0 & \frac{-\mu+\omega}{\eta g} & \frac{-\mu-\omega}{\eta g} \\ -\eta & 1 & 1 \\ 1 & \eta & \eta \end{pmatrix} , \qquad \Lambda = \begin{pmatrix} -\kappa & 0 & 0 \\ 0 & -\Gamma + \mathrm{i}\omega & 0 \\ 0 & 0 & -\Gamma + \mathrm{i}\omega \end{pmatrix} , \tag{4.24}$$

where

$$\Gamma \equiv \frac{\gamma/2 + \kappa}{2} , \qquad \mu \equiv \frac{\gamma/2 - \kappa}{2} , \qquad \omega \equiv \sqrt{g^2(1+\eta^2) - \mu^2} . \tag{4.25}$$

With these definitions we find

$$\dot{A}(t) = D_A A(t) + d_A \quad \Rightarrow \quad \frac{\mathrm{d}}{\mathrm{d}t}\big(T^{-1}A(t)\big) = \Lambda\big(T^{-1}A(t)\big) + T^{-1} d_A , \tag{4.26}$$

from which it follows that

$$A(t) = T e^{\Lambda t} T^{-1}\big(A(0) - A_{ss}\big) + A_{ss} . \tag{4.27}$$

With T and Λ from equation (4.24) and the initial conditions from equations (4.22), we find for the correlation functions:

Second-order photon correlation functions for single, non-degenerate, two-level atom, two-mode cavity QED in the weak excitation limit

In the weak excitation limit, the second-order correlation functions for a two-mode optical cavity interacting with a single non-degenerate two-level atom are

$$g^{(2)}_{aa}(\tau) = \big(1 - L\Omega(\tau) e^{-\Gamma\tau}\big)^2 , \tag{4.28a}$$

$$g^{(2)}_{ab}(\tau) = g^{(2)}_{ba}(\tau) = \big(1 - KL\Omega(\tau) e^{-\Gamma\tau}\big)^2 , \tag{4.28b}$$

$$g^{(2)}_{bb}(\tau) = \big(1 - K^2 L\Omega(\tau) e^{-\Gamma\tau}\big)^2 , \tag{4.28c}$$

where $\tau \geq 0$ and

$$K \equiv -\frac{C}{1 + C\eta^2} , \tag{4.29a}$$

$$L \equiv \frac{\kappa}{2\Gamma + C'\gamma/2} , \tag{4.29b}$$

$$\Omega(\tau) \equiv \cos(\omega\tau) + \frac{\Gamma}{\omega}\sin(\omega\tau) . \tag{4.29c}$$

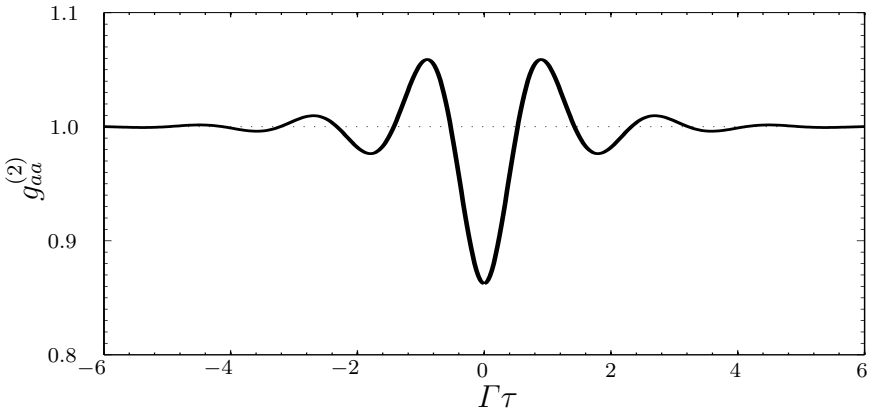

(a)

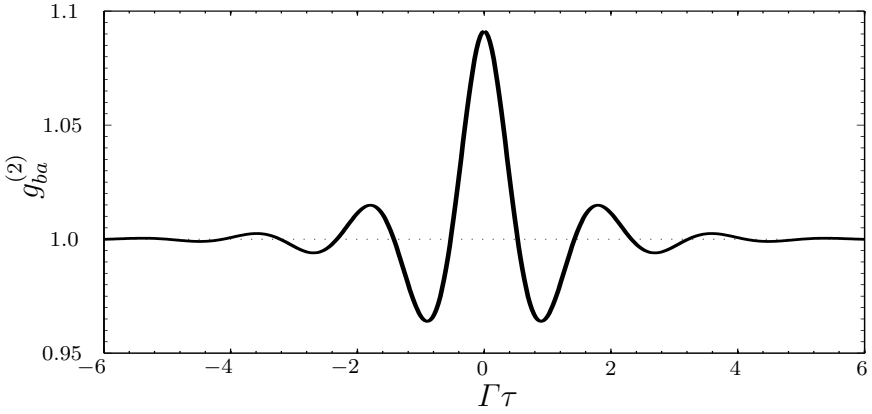

(b)

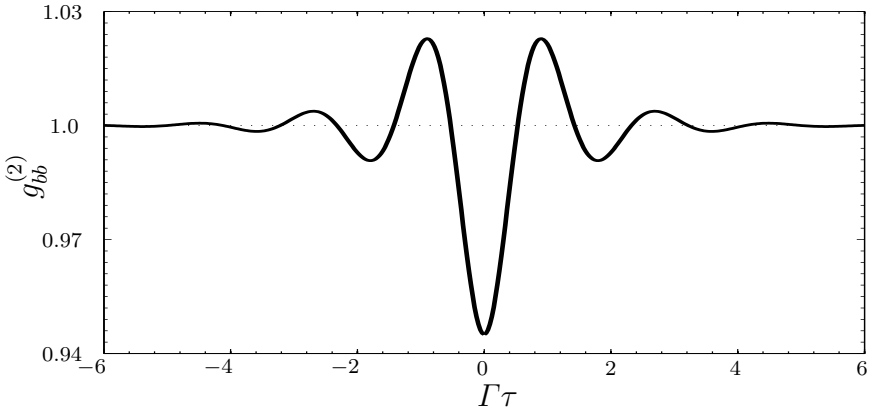

(c)

Figure 4.1 Analytic second-order correlation functions for a non-degenerate two-level atom in a two-mode cavity in the weak-excitation regime for $\gamma/\kappa = 6$, $g/\kappa = 5$, and $\eta = 1$: (a) driven-mode self-correlation function, (b) two-mode cross-correlation function, (c) non-driven-mode self-correlation function.

Figure 4.1 shows the second-order correlation functions for an illustrative set of parameters. The self-correlation functions of both the driven and the non-driven mode show photon antibunching similar to that observed in [14, 15, 16] for many-atom systems. All correlation functions show decaying oscillations, with the decay time determined by the atomic and cavity lifetimes. The oscillations, which only occur for strong coupling ($g > \kappa, \gamma/2$), are determined by the dipole coupling strength g and decay on a time-scale determined by the inverse of the average of the damping rates $\gamma/2$ and κ.

So far the considerations included the degeneracy of the atom only in terms of the different coupling strengths of the atom to the two modes. In the next section we take the degeneracy explicitly into account, and we see that this changes the dynamics of the system dramatically.

4.3 Two-level atom with Zeeman substructure

4.3.1 Possible system states

Initial condition

In the experiment we model, the atom is prepared in the $m_F = 0$ ground state of an $F = 3$ to $F' = 4$ transition when it enters the cavity. All possible initial system states in the two-quanta basis are shown in figure 4.2, where a system state is labelled with the photon numbers of the two cavity modes written next to the atomic state.

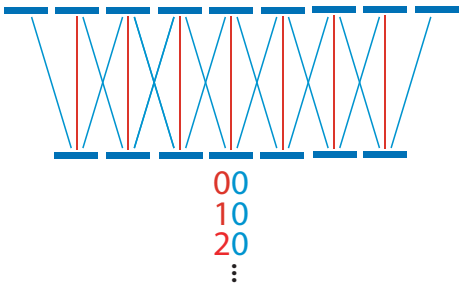

Figure 4.2 Initial condition of the investigated two-mode cavity QED system: the atom is prepared in the $m_F = 0$ ground state, and there are no photons in the non-driven cavity mode.

Before the first photon leaves the cavity, the atom interacts with the cavity field by absorbing and emitting photons, and the driving laser might increase or decrease the number of photons in the driven mode. All system states that can be reached by these interaction process can be expressed as a superposition of a manifold M_1 of basis states as shown in figure 4.3a. It is notable that not all imaginable two-quanta states occur in this basis, e. g. the $m_F = \pm 1$ atomic ground state with no photons in the cavity is not present.

After the system reaches a stationary state, at some point a photon is emitted through the cavity mirror, and the steady state wavefunction collapses.

Collapsed wavefunctions

If a photon of the driven mode is emitted, the wavefunction will collapse. The reduced wavefunction can also be expanded in the basis states of the manifold M_1. This is not too surprising, since all the states that can emit a photon of the driven mode are pumped by the laser in the first place.

After the first emission of a photon of the non-driven mode, the wave function collapses as well. But this time the reduced wavefunction cannot be expanded in the basis states of the manifold M_1. A new manifold of basis states, M_2, is necessary. The basis states of this manifold, which is orthogonal to M_1, are shown in figure 4.3b.

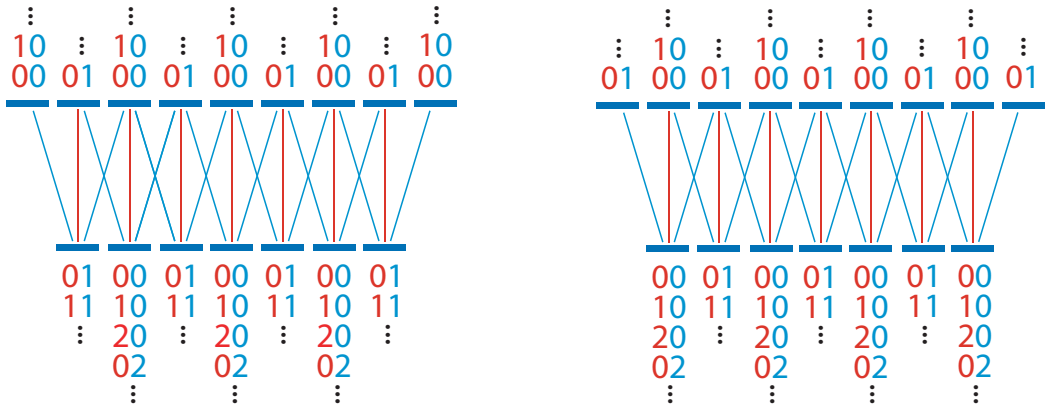

(a) Manifold M_1 **(b)** Manifold M_2

Figure 4.3 In the weak-excitation limit there exist two orthogonal manifolds of basis states, M_1 and M_2.

4.3.2 Identification of two correlation time-scales

The two identified manifolds M_1 and M_2 of basis states have in common that the system state stays within each manifold if a photon of the driven mode is emitted, but flips to the other manifold if the emitted photon is from the non-driven mode. This is illustrated in figure 4.4.

As a consequence of this behaviour, the system dynamics is correlated on two distinct time-scales:

- One time-scale reflects the intra-manifold relaxation of the system after each photon emission. This time-scale is determined by the atomic and cavity

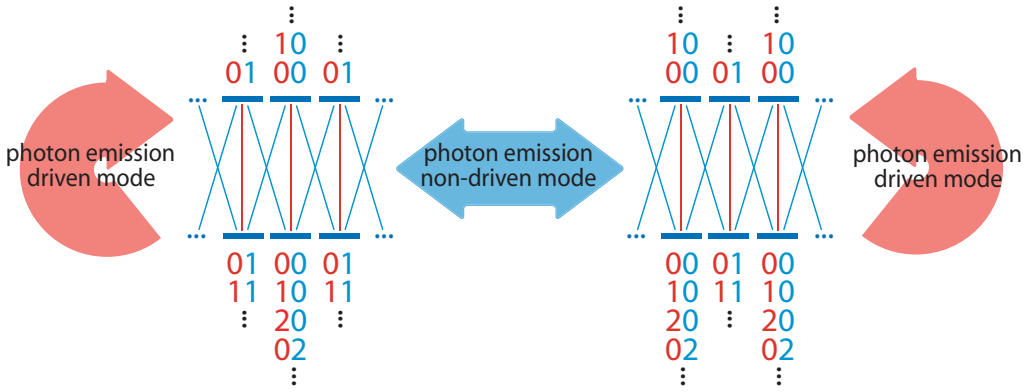

Figure 4.4 The system switches back and forth between the two manifolds of basis states each time a photon of the non-driven mode is emitted from the cavity.

lifetimes, and is very similar to the correlation time scale observed for the non-degenerate two-level atom in the previous section.

- The second time-scale, not previously present, reflects the back-and-forth switching between the two manifolds of basis states each time a photon of the non-driven mode is emitted. This time-scale is determined by the inverse of the photon emission rate of the non-driven mode—hence, for $\mathcal{E}/\kappa \to 0$ it approaches infinity, and is shortened when the level of excitation is increased.

Correlation time for a single-atom, two-mode cavity QED system with atomic Zeeman substructure

In the weak excitation limit the density matrix of a single-atom two-mode cavity QED system with Zeeman substructure is a mixture of two pure states. Transitions between these two states occur each time a photon of the non-driven mode is emitted from the cavity field. Consequently, the correlation time of the system displays two distinct time scales, one determined by the atomic and cavity lifetimes, and the other determined by the inverse of the non-driven mode emission rate.

To calculate correlation functions for this two-mode cavity QED system with atomic Zeeman substructure, we could use the same perturbation expansion in the driving field strength $\mathcal{E}$, like we did for the case of a non-degenerate two-level atom. However, this calculation would be very complex: first, because the two-quanta basis has 69 elements, and second, because we have to calculate the equilibrium between the steady states of the two manifolds.

For this reasons we refrain from calculating analytic results for the steady state characteristics and correlation functions. Instead we numerically solve the master equation and use standard quantum regression formulas to find these properties. This is the subject of the following chapter.

Chapter 5

Two-Mode Cavity Quantum Electrodynamics II: Numerical Solution of the Master Equation

When considering a two-level atom with Zeeman substructure, the analytic investigations in the previous chapter have predicted two distinct time scales for the correlations of our two-mode cavity QED system. Since finding analytic solutions to the system dynamics is overly complex, we will use numerical methods to solve the master equation in this chapter.

Performing numerical calculations requires the problem to be set up in a manner that is suitable for computers. Due to the finite size of a computer, two factors require attention at this point:

1. Computers can only represent a subset of the real numbers; this can lead to inaccuracy and rounding errors in the calculations. In particular, combining numbers that differ by many orders of magnitude should be avoided.

2. The memory and capacity of the hard drive are limited.

To address these factors, we recast the master equation into a dimensionless form, so that the scaled parameters are of similar orders of magnitude. We also make the Hilbert space of our system finite by truncating the Fock spaces of the two cavity modes. These considerations are discussed in the first section of this chapter.

In the second section, we present results for the steady state. Mean photon numbers of the cavity mode are calculated to evaluate the quality of the Fock space truncation. The key result in this section is the observation of the two predicted time scales of the correlation function.

5.1 Computational considerations

Since the master equation (3.43) for a two-level atom with Zeeman substructure ($F = 3$ to $F' = 4$ transition) in a driven two-mode cavity is too complex to solve analytically with a reasonable amount of effort, we will use numerical methods for our further investigations. A few considerations are necessary when carrying out calculations on a computer. In order to implement numerical methods we have to be aware of the computer as a finite-sized machine regarding memory and disk space.

5.1.1 Dimensionless master equation

On the hardware of computers, floating point numbers are represented in a binary numeral system, where for each floating point number only a limited number of bits is available. Restrictions on both the precision and the magnitude of the floating point numbers that have a hardware representation are the consequences. This leads to accuracy problems, and is especially an issue when adding two non-zero numbers that differ by many orders of magnitude. In an extreme case, the sum of two non-zero numbers may evaluate to be equal to the larger summand.

To avoid such computational issues we rewrite our master equation such that all terms are of a similar order of magnitude. A dimensionless master equation that satisfies these criteria is a rescaled version of (3.43):

$$\begin{aligned}\frac{\mathrm{d}\rho(t)}{\mathrm{d}(\kappa t)} = &\left[\frac{H_S}{\mathrm{i}\hbar\kappa}, \rho(t)\right] + \left(2\hat{a}\rho(t)\hat{a}^\dagger - \hat{a}^\dagger\hat{a}\rho(t) - \rho(t)\hat{a}^\dagger\hat{a}\right) \\ &+ \left(2\hat{b}\rho(t)\hat{b}^\dagger - \hat{b}^\dagger\hat{b}\rho(t) - \rho(t)\hat{b}^\dagger\hat{b}\right) \\ &+ \frac{\gamma}{2\kappa}\sum_{p=0,\pm1}\left(2\hat{\Sigma}_p\rho(t)\hat{\Sigma}_p^\dagger - \hat{\Sigma}_p^\dagger\hat{\Sigma}_p\rho(t) - \rho(t)\hat{\Sigma}_p^\dagger\hat{\Sigma}_p\right) ,\end{aligned} \tag{5.1}$$

with

$$\frac{H_S}{\mathrm{i}\hbar\kappa} = \frac{\mathcal{E}}{\kappa}(\hat{a}^\dagger - \hat{a}) + \frac{g}{\kappa}\left(\hat{a}^\dagger\hat{\Sigma}_0 - \hat{a}\hat{\Sigma}_0\right) + \frac{g}{\kappa}\left(\hat{b}^\dagger\,\frac{\hat{\Sigma}_{-1} + \hat{\Sigma}_{+1}}{\sqrt{2}} - \hat{b}\,\frac{\hat{\Sigma}_{-1} + \hat{\Sigma}_{+1}}{\sqrt{2}}\right) , \tag{5.2}$$

where $\hat{\Sigma}_p$ with $p = -1, 0, 1$ is defined in equation (1.73a).

5.1.2 Fock space truncation

As discussed in the previous chapter, for a given driving field strength it is very unlikely that the number of photons in a cavity mode α reaches an appropriately chosen maximum number N_α. It is thus a good approximation to neglect all Fock states with a photon number larger than N_α, i. e. to truncate the Fock space of the cavity mode α.

If N_a and N_b are the maximum considered numbers of photons in the driven and non-driven cavity modes, respectively, the Hilbert space $\mathcal{H}$ of our atom-cavity system

with truncated Fock spaces for the cavity modes,

$$\mathcal{H} = \mathcal{H}_{\text{atom}} \otimes \mathcal{H}_{\text{driven mode}} \otimes \mathcal{H}_{\text{non-driven mode}} \ , \tag{5.3}$$

is $16(N_a+1)(N_b+1)$-dimensional, assuming an atom with 16 sub-levels. Consequently, solving the master equation for the system density operator requires the solution of a set of $(16(N_a+1)(N_b+1))^2$ coupled ordinary differential equations. This allows us to describe the dynamics of our cavity QED system on a finite-sized computer disk. For small N_a and N_b it is a straightforward numerical task to solve these coupled differential equations. In the results presented in the remaining parts of this chapter we have considered up to two photons in each cavity mode, i. e. $N_a = N_b = 2$.

5.2 Results for the steady state in the weak excitation regime

The steady state can be characterised by the means of various operators. The mean of an arbitrary system operator $\hat{O}$ is related to the steady-state density operator ρ_{ss} by

$$\langle \hat{O} \rangle_{ss} = \text{Tr}_S \{ \hat{O} \rho_{ss} \} \ . \tag{5.4}$$

For the numerical work presented in this chapter we used the Quantum Optics Toolbox [48] for MATLAB®. To calculate the steady-state density operator we used the toolbox function `steady(L)`, which returns the steady-state density operator for an arbitrary Liouvillian $\mathcal{L}$, while operator averages were determined with the toolbox function `expect(O,rhoss)`.

5.2.1 Steady state properties

Mean photon numbers of the cavity modes

The mean photon numbers of the cavity modes indicate how well the Fock space truncation approximates the full Fock space. If the mean photon number is not much larger than one-tenth of the maximum considered photon number, then the truncation might be said to be a reasonable approximation. In this case the system is very seldom in a state that cannot be represented in the truncated Fock space.

Figure 5.1 shows the mean photon numbers of the driven and non-driven cavity mode, given by

$$\langle \hat{\nu}^\dagger \hat{\nu} \rangle = \text{Tr}_S \left\{ \hat{\nu}^\dagger \hat{\nu} \rho_{ss} \right\} \ , \tag{5.5}$$

where $\hat{\nu} = \hat{a}, \hat{b}$, for varying dipole coupling and driving strengths. We observe that, in general, the mean photon number in the driven mode is much larger than that in the non-driven mode.

Dipole coupling strength variation: If the dipole coupling strength is switched on and increased, two effects are particular interesting: firstly, due to the coupling between the atom and the cavity modes, the atom can be excited. As a consequence, photons are scattered from the driven mode into both the non-driven cavity mode and into the free space modes exiting out the side of the cavity. Secondly, the magnitude of the vacuum Rabi splitting increases with increasing coupling strength. Therefore, the effective resonance frequency of the atom-cavity system is more and more detuned from the laser frequency, and hence, fewer photons enter the cavity. At the same time, the cavity-mode decay rate remains constant.

Both of these effects lead to a decrease in the mean photon number in the driven mode when the coupling strength is increased.

For the mean photon number in the non-driven mode, the two effects have opposite character. All the photons in the non-driven mode originate from emission events of the atom. This yields an initial increase in the mean photon number in this mode when the dipole coupling strength is increased. For larger coupling, however, the effects of the vacuum Rabi splitting dominate: since there are fewer photons in the driven mode, fewer photons can be scattered into the non-driven mode. The mean photon number in the non-driven mode therefore decreases as well.

Driving field strength variation: If the strength of the driving field is increased, more photons are provided by the laser; consequently, the mean photon number in the driven mode increases. With a larger average photon number in the driven mode, more photons are scattered into the non-driven mode. However, this scattering is not in general proportional. A single atom is only able to scatter photons into the non-driven mode at a limited rate, even if a large number of photons in the driven mode is present. This effect will become more apparent when we investigate a larger driving field in the next chapter.

Field amplitude of the driven mode

As a second steady state property we calculate the mean amplitude of the driven mode,

$$\langle \hat{a} \rangle = \mathrm{Tr}_S \left\{ \hat{a} \rho_{ss} \right\} \ , \tag{5.6}$$

for varying coupling and driving field strengths (see Figure 5.2). The amplitude of the driven mode has a coherent part from the driving field and an incoherent part from the interaction with the atom. Since the coherent part does not average out, the amplitude of the driven mode has a non-zero mean. By contrast, the mean amplitude of the non-driven cavity mode is zero since all the light in this mode originates from phase-uncorrelated photon emissions of the atom.

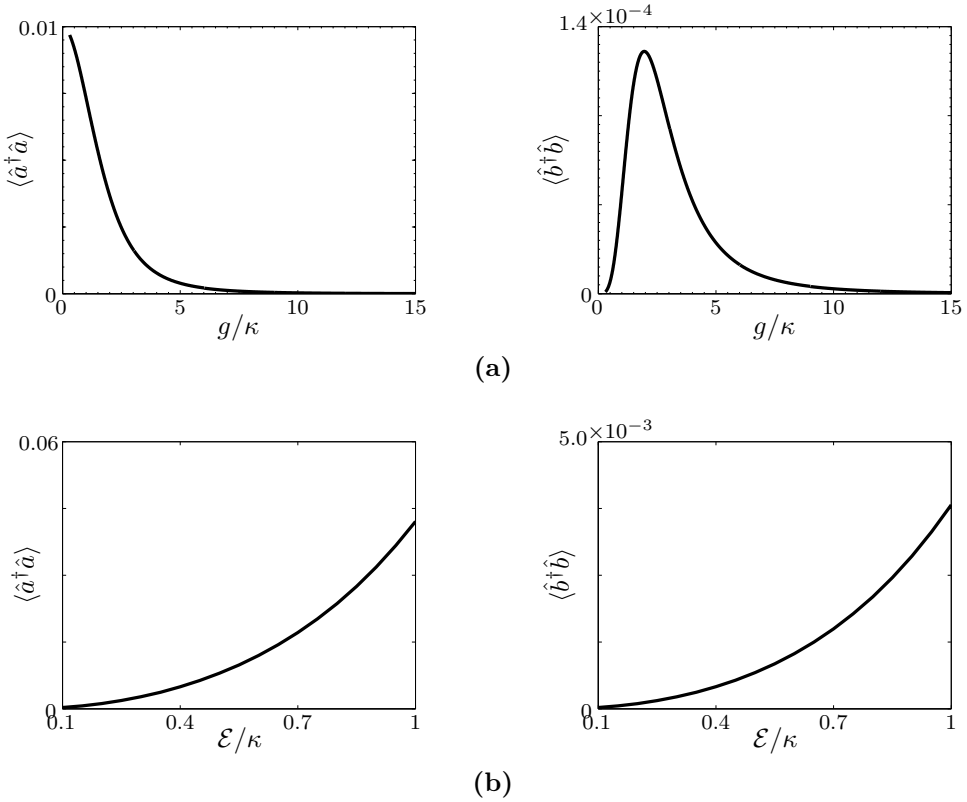

Figure 5.1 Mean photon numbers of the driven and non-driven cavity modes for $\gamma/\kappa = 6$, and (a) $\mathcal{E}/\kappa = 0.1$ and varying coupling constant g, (b) $g/\kappa = 5$ and varying driving field strength $\mathcal{E}$.

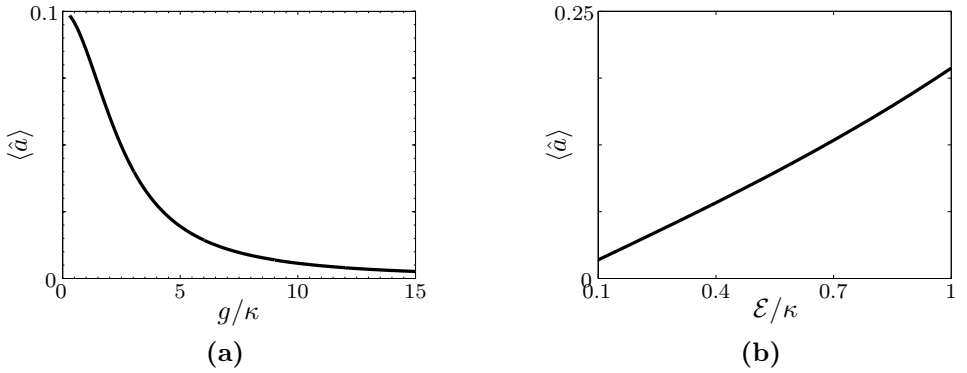

Figure 5.2 Mean field amplitude of the driven cavity mode for $\gamma/\kappa = 6$, and (a) $\mathcal{E}/\kappa = 0.1$ and varying coupling constant g, (b) $g/\kappa = 5$ and varying driving strength $\mathcal{E}$.

Atom population distribution

The atom population distribution tells us which atomic states must be taken into account if one wants to find a reduced level scheme that well approximates the full scheme. The atom population distribution for varying coupling and driving field strength are shown in Figures 5.3 and 5.4, respectively. We find that the atom is mainly in the ground state, and in states with $|m_F| \lessapprox 2$.

5.2.2 Second-order photon correlation functions

The steady state second-order photon correlation functions are calculated according to the quantum regression formula in Equation (2.46),

$$g^{(2)}_{\mu\nu}(\tau) = \frac{\langle \hat{\mu}^\dagger(0)\hat{\nu}^\dagger(\tau)\hat{\nu}(\tau)\hat{\mu}(0)\rangle_{ss}}{\langle \hat{\mu}^\dagger\hat{\mu}\rangle_{ss}\langle \hat{\nu}^\dagger\hat{\nu}\rangle_{ss}} = \frac{\mathrm{Tr}_S\left\{\hat{\nu}^\dagger\hat{\nu}e^{\mathcal{L}\tau}\left(\frac{\hat{\mu}\rho_{ss}\hat{\mu}^\dagger}{\langle \hat{\mu}^\dagger\hat{\mu}\rangle_{ss}}\right)\right\}}{\langle \hat{\nu}^\dagger\hat{\nu}\rangle_{ss}} \,. \tag{5.7}$$

The normalisation of the collapsed density matrix, namely $\frac{\hat{\mu}\rho_{ss}\hat{\mu}^\dagger}{\langle \hat{\mu}^\dagger\hat{\mu}\rangle_{ss}}$, is important for numerical reasons; it ensures that the matrix elements do not become too small compared with the other numbers involved in the calculation. The integration over time was carried out using the toolbox functions `ode2file` and `odesolve`.

The correlation functions for an illustrative set of parameters are shown in Figure 5.5. We see several important features:

- The driven mode self-correlation shows photon antibunching similar to the observations in one-mode cavity QED [14, 15, 16].

- The two-mode cross-correlation is asymmetric in time. This is an example of the breakdown of *detailed balance* reported by Denisov *et al.* [49] for one-mode cavity QED.

  Detailed balance is the equality of the probabilities of the direct and inverse transition for each pair of system states in the steady state. In our case the breakdown of detailed balance is possible due to the considered atomic level structure and the open-system character of our model. The balance of transitions between pairs of system states, i. e. the detailed balance, is no longer required; instead, a more complicated balanced cycle of transitions (*cyclic balance*) is sufficient.

- Most notable are the correlations on two distinct time scales, as predicted by our analytic investigations in the last chapter. As anticipated, the correlations at the lowest level of excitation decay very slowly, and this long decay time is shortened as the level of excitation—and therewith the photon emission rate of the non-driven mode—is increased.

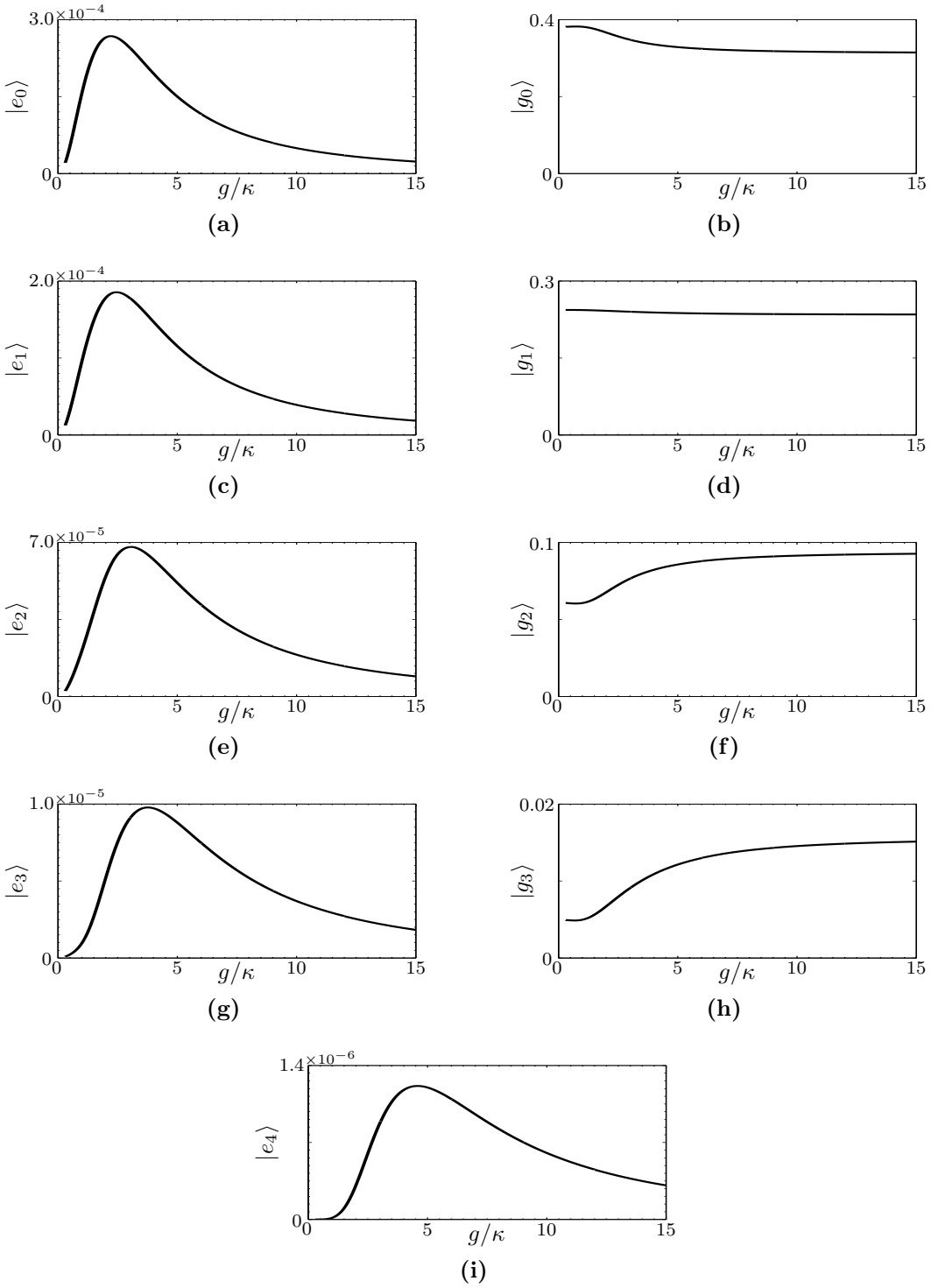

Figure 5.3 Atomic population distribution for $\gamma/\kappa = 6$, $\mathcal{E}/\kappa = 0.1$, and varying coupling constant g. Atomic state populations for states with negative m_F are omitted since for symmetry reasons they are the same as for positive m_F.

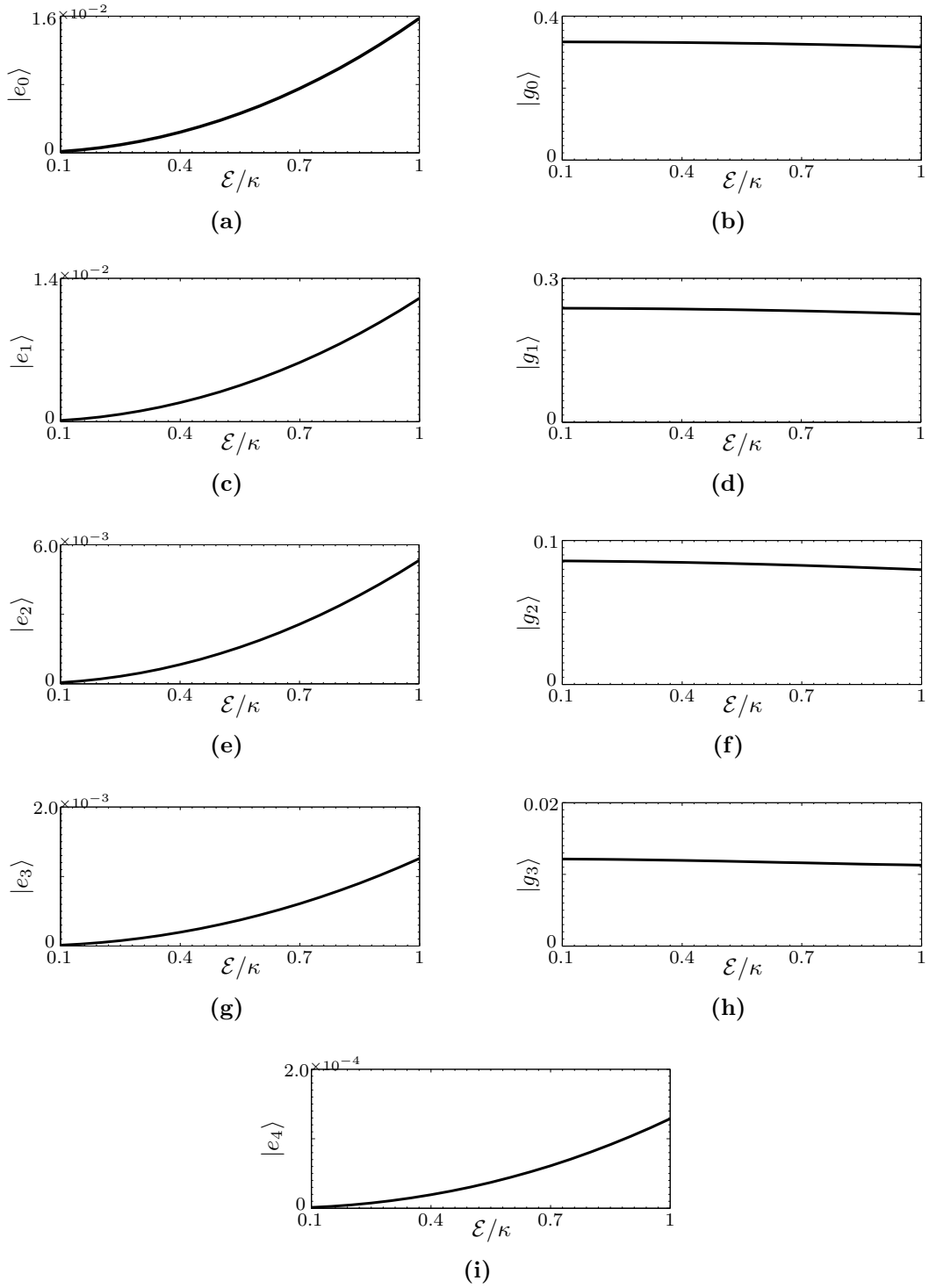

Figure 5.4 Atomic population distribution for $\gamma/\kappa = 6$, $g/\kappa = 5$, and varying driving strength $\mathcal{E}$. Atomic state populations for states with negative m_F are omitted since for symmetry reasons they are the same as for positive m_F.

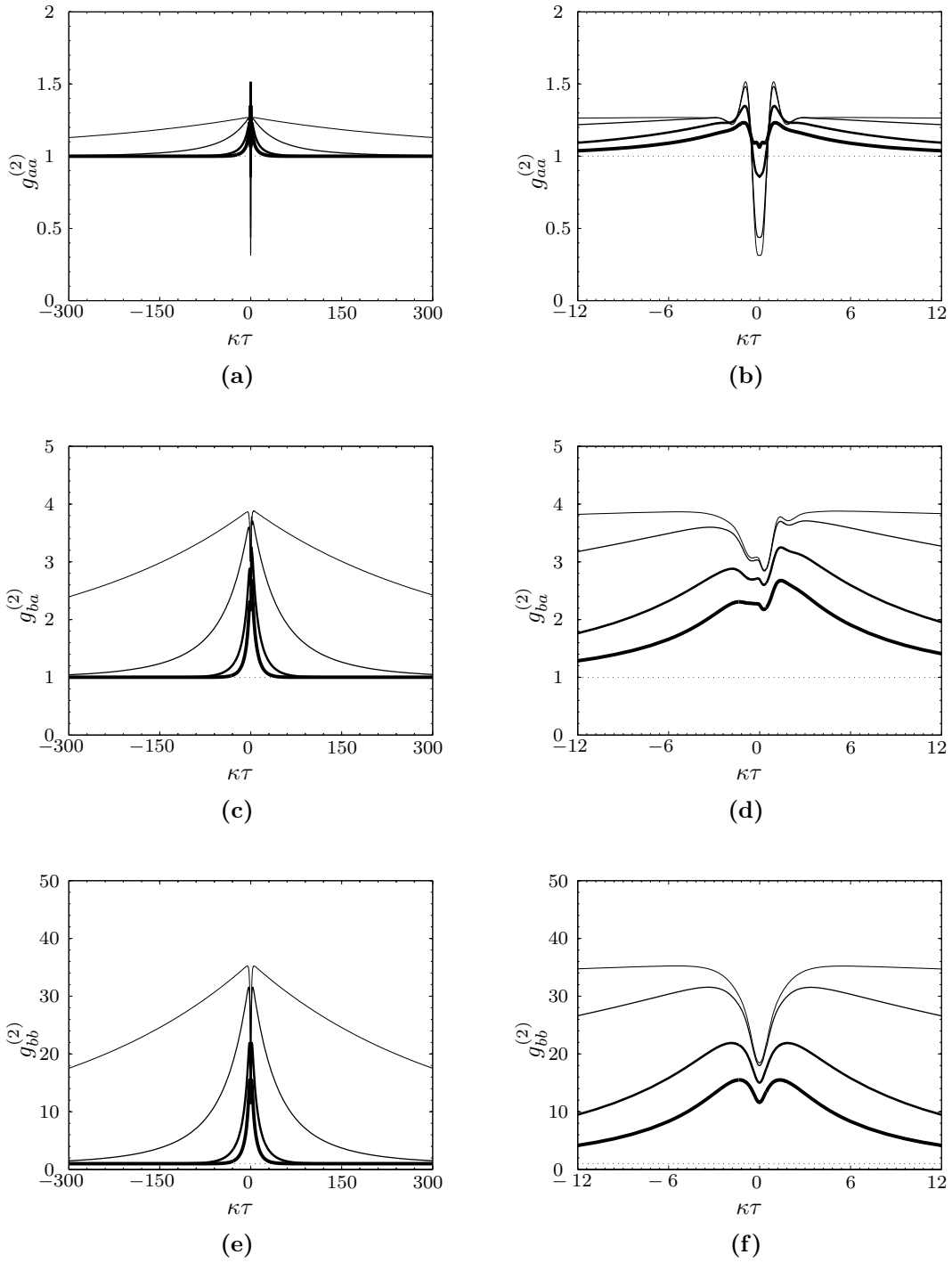

Figure 5.5 Steady state second-order photon correlation functions for $\gamma/\kappa = 6$, $g/\kappa = 5$, and $\mathcal{E}/\kappa = 0.1, 0.3, 0.7,$ and 1.0 (thinnest line to thickest line): (a) and (b) driven mode self-correlation, (c) and (d) two-mode cross-correlation, and (e) and (f) non-driven mode self-correlation. Each correlation function is plotted twice, for a large time scale on the left hand side, and for a short time scale on the right hand side.

If we kept increasing the strength of the driving field, the mean photon number in the cavity would increase as well, and our chosen truncation of the Fock space would become a bad approximation. To compensate for larger driving fields we have to consider a larger Fock space for the cavity modes. However, a larger Fock space has the disadvantage that the master equation yields a larger number of coupled differential equations. Since the number of differential equations increases quadratically with the dimension of the Fock space, we run into numerical difficulties very soon. For larger driving field strengths, we therefore use a quantum trajectory approach, where the number of coupled differential equations increases only linearly with the dimension of the Fock space. This is the subject of the next chapter.

Chapter 6

Two-Mode Cavity Quantum Electrodynamics III: Quantum Simulations

The numerical integration of the master equation confirms the qualitative predictions from our analytic analysis in Chapter 4 (regarding correlations of the system on two distinct time scales). Both of these approaches are limited to weak excitations—the analytic conceptually, and the numerical practically. In this chapter, we explore driving field strengths away from the weak excitation regime, using a simulation of our system based on quantum trajectory theory. Besides exploring the new regime, we use the trajectory simulation to quantitatively verify our results from the numerical integration.

In the first section we briefly discuss how to "unravel" the master equation of our two-mode cavity QED system. We determine the appropriate non-unitary Schrödinger equation for the time evolution of the wavefunction, and identify the collapse operators that interrupt this coherent time evolution.

Once we have found the Schrödinger equation for the time evolution, and the collapse operators for the quantum jumps, we can adopt the Monte-Carlo algorithm described in Chapter 2 to simulate the quantum trajectory of the wavefunction. The algorithm we use in this chapter is slightly modified to optimise the numerical efficiency. A discussion of this optimisation is given in the second section of this chapter.

In the final section we present the steady state properties and second order correlation functions resulting from the quantum trajectory simulations. The dynamics found from the numerical integration of the master equation in the previous chapter are recovered and extended to the higher excitation regime.

6.1 Stochastic wavefunction for a two-mode cavity QED system

To apply the quantum trajectory formalism, we unravel the dimensionless master equation (5.1) according to the procedure described in subsection 2.2.1.

The considered two-mode cavity QED system radiates five fields: The cavity radiates two fields, one for each cavity mode, which are transmitted through the cavity output mirror; we assume vacuum input fields at this mirror. Three fields of different polarisations are radiated out the side of the cavity by atomic spontaneous emission. Thus, the reduced density operator experiences five types of collapses, represented by the five dimensionless collapse superoperators

$$\mathcal{S}_{\hat{\nu}}\cdot = 2\hat{\nu}\cdot\hat{\nu}^\dagger \ , \qquad\qquad \mathcal{S}_p\cdot = \frac{\gamma}{\kappa}\,\hat{\Sigma}_p\cdot\hat{\Sigma}_p^\dagger \ , \tag{6.1}$$

where $\hat{\nu} = \hat{a}, \hat{b}$ and $p = -1, 0, 1$, and we scale time by κ^{-1}.

Since the system is initially prepared in a pure state (the atom in the $m_F = 0$ ground state and no photons in the non-driven mode), the unravelling of the master equation results in a non-unitary time evolution for the conditioned system wavefunction:

$$|\bar{\psi}_c(\kappa t + \Delta(\kappa t))\rangle = e^{-\frac{\mathrm{i}H_{\mathrm{eff}}}{\kappa\hbar}\Delta(\kappa t)}|\bar{\psi}_c(\kappa t)\rangle \tag{6.2}$$

with

$$\frac{\mathrm{i}H_{\mathrm{eff}}}{\kappa\hbar} = -\frac{H_S}{\mathrm{i}\hbar\kappa} + \sum_{\nu=a,b}\hat{\nu}^\dagger\hat{\nu} + \frac{\gamma}{2\kappa}\sum_{p=0,\pm1}\hat{\Sigma}_p^\dagger\hat{\Sigma}_p \ , \tag{6.3}$$

where $\frac{H_S}{\mathrm{i}\hbar\kappa}$ is given by equation (5.2). The coherent time evolution of the system wavefunction is interrupted by five types of collapses:

$$|\bar{\psi}_c\rangle \to \hat{C}_{\hat{\nu}}|\bar{\psi}_c\rangle \ , \qquad\qquad |\bar{\psi}_c\rangle \to \hat{C}_p|\bar{\psi}_c\rangle \ , \tag{6.4}$$

where $\hat{C}_{\hat{\nu}} = \sqrt{2}\hat{\nu}$ and $\hat{C}_p = \sqrt{\gamma/\kappa}\hat{\Sigma}_p$ are the collapse operators associated with the five superoperators defined in equation (6.1), i. e. $\mathcal{S}\cdot \equiv \hat{C}\cdot\hat{C}$. The collapse probabilities of the wavefunction within a small time interval of length $\Delta(\kappa t)$ are given by

$$p_{c,\nu}(\kappa t) = 2\Delta(\kappa t)\frac{\langle\bar{\psi}_c(\kappa t)|\hat{\nu}^\dagger\hat{\nu}|\bar{\psi}_c(\kappa t)\rangle}{\langle\bar{\psi}_c(\kappa t)|\bar{\psi}_c(\kappa t)\rangle} \ , \tag{6.5a}$$

$$p_{c,p}(\kappa t) = \frac{\gamma}{\kappa}\,\Delta(\kappa t)\frac{\langle\bar{\psi}_c(\kappa t)|\hat{\Sigma}_p^\dagger\hat{\Sigma}_p|\bar{\psi}_c(\kappa t)\rangle}{\langle\bar{\psi}_c(\kappa t)|\bar{\psi}_c(\kappa t)\rangle} \ . \tag{6.5b}$$

We can now apply the Monte-Carlo algorithm summarised on page 40 to simulate the two-mode cavity QED system with atomic Zeeman substructure.

Nevertheless, a few considerations about the numerical implementation of the algorithm are advisable to optimise the numerical efficiency of our code. This is the subject of the following section.

6.2 Monte-Carlo simulation

6.2.1 Computational considerations

Time evolution

The Monte-Carlo algorithm requires the system state to be evolved in time between successive wavefunction collapses. The time-evolution operator is an exponential that cannot be implemented exactly on a computer. However, for exponents with small modulus we can use Euler's method for the time integration:

$$|\bar{\psi}_c(\kappa t + \Delta(\kappa t))\rangle \approx \left(1 - \frac{\mathrm{i}H_{\mathrm{eff}}}{\kappa\hbar}\,\Delta(\kappa t)\right)|\bar{\psi}_c(\kappa t)\rangle\ . \tag{6.6}$$

Although the Euler method is the most simple numerical integration method, it is reluctantly applied, since it is numerically not very stable. Nonetheless, in a damped system like ours, the damping acts to increase the stability, if the size of the time step is chosen small enough.

Wavefunction collapses

The unravelling of the master equation is based on the assumption that an interaction of our system with the environment via a photon emission, and therewith a wavefunction collapse, occurs very seldom. The system mostly evolves coherently in time according to the non-unitary Schrödinger equation.

In our simulation we decide whether or not a wavefunction collapse occurs within a small time step $\Delta(\kappa t)$ by using a variation of the algorithm introduced in chapter 2: we compare the collapse probabilities for each possible type of collapse one by one with uncorrelated random numbers. The first random number that is smaller than or equal to the compared collapse probability decides that this collapse occurs, and we move on to the next time step. If all random numbers are larger than the compared collapse probabilities, we evolve the wavefunction in time. The order in which we compare the five collapses is not important as long as the collapse probabilities, which can be tuned by the size of the time step, are very small.

Time-step size

The size of the time step has a huge impact on the execution time of our simulation. The larger the time step, the faster we evolve our system through time, and the more quickly we can calculate the system properties. However, as discussed before, there are two upper limits on the size of the time step: it has to be small enough for Euler's approximation to hold, and small enough to ensure very small collapse probabilities.

To ensure the validity of the Euler method we use $\min\{(\frac{2\pi}{g/\kappa}, 2\pi, \frac{2\pi}{\gamma/\kappa})/100\}$ as an upper limit of $\Delta(\kappa t)$. The average collapse probability is chosen to be smaller than 0.01 to ensure the validity of our Monte-Carlo algorithm. However, since we need to know the mean photon number in the cavity mode to determine the average collapse

probability, the upper limit on the time step that the Monte-Carlo algorithm dictates can only be determined empirically.

Wavefunction normalisation

Neither the non-unitary Schrödinger equation nor the collapse operators preserve the norm of the wavefunction. Thus, the normalisation of the wavefunction has to be explicitly implemented in our simulation. Normalising the wavefunction is numerically expensive, since every element of the wavefunction must be divided by a number. Fortunately, it is not necessary to normalise the wavefunction after every time step; instead, we work with the unnormalised wavefunction, normalising it only if the norm becomes very small or large—we have chosen 0.001 and 1000 as the limits.

6.2.2 Monte-Carlo algorithm

Due to the considerations of the previous subsection, we use a slightly different Monte-Carlo algorithm than the one described in chapter 2. To simulate the dynamics of our two-mode cavity QED system we use a discrete time integration described by the following algorithm:

1. Calculate the norm $\langle\bar{\psi}_c(\kappa t_n)|\bar{\psi}_c(\kappa t_n)\rangle$ of the wavefunction, and decide whether a normalisation is necessary or not according to:

   If ($(\langle\bar{\psi}_c(\kappa t_n)|\bar{\psi}_c(\kappa t_n)\rangle \leq 0.001)$ **or** $(\langle\bar{\psi}_c(\kappa t_n)|\bar{\psi}_c(\kappa t_n)\rangle \geq 1000)$ **) then**

   $$|\bar{\psi}_c(\kappa t_n)\rangle = \frac{|\bar{\psi}_c(\kappa t_n)\rangle}{\sqrt{\langle\bar{\psi}_c(\kappa t_n)|\bar{\psi}_c(\kappa t_n)\rangle}} \; . \tag{6.7}$$

2. Calculate the five probabilities $p_{c,i}(\kappa t_n)$, $i = a, b, -1, 0, +1$, for a collapse in the interval $[\kappa t_n, \kappa t_n + \Delta(\kappa t)]$:

   $$p_{c,i}(t_n) = \frac{\langle\bar{\psi}_c(\kappa t_n)|\hat{C}_i^\dagger \hat{C}_i|\bar{\psi}_c(\kappa t_n)\rangle}{\langle\bar{\psi}_c(\kappa t_n)|\bar{\psi}_c(\kappa t_n)\rangle}\,\Delta(\kappa t) \; . \tag{6.8}$$

3. Draw five random numbers $r_{n,i}$ from an uniformly distribution of the interval $[0, 1]$.

4. Compare the collapse probability $p_{c,i}(\kappa t_n)$ with the random number $r_{n,i}$ and determine the unnormalised state at time κt_{n+1} according to:

   If ($p_{c,a}(\kappa t_n) \geq r_{n,a}$ **) then**

   $$|\bar{\psi}_c(\kappa t_{n+1})\rangle = \hat{C}_a|\bar{\psi}_c(\kappa t_n)\rangle \tag{6.9a}$$

   elseif ($p_{c,b}(\kappa t_n) \geq r_{n,b}$ **) then**

   $$|\bar{\psi}_c(\kappa t_{n+1})\rangle = \hat{C}_b|\bar{\psi}_c(\kappa t_n)\rangle \tag{6.9b}$$

elseif ($p_{c,-1}(\kappa t_n) \geq r_{n,-1}$) **then**

$$|\bar{\psi}_c(\kappa t_{n+1})\rangle = \hat{C}_{-1}|\bar{\psi}_c(\kappa t_n)\rangle \tag{6.9c}$$

elseif ($p_{c,0}(t_n) \geq r_{n,0}$) **then**

$$|\bar{\psi}_c(\kappa t_{n+1})\rangle = \hat{C}_{0}|\bar{\psi}_c(\kappa t_n)\rangle \tag{6.9d}$$

elseif ($p_{c,+1}(\kappa t_n) \geq r_{n,+1}$) **then**

$$|\bar{\psi}_c(\kappa t_{n+1})\rangle = \hat{C}_{+1}|\bar{\psi}_c(\kappa t_n)\rangle \tag{6.9e}$$

else calculate

$$|\bar{\psi}_c(\kappa t_{n+1})\rangle = \left(1 - \frac{\mathrm{i}H_{\mathrm{eff}}}{\kappa\hbar}\,\Delta(\kappa t)\right)|\bar{\psi}_c(\kappa t_n)\rangle\ . \tag{6.9f}$$

In a statistical sense, the stochastic wavefunction described by the above algorithm will eventually become stationary in time. From this stationary state we can extract steady state properties.

6.3 Results for the steady state

6.3.1 Steady state properties

To determine the steady state properties we calculate expectation values 'on the fly' during the simulation and take a time average of them. Instead of calculating the properties after every time step, we take samples separated by a time interval of the order of the largest correlation time, which we determined by a preliminary simulation. This has two advantages: firstly, our simulation is sped up because fewer operations are performed, and secondly, the error in our sample average drops more quickly since the samples are statistically independent.

Mean photon numbers

The mean photon numbers in the driven and non-driven mode for varying driving field strength are shown in figure 6.1. The presence of the atom in the cavity reduces the mean photon number of the driven mode compared to the situation of a resonantly-driven empty cavity (dotted line in figure 6.1a). This reduction is due to photon absorptions and emissions of the atom: missing photons in the driven mode are emitted by the atom either through the side of the cavity, or into the non-driven cavity mode. The reduction is especially significant for small driving field strengths .

For large driving field strengths a single atom has a limited impact on the mean photon number of the driven mode, since the atomic photon emission rate approaches a constant when the cavity mode intensity exceeds the atomic saturation intensity. In

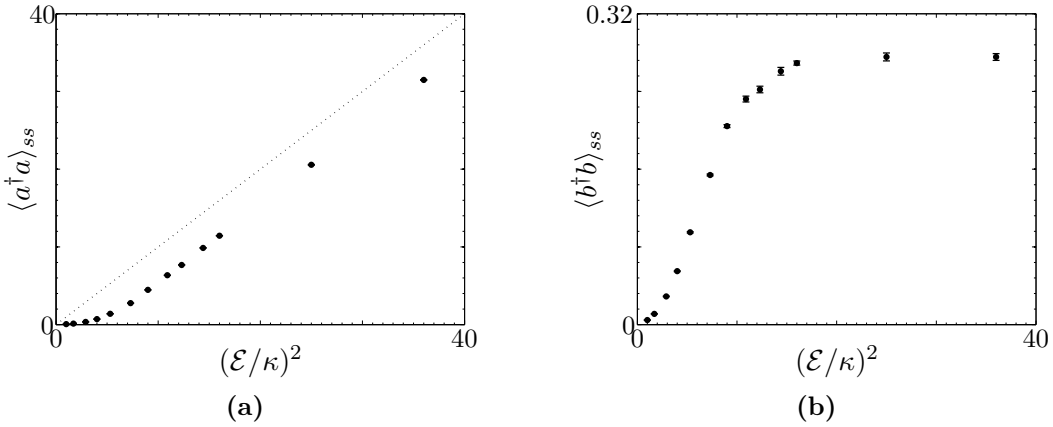

Figure 6.1 Mean photon numbers of the two cavity modes for $\gamma/\kappa = 6$, $g/\kappa = 5$, and various driving field strength: (a) for the driven cavity mode; (b) for the non-driven cavity mode. The bars indicate statistical uncertainties corresponding to one standard deviation. For comparison, the dotted line is the mean photon number of a resonantly driven empty cavity.

figure 6.1 this saturation can be seen by the fact that for strong driving field strengths the mean photon number in the driven mode tends toward a constant offset from the mean photon number of a resonantly-driven empty cavity, while at the same time, the mean photon number of the non-driven cavity mode approaches a constant value.

The atomic saturation can also be seen if we consider the photon flux out the side of the cavity, and its dependence on the driving field strength, shown in figure 6.2. Since only a small fraction of the atomic photon emissions into 4π is absorbed by the cavity modes, the photon flux through the side of the cavity tends asymptotically to half of the total photon scattering rate γ of the atom as the driving field strength is increased. The factor $\frac{1}{2}$ arises since the atom evolves, once the saturation threshold is passed, into a steady configuration in which both the atomic ground level and excited level are equally populated.

Second-order photon correlation functions at zero time delay

Figure 6.3 shows the second-order correlation functions at zero time delay for various driving field strengths. The plotted results from the trajectory simulations are supplemented with data from the numerical integration of the master equation.

For large driving field strengths the values of the driven-mode self-correlation and two-mode cross-correlation functions at zero delay become unity. This is another manifestation of the diminishing influence of the atom on the driven mode once the atom is saturated and the field strength is increased further.

For the self-correlation function of the non-driven mode the behaviour for large driving field strengths is different. Since all photons of the non-driven mode originate

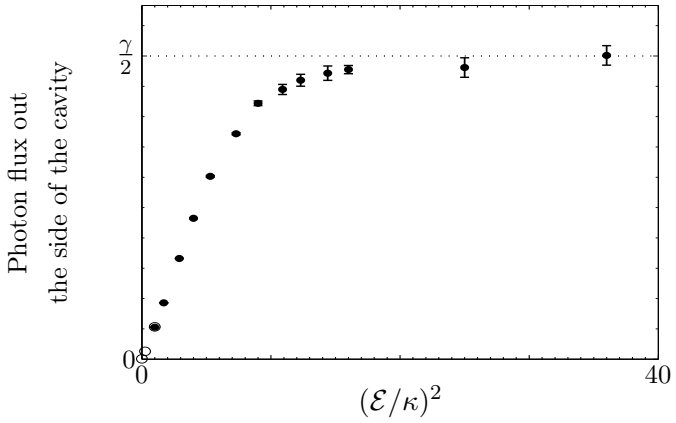

Figure 6.2 Photon flux out the side of the cavity for $\gamma/\kappa = 6$, $g/\kappa = 5$, and various driving field strength. The points are from the trajectory simulation; the bars indicate statistical uncertainties corresponding to one standard deviation. The circles are from the numerical integration of the master equation. The dotted line is half of the atomic decay rate.

from atom-mediated photon emission events, the light in this mode does not develop a mean amplitude and the correlation function at zero time delay does not approach unity if the driving field strength is increased.

6.3.2 Second-order photon correlation functions

An intuitive but very inefficient way of extracting the correlation functions from the data of the simulation would be to keep a record of all occurring separation times of (not necessarily successive) photon emission pairs through the cavity mirror. The distribution of these separation times determines the second-order correlation function.

Much more efficient, and the method we have used, is to record the photon emission probability $P(E_2|E_1)$ conditioned on a photon emission event E_1 through the cavity mirror some time earlier. Averaging over all records allows the calculation of the second-order correlation function according to equation (1.9b).

Correlation functions for the same set of parameters as in the last chapter, but for a larger driving field strength, are shown in figure 6.4. To compare the results from the quantum trajectory simulation with the results from the numerical integration of the master equation, the correlation functions for a driving field strength of $\mathcal{E}/\kappa = 1$ are displayed for both methods. They agree well with each other.

For driving field strengths away from the weak excitation regime, the correlations decay further, similar to what was observed from the numerical investigations in the previous chapter. In the strong excitation regime, where the atom has only a minor influence on the driven cavity mode, the cavity output field that couples to the driven mode becomes coherent, and both the driven-mode self-correlation function and the two-mode cross-correlation function become unity.

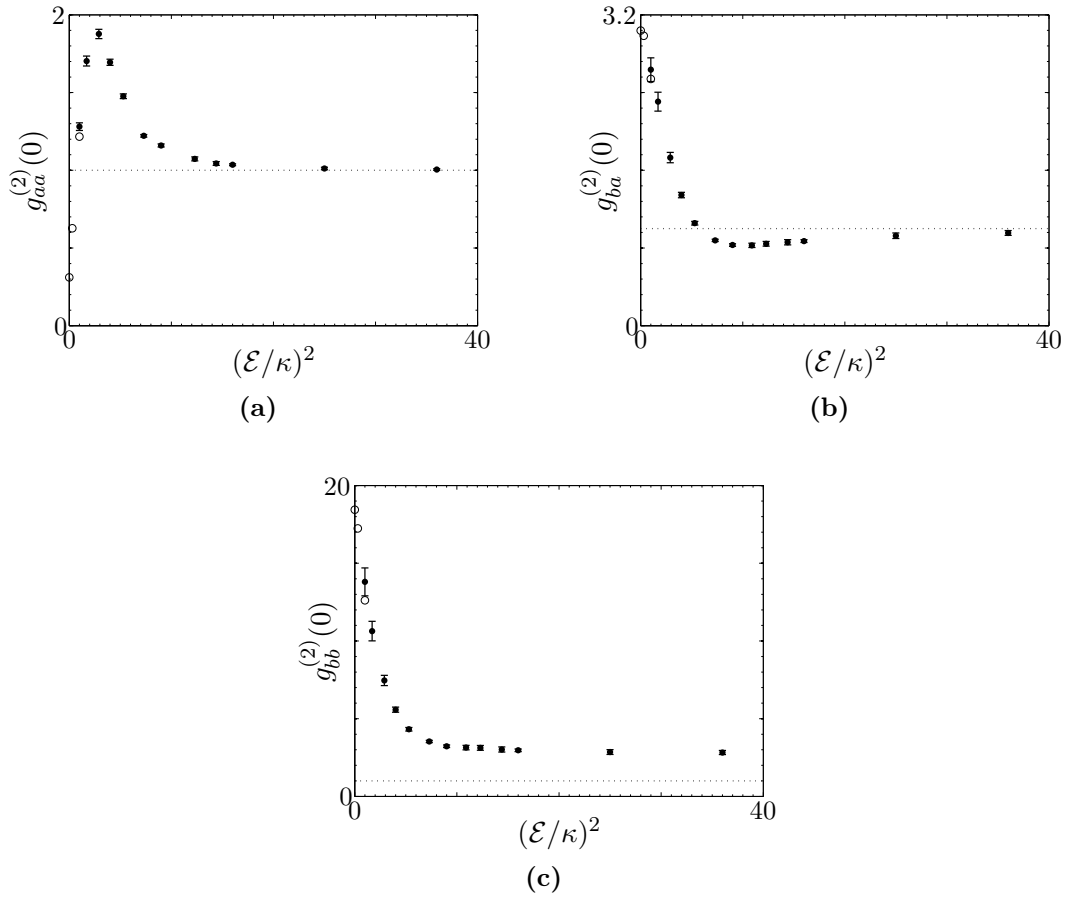

Figure 6.3 Steady state second-order correlation functions at zero time delay for $\gamma/\kappa = 6$, $g/\kappa = 5$, and various driving field strengths (from $(\mathcal{E}/\kappa)^2 = 0.01$ to 36): (a) driven-mode self-correlations, (b) two-mode cross-correlations, (c) non-driven-mode self-correlations. The points are from the trajectory simulation; the bars indicate statistical uncertainties corresponding to one standard deviation. The circles are from the numerical integration of the master equation.

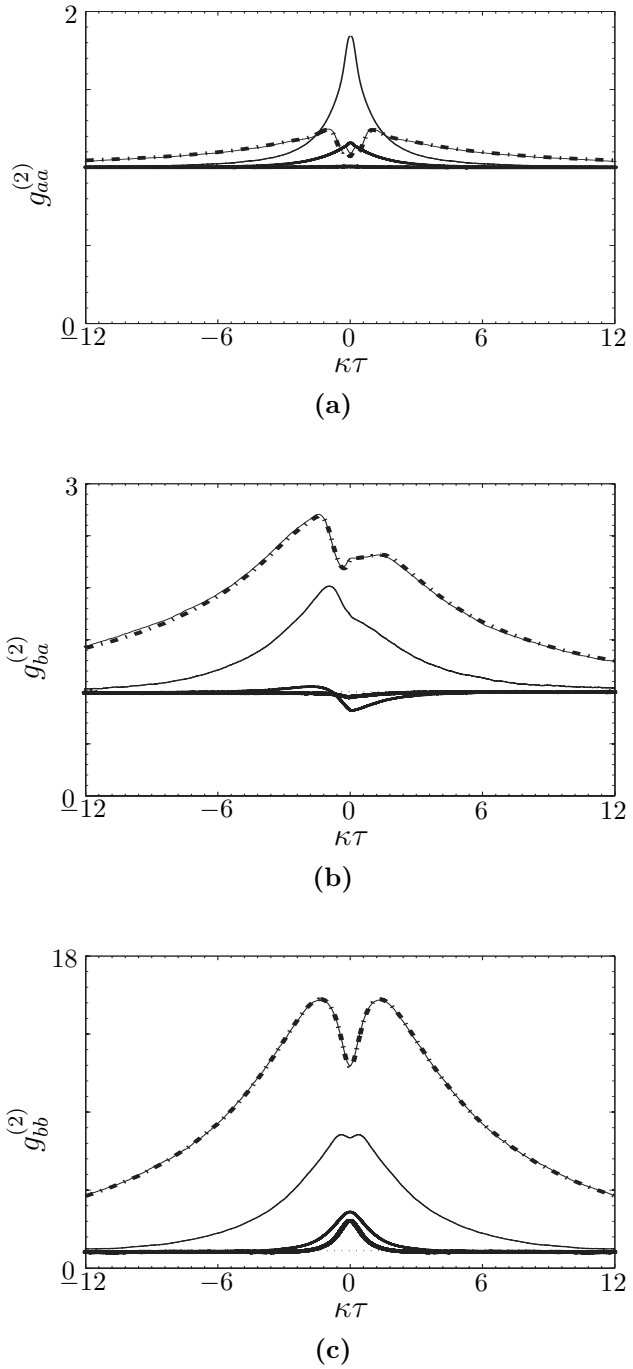

Figure 6.4 Steady state second-order photon correlation functions for $\gamma/\kappa = 6$, $g/\kappa = 5$, and $\mathcal{E}/\kappa = 1.0, 1.7, 3.0,$ and 6.0 (thinnest line to thickest line): (a) driven-mode self-correlation; (b) two-mode cross-correlation; (c) non-driven mode self-correlation. The dashed lines are the results from the numerical integration of the master equation for $\mathcal{E}/\kappa = 1.0$, and agree well with the quantum trajectory theory approach.

Chapter 7

Conclusion

7.1 Summary

In this thesis we have presented the results of an investigation into the dynamics of a cavity QED system where a single atom interacts with two orthogonal linearly polarised cavity modes. One cavity mode is resonantly driven by a coherent field, with light in the other cavity mode being generated only by atomic emission. We took the full atomic level structure for an $F = 3$ to $F' = 4$ transition into account.

We analytically investigated the weak-excitation limit and showed that there exist two orthogonal manifolds of basis states. Before the first photon emission from the non-driven cavity mode, the system evolves entirely within one of these manifolds, and transitions between the two manifolds occur each time a photon of the non-driven mode is emitted. As a qualitative result, the system displays correlations on two distinct time scales, one, a short time scale, determined by the atomic and cavity-mode decay rates, and the other, a much longer time scale, determined by the non-driven mode emission rate.

We used standard quantum regression formulas and a numerical solution of the master equation for a quantitative treatment in the weak-excitation regime, where we made a truncation of the cavity mode Hilbert spaces at two-photon states. We computed steady-state properties and second-order photon correlation functions. In agreement with our analytical considerations, we identified an extremely long correlation time at the lowest level of excitation (where the non-driven emission rate is very small), and a shortening of this correlation time as the level of excitation is increased.

We recovered this dynamic from a Monte-Carlo simulation based on a quantum trajectory unravelling of the master equation. The simulations also enabled us to explore higher levels of excitations up to the point of cavity mode intensities exceeding the atomic saturation intensity.

With the numerical integration of the master equation in the weak excitation regime and the quantum trajectory approach at higher levels of excitations, we have efficient tools to cover the full range of the driving field strength.

7.2 Future work

First experimental results became available during the stage of writing this thesis. Qualitatively in agreement with our investigations, they show correlations on an extremely long time scale especially at the lowest level of excitation. However, the results differ quantitatively from our calculations. This is partly due to the fact that the experiment is carried out in a slightly different parameter regime. A graver reason for the quantitative mismatch is that, even though incorporating the full atomic level structure, our model disregards a few effects present in the experiments:

- In the experiment an external magnetic field is used to define the quantisation axis. The precession of the magnetic moment of the electron about the external magnetic field results in a Zeeman splitting of the atomic sub-levels. Consequently, the correlation function shows an additional oscillation determined by the Larmor frequency.

- Our assumption of an atom at rest in the centre of the cavity is not valid. In the experiment, single atoms are launched from a magneto-optical trap (MOT), which is located below the cavity. The atoms fly through the cavity and experience a varying dipole coupling strength during their flight. The magnitude of the vacuum splitting varies therefore as well, which has a bearing on the Rabi oscillations of the correlation functions.

- In the experiment, the laser and cavity-mode frequencies are locked to the atomic resonance frequency with limited accuracy. This gives rise to possible slight frequency detuning.

To include these effects into our model is the future work in this project. The Zeeman splitting, and the laser and cavity-mode frequency detuning result in additional terms in the system Hamiltonian—which is feasible in both of the numerical methods we used. The varying dipole coupling strength due to the motion of the atom is more straightforwardly implemented in the Monte-Carlo simulation, following the work of [50].

Appendix

Different Pictures in Quantum Mechanics

The subject of this appendix is the dynamics of quantum mechanical state vectors and operators, and their representation for system states and observables.

A.1. Some general properties of non-relativistic quantum mechanics

We may start by recalling some postulates of non-relativistic quantum mechanics:

Postulate 1 The quantum mechanical state of a system is described by a non-zero state vector $|\varphi(t)\rangle$ of a complex Hilbert space. Two vectors specify the same state if, and only if, they are scalar multiples of each other.

Postulate 2 Physical observables A are experimentally measurable quantities. They can be represented by linear, Hermitian operators $\hat{A}(t)$, i. e. the operators have real eigenvalues. [51]

Postulate 3 The expectation value of an observable represented by an operator $\hat{A}(t)$ is given by

$$\langle \hat{A}(t) \rangle = \langle \varphi(t) | \hat{A}(t) | \varphi(t) \rangle \ . \tag{A.1}$$

Postulate 4 If the system is not perturbed, e. g. by a measurement, the time-evolution of a state vector $|\varphi(t)\rangle$ is determined by the *Schrödinger equation*

$$\mathrm{i}\hbar \frac{\mathrm{d}}{\mathrm{d}t} |\varphi(t)\rangle = H(t) |\varphi(t)\rangle \ , \tag{A.2}$$

where $H(t)$ is an Hermitian operator, the so-called *Hamiltonian*.

The postulates raise the question of how many possible representations there are for the states and the observables. It turns out that there are an infinite number of possible representations, all related by unitary transformations. This becomes

apparent by a simple mathematical observation: we find for a state vector $|\varphi\rangle$, an observable A, and a unitary operator $\hat{U}$ (i. e. $\hat{U}^\dagger = \hat{U}^{-1}$):

$$\langle\varphi|\hat{A}|\varphi\rangle = \langle\varphi|\hat{U}\hat{U}^\dagger\hat{A}\hat{U}\hat{U}^\dagger|\varphi\rangle = \big(\langle\varphi|\hat{U}\big)\big(\hat{U}^\dagger\hat{A}\hat{U}\big)\big(\hat{U}^\dagger|\varphi\rangle\big) \ . \tag{A.3}$$

We can now define a new representation by

$$|\varphi'(t)\rangle \equiv U^\dagger(t,t_0)|\varphi(t)\rangle \ , \tag{A.4a}$$

$$\hat{A}'(t) \equiv U^\dagger(t,t_0)\hat{A}(t)U(t,t_0) \ . \tag{A.4b}$$

Such a transformation of the state vectors and the operators keeps the expectation value in our example, and all observable quantities in general, unchanged.

The time evolution of the state vectors $|\varphi\rangle$ and $|\varphi'\rangle$ is governed by a Schrödinger equation with Hamiltonian H and H', respectively. However, the Hamiltonian H' is not just the transformed Hamiltonian H since in general $U^\dagger \mathrm{d}|\varphi\rangle/\mathrm{d}t \neq \mathrm{d}(U^\dagger|\varphi\rangle)/\mathrm{d}t$. Instead, if $\hat{U}(t,t_0)$ satisfies the operator equation

$$\mathrm{i}\hbar\frac{\mathrm{d}}{\mathrm{d}t}\hat{U}(t,t_0) = \hat{H}_U(t)\hat{U}(t,t_0) \ , \tag{A.5}$$

we find

$$\begin{aligned}
\mathrm{i}\hbar\frac{\mathrm{d}}{\mathrm{d}t}|\varphi'(t)\rangle &= \mathrm{i}\hbar\Big(\frac{\mathrm{d}\hat{U}^\dagger}{\mathrm{d}t}(t,t_0)|\varphi(t)\rangle + \hat{U}^\dagger(t,t_0)\frac{\mathrm{d}}{\mathrm{d}t}|\varphi(t)\rangle\Big) \\
&= -\hat{U}^\dagger(t,t_0)\hat{H}_U(t)|\varphi(t)\rangle + \hat{U}^\dagger(t,t_0)H(t)|\varphi(t)\rangle \\
&= \hat{U}^\dagger(t,t_0)\big(H(t)-\hat{H}_U(t)\big)\hat{U}(t,t_0)|\varphi'(t)\rangle \ .
\end{aligned} \tag{A.6}$$

Therefore,

$$H'(t) \equiv \hat{U}^\dagger(t,t_0)H(t)\hat{U}(t,t_0) - H'_U(t) \tag{A.7}$$

is the Hamiltonian of the Schrödinger equation in the primed representation.

Note A.1 To remind us of the particular role of the Hamiltonian, we do not put a hat on it like we do for every ordinary operator. ◀

The time evolution of an operator in the primed and unprimed representation is related by

$$\begin{aligned}
\mathrm{i}\hbar\frac{\mathrm{d}}{\mathrm{d}t}\hat{A}'(t) &= \mathrm{i}\hbar\left(\frac{\mathrm{d}\hat{U}^\dagger}{\mathrm{d}t}\hat{A}(t)\hat{U} + \hat{U}^\dagger\frac{\mathrm{d}\hat{A}(t)}{\mathrm{d}t}\hat{U} + \hat{U}^\dagger\hat{A}(t)\frac{\mathrm{d}\hat{U}}{\mathrm{d}t}\right) \\
&= -\hat{U}^\dagger\hat{H}_U\hat{A}(t)\hat{U} + \mathrm{i}\hbar\hat{U}^\dagger\frac{\mathrm{d}\hat{A}(t)}{\mathrm{d}t}\hat{U} + \hat{U}^\dagger\hat{A}^\dagger(t)\hat{H}_U\hat{U} \\
&= \Big[\hat{A}'(t),\hat{H}'_U(t)\Big] + \mathrm{i}\hbar\hat{U}^\dagger\frac{\mathrm{d}\hat{A}(t)}{\mathrm{d}t}\hat{U} \ .
\end{aligned} \tag{A.8}$$

For an operator with no implicit time-dependence in the unprimed representation (i. e. $\mathrm{d}\hat{A}/\mathrm{d}t = \partial\hat{A}/\partial t$), equation (A.8) can be simplified further by noting that $\frac{\partial\hat{A}(t)}{\partial t}$ itself is an operator (i. e. $\frac{\partial}{\partial t}\hat{A}'(t) = \hat{U}^\dagger\frac{\partial\hat{A}(t)}{\partial t}\hat{U}$). We find the so-called *Heisenberg equation of motion*,

$$\frac{\mathrm{d}}{\mathrm{d}t}\hat{A}'(t) = \frac{1}{\mathrm{i}\hbar}\left[\hat{A}'(t), \hat{H}'_U(t)\right] + \frac{\partial\hat{A}'(t)}{\partial t} \ . \tag{A.9}$$

A.2. The Schrödinger, Heisenberg, and Dirac pictures

Among the infinite number of possible representations, three are frequently preferred, namely the Schrödinger, the Heisenberg, and the Dirac pictures:

Schrödinger picture

The Schrödinger picture is characterised by time-dependent state vectors, and operators with no implicit time-dependence. The time-evolution of the state vectors and operators is governed by

$$\mathrm{i}\hbar\frac{\mathrm{d}}{\mathrm{d}t}|\varphi_S(t)\rangle = H_S(t)|\varphi_S(t)\rangle \ , \tag{A.10a}$$

$$\mathrm{i}\hbar\frac{\mathrm{d}}{\mathrm{d}t}\hat{A}_S(t) = \mathrm{i}\hbar\frac{\partial}{\partial t}\hat{A}_S(t) \ . \tag{A.10b}$$

Heisenberg picture

The Heisenberg picture is obtained from the Schrödinger picture by choosing $\hat{H}_U(t) = H_S(t)$ in the operator equation (A.5) for the unitary transformation operator:

$$|\varphi_H\rangle \equiv \hat{U}_S^\dagger(t,t_0)|\varphi_S(t)\rangle = |\varphi_S(t_0)\rangle \ , \tag{A.11a}$$

$$\hat{A}_H(t) \equiv \hat{U}_S^\dagger(t,t_0)\hat{A}_S(t)\hat{U}_S(t,t_0) \ , \tag{A.11b}$$

where the unitary operator $\hat{U}_S(t,t_0)$ satisfies the operator equation

$$\mathrm{i}\hbar\frac{\mathrm{d}}{\mathrm{d}t}\hat{U}_S(t,t_0) = H_S\hat{U}_S(t,t_0) \ . \tag{A.12}$$

Consequently, in the Heisenberg picture the state vectors are time-independent and the operators are time-dependent:

$$\mathrm{i}\hbar\frac{\mathrm{d}}{\mathrm{d}t}|\varphi_H\rangle = \big(H_S(t) - H_S(t)\big)|\varphi_H\rangle = 0 \ , \tag{A.13a}$$

$$\mathrm{i}\hbar\frac{\mathrm{d}}{\mathrm{d}t}\hat{A}_H(t) = \left[\hat{A}_H(t), \hat{H}_H(t)\right] + \mathrm{i}\hbar\frac{\partial}{\partial t}\hat{A}_H(t) \ , \tag{A.13b}$$

where $\hat{H}_H(t) = \hat{U}_S^\dagger(t,t_0)H_S(t)\hat{U}_S(t,t_0)$.

Dirac picture

The Dirac picture is obtained from the Schödinger picture by choosing the time-independent part of the Hamiltonian as $H_U(t)$ in equation (A.5), i. e. if

$$H_S(t) = \hat{H}_S^{(0)} + \hat{W}_S(t) \tag{A.14}$$

then $\hat{H}_U(t) = \hat{H}_S^{(0)}$, and we find

$$|\varphi_D\rangle = \hat{U}_0^\dagger(t, t_0)|\varphi_S(t)\rangle \ , \tag{A.15a}$$
$$\hat{A}_D(t) = \hat{U}_0^\dagger(t, t_0)\hat{A}_S(t)\hat{U}_0(t, t_0) \ , \tag{A.15b}$$

where the unitary operator $\hat{U}_0(t, t_0)$ satisfies the operator equation

$$\mathrm{i}\hbar\frac{\mathrm{d}}{\mathrm{d}t}\hat{U}_0(t, t_0) = \hat{H}_S^{(0)}\hat{U}_0(t, t_0) \ . \tag{A.16}$$

In the Dirac picture the states and the operators are time-dependent. The time-evolution of the state vectors and operators is governed by

$$\mathrm{i}\hbar\frac{\mathrm{d}}{\mathrm{d}t}|\varphi_D(t)\rangle = H_D(t)|\varphi_I(t)\rangle \qquad \text{with} \qquad H_D(t) = \hat{W}_D(t) \ , \tag{A.17a}$$
$$\mathrm{i}\hbar\frac{\mathrm{d}}{\mathrm{d}t}\hat{A}_D(t) = \left[\hat{A}_D(t), \hat{H}_D^{(0)}(t)\right] + \mathrm{i}\hbar\frac{\partial}{\partial t}\hat{A}_D(t) \ . \tag{A.17b}$$

Bibliography

[1] G. R. Kirchhoff, *Über den Zusammenhang von Emission und Absorption von Licht und Wärme*, Monatsberichte der Akademie der Wissenschaften zu Berlin (1859), 783–787.

[2] O. Lummer and E. Pringsheim, *Über die Strahlung des schwarzen Körpers für lange Wellen*, Verhandlungen der Deutschen Physikalischen Gesellschaft **2** (1900), 163–180.

[3] H. Rubens and F. Kurlbaum, *Über die Emission langwelliger Wärmestrahlen durch den schwarzen Körpers bei verschiedenen Temperaturen*, (Monatsberichte) Sitzungsberichte der Königlich-Preussischen Akademie der Wissenschaften, Berlin, Mathematik-Naturwissenschaftliche Klasse (1900), 929–941.

[4] J. C. Maxwell, *Dynamical theory of the electromagnetic field*, Royal Society Transactions **155** (1865), 459–512.

[5] W. Wien, *Über die Energieverteilung im Emissionsspektrum eines schwarzen Körpers*, Wiedemannsche Annalen der Physik **58** (1896), 662–669.

[6] L. Rayleigh, *Remarks upon the law of complete radiation*, Philosophical Magazine **49** (1900), 539–540.

[7] M. Planck, *Über eine Verbesserung der Wienschen Spektralgleichung*, Verhandlungen der Deutschen Physikalischen Gesellschaft **2** (1900), 202–204.

[8] L. Boltzmann, *Über die Beziehung zwischen dem zweitem Hauptsatze der mechanischen Wärmetheorie und der Wahrscheinlichkeitsrechnung, resp. den Sätzen über das Wärmegleichgewicht*, Sitzungsberichte der Kaiserlichen Akademie der Wissenschaften (Vienna) **76** (1877), 373–435.

[9] A. Einstein, *Über einen die Erzeugung und Verwandlung des Lichtes betreffenden heuristischen Gesichtspunkt*, Annalen der Physik **17** (1905), 132–148.

[10] G. N. Lewis, *The conservation of photons*, Nature **118** (1926), 874–875 ("I therefore take the liberty of proposing for this hypothetical new atom, which is not light but plays an essential part in every process of radiation, the name photon.").

[11] L. de Broglie, *Recherches sur la théorie des quanta*, PhD thesis, Université de Paris, Paris, 1924.

[12] R. H. Brown and R. Q. Twiss, *Correlation between photons in two coherent beams of light*, Nature **177** (1956), 27–29.

[13] H. J. Kimble, M. Dagenais, and L. Mandel, *Photon antibunching in resonance fluorescence*, Phys. Rev. Lett. **39** (1977), 691–695.

[14] G. Rempe, R. J. Thompson, R. J. Brecha, W. D. Lee, and H. J. Kimble, *Optical bistability and photon statistics in cavity quantum electrodynamics*, Phys. Rev. Lett. **67** (1991), 1727–1730.

[15] S. L. Mielke, G. T. Foster, and L. A. Orozco, *Nonclassical intensity correlations in cavity QED*, Phys. Rev. Lett. **80** (1998), 3948–3951.

[16] G. T. Foster, S. L. Mielke, and L. A. Orozco, *Intensity correlations in cavity QED*, Phys. Rev. A **61** (2000), 053821.

[17] H. J. Carmichael, R. J. Brecha, and P. R. Rice, *Quantum interference and collapse of the wavefunction in cavity QED*, Optics Communications **82** (1991), 73–79.

[18] T. Fischer, P. Maunz, P. W. H. Pinkse, T. Puppe, and G. Rempe, *Feedback on the motion of a single atom in an optical cavity*, Physical Review Letters **88** (2002), 163002.

[19] K. M. Birnbaum, A. Boca, R. Miller, A. D. Boozer, T. E. Northup, and H. J. Kimble, *Photon blockade in an optical cavity with one trapped atom*, Nature **436** (2005), 87–90.

[20] J. I. Cirac, P. Zoller, H. J. Kimble, and H. Mabuchi, *Quantum state transfer and entanglement distribution among distant nodes in a quantum network*, Phys. Rev. Lett. **78** (1997), 3221–3224.

[21] M. L. Terraciano, R. Olson Knell, D. L. Freimund, L. A. Orozco, J. P. Clemens, and P. R. Rice, *Enhanced spontaneous emission into the mode of a cavity QED system*, Optics Letters **32** (2007), 982–984.

[22] X. T. Zou and L. Mandel, *Photon-antibunching and sub-Poissonian photon statistics*, Phys. Rev. A **41** (1990), 475–476.

[23] H. Friedrich, *Theoretical Atomic Physics*, 3 edition, Springer-Verlag Berlin Heidelberg, 2006 (Chapter 2).

[24] M. O. Scully and M. S. Zubairy, *Quantum Optics*, Cambridge University Press, 1997.

[25] J. J. Sakurai, *Modern Quantum Mechanics*, The Benjamin/Cummings Publishing Company, Inc., 1985.

[26] C. Eckart, *The application of group theory to the quantum dynamics of monatomic systems*, Rev. Mod. Phys. **2** (1930), 305–380.

[27] E. Wigner, *Einige Folgerungen aus der Schrödingerschen Theorie für die Termstrukturen*, Zeitschrift für Physik **43** (1927), 624–652.

[28] H. J. Carmichael, *An Open Systems Approach to Quantum Optics*, Springer-Verlag Berlin Heidelberg, 1993.

[29] R. Dum, P. Zoller, and H. Ritsch, *Monte Carlo simulation of the atomic master equation for spontaneous emission*, Phys. Rev. A **45** (1992), 4879–4887.

[30] R. Dum, A. S. Parkins, P. Zoller, and C. W. Gardiner, *Monte Carlo simulation of master equations in quantum optics for vacuum, thermal, and squeezed reservoirs*, Phys. Rev. A **46** (1992), 4382–4396.

[31] K. Molmer, Y. Castin, and J. Dalibard, *Monte Carlo wavefunction method in quantum optics*, J. Opt. Soc. Am. B **10** (1993), 524–.

[32] H. J. Carmichael, *Statistical Methods in Quantum Optics*, Vol. 1, Springer-Verlag Berlin Heidelberg, 1999.

[33] (Physically, condition (2.12) holds for all interactions that exclude purely phase destroying effects.).

[34] F. Haake, *On a non-Markoffian master equation*, Zeitschrift für Physik **223** (1969), 335–363.

[35] ———, *On a non-Markoffian master equation*, Zeitschrift für Physik **223** (1969), 364–377.

[36] A. G. Redfield, Advances in Magnetic Resonances **1** (1965), 1.

[37] J. Wilkie, *Positivity preserving non-Markovian master equations*, Phys. Rev. E **62** (2000), 8808–8810.

[38] G. Lindblad, *On the generators of quantum dynamical semigroups*, Communications in Mathematical Physics **48** (1976), 119–130.

[39] J. P. Clemens, L. Horvath, B. C. Sanders, and H. J. Carmichael, *Collective spontaneous emission from a line of atoms*, Phys. Rev. A **68** (2003), 023809.

[40] H. J. Carmichael and K. Kim, *A quantum trajectory unraveling of the superradiance master equation*, Optics Communications **179** (2000), 417–427.

[41] H. J. Carmichael, *Statistical Methods in Quantum Optics*, Vol. 2, Springer-Verlag Berlin Heidelberg, 2007.

[42] E. T. Jaynes and F. W. Cummings, Proc. IEEE **51**.

[43] M. Fox, *Quantum Optics*, 1 edition, Oxford University Press, 2006.

[44] (This approximation is reasonable since at optical frequencies $\hbar\omega_i \gg k_B T$ and thermal effects can be neglected.).

[45] (For the definition of an eigenoperator see equation (2.20).).

[46] V. G. Weisskopf and E. Wigner, Zeitschrift für Physik **63** (1930), 54.

[47] H. Eleuch and H. J. Carmichael, *2-mode correlation function of a cavity QED system*, unpublished notes (2006), (We follow Eleuch's calculation given in section III.).

[48] S. M. Tan *Quantum Optics and Computation Toolbox for* MATLAB, 2002.

[49] A. Denisov, H. M. Castro-Beltran, and H. J. Carmichael, *Time-asymmetric fluctuations of light and the breakdown of detailed balance*, Phys. Rev. Lett. **88** (2002), 243601.

[50] L. Horvath and H. J. Carmichael, *Atomic motion and density fluctuations in cavity QED with atomic beams*, Vol. 6038 SPIE, 2005, p. 603801.

[51] (It might be more precise to say: by linear, self-adjoint operators (which can be represented by Hermitian matrices).).